UNDERGROUND CONDUCTIVITY STRUCTURE IN TASMANIA

BY

M. RAHMAT HERMANTO

Submitted in partial fulfilment
of the requirements for the
degree of Master of Science

UNIVERSITY OF TASMANIA
HOBART
1985

graduating
1985

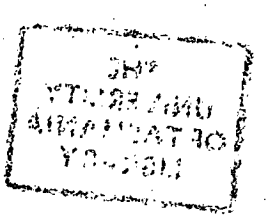

To my family

This thesis contains no material which has been accepted for the award of any other degree or diploma in any University and to the best of my knowledge and belief, contains no copy or paraphrase of material previously published or written by another person, except where due reference is made in the text of this thesis.

M. Rahmat Hermanto

June, 1985.

AKNOWLEDGEMENTS.

I record my gratitude to my supervisors Dr. W.D. Parkinson and Dr. R.J.G. Lewis for their supervision during the course of this study, and also for their encouragement, suggestions and wide ranging assistance in all stages of the work.
I would like to thank all the property owners who allowed me to use their land for recording data. To my friends, Mr. Suhartono Sudargo, Mr. Sutrisno, and Mr. Rudy Oei, their help and company during some of the field trips are gratefully appreciated. I would like also to express my thanks to Mrs. Pongratz for editing and proof-reading the final draft of the thesis.
Finally, I must acknowledge my parents and my wife for their encouragement, support, and endless prayer.

ABSTRACT

Geomagnetic variations were measured at 35 temporary stations in the north, north-east and centre of Tasmania. The surveys were carried out from early in 1983 to the middle of 1984. The surveys were designed to map the southern extension of the anomaly discovered by Buyung (1980) and revealed two types of anomalies, i.e. inland and coast effect. The inland anomaly is characterized by oppositely directed in-phase induction arrows at close locations for periods from 4 to 20 minutes, indicating the presence of a concentration of current in a highly conductive zone. This anomaly is coincident with the Tamar Fracture Zone. Meanwhile, the gradual change in the direction of induction arrows with increasing period from various directions to almost south-east illustrates the significant effect of the coast. This is probably due either to current induced in the conducting ocean water or to high conductivity contrasts between the resistive block in the eastern part of Tasmania and the conducting ocean floor.

The finite difference method of Jones and Pascoe (1971) and Pascoe and Jones (1972) was used to calculate the induction response of two-dimensional models and to interpret the observations. Modelling reveals that a highly conductive zone, responsible for the inland anomaly, is located at a depth of about 2 km from the surface. This zone, which is bounded by resistive blocks to the east and west, has a resistivity of 0.5Ω m and thickness of 2 to 3 km. This model agrees with magneto-telluric observations of previous workers. The most likely cause of this highly conductive zone is a large quantity of saline water or conducting liquid in porous or cracked rocks.

Analogue modelling of the coast effect around Tasmania by Dosso et al. (in press) has been used in an attempt to isolate the effect of inland structures. This was only partly successful, probably because the analogue models assume that the island is a perfect insulator.

CONTENTS.

LIST OF FIGURES.

LIST OF TABLES.

CHAPTER 1

INTRODUCTION

The study of electrical conductivity structure by means of the magneto-variational (m-v) method has contributed to our knowledge of the distribution of lateral conductivity inhomogeneities. The term magneto-variational follows its use by Rokityansky when determining lateral conductivity inhomogeneities in the earth's crust and upper mantle (Rokityansky, 1982, p.247). This method utilizes the natural varying field which originates outside the earth. The geomagnetic variations found to be most suitable as a source field are those that are associated with substorms and similar types of bays. The current systems responsible for these variations are concentrated in the auroral zones and flow either through the temperate latitude ionosphere or the magnetosphere. Electric fields which are generated by such variations cause eddy currents to flow in the conducting part of the earth. These variations which penetrate down into the earth, ~~depending~~ to a depth which depends on the period of the variations and conductivity of the medium, are used as a tool in probing the lateral conductivity contrast.

The primary concern of this study was to investigate the underground conductivity structure in Tasmania and to trace the southern extension of the highly conductive zone previously discovered by Buyung (1980) in the Tamar Graben area. Buyung's work was suggested by the peculiar behaviour of the induction arrows which were observed by Lilley (1976) at Devonport and Bridport and which both pointed toward the mouth of Tamar River. The present study involved the occupation of 32 temporary m-v stations during the period from early 1983 to mid 1984.

The area is of interest because it contains the boundary between two geological provinces of different composition and structural style, as described in section 5.3. Despite its geological significance the nature and structure of the Tamar Fracture Zone cannot be adequately determined from the surface geology as it is overlain by dolerite and Tertiary sediments.

1.1 PREVIOUS STUDY

1.1.1 MAGNETO-VARIATIONAL METHOD

The first magneto-variational observation in Tasmania was conducted by Parkinson (1962) at Hobart. This observation was made as a part of a world-wide survey to study the effect of oceans on the geomagnetic field at coastal stations and showed the normal coast effect (see figure 1.1).

Intensive magneto-variational studies in the north-east of Tasmania, however, originated with the interesting results shown by Lilley (1976) on either side of the Tamar River. Lilley's m-v observations in the north of Tasmania were a part of his study on geomagnetic variations in south-east Australia. Although the induction vectors at Devonport and Bridport (see figure 1.1) appear to be deflected by the effect of currents induced in Bass Strait, the vectors at these stations (both pointing almost towards the off-shore projection of the Tamar Valley) suggest that they may be due to an anomalous region beneath the mouth of the Tamar River. These results led to Buyung (1980) carrying out a preliminary induction study in the north-east of Tasmania. Eleven temporary stations scattered on the eastern and western sides of the Tamar River were occupied during his study. Induction vectors at periods of 13 and 24 minutes derived from this study followed an approximately similar pattern to those of Lilley's results (see figures 1.2 and 1.3). Buyung concluded that the reversal in direction of induction vectors on the eastern and western sides of the river at periods less than 1 hour could be due to a zone of high conductivity under the Tamar River. More localized surveys in the north-east and east of Tasmania were carried out by Parkinson at Golconda (GOL), Myrtle Bank (MTB), Lilydale (LIL), Triabunna (TRI), and Cambridge (CAM), (W.D. Parkinson, personal communication). With his permission the results from GOL and MTB are used in this thesis. M-v data from NTS, a magneto-telluric site occupied by Bindoff (1983) and calculated by W.D. Parkinson, are also used here. These results together with the present observations will be discussed in a later section.

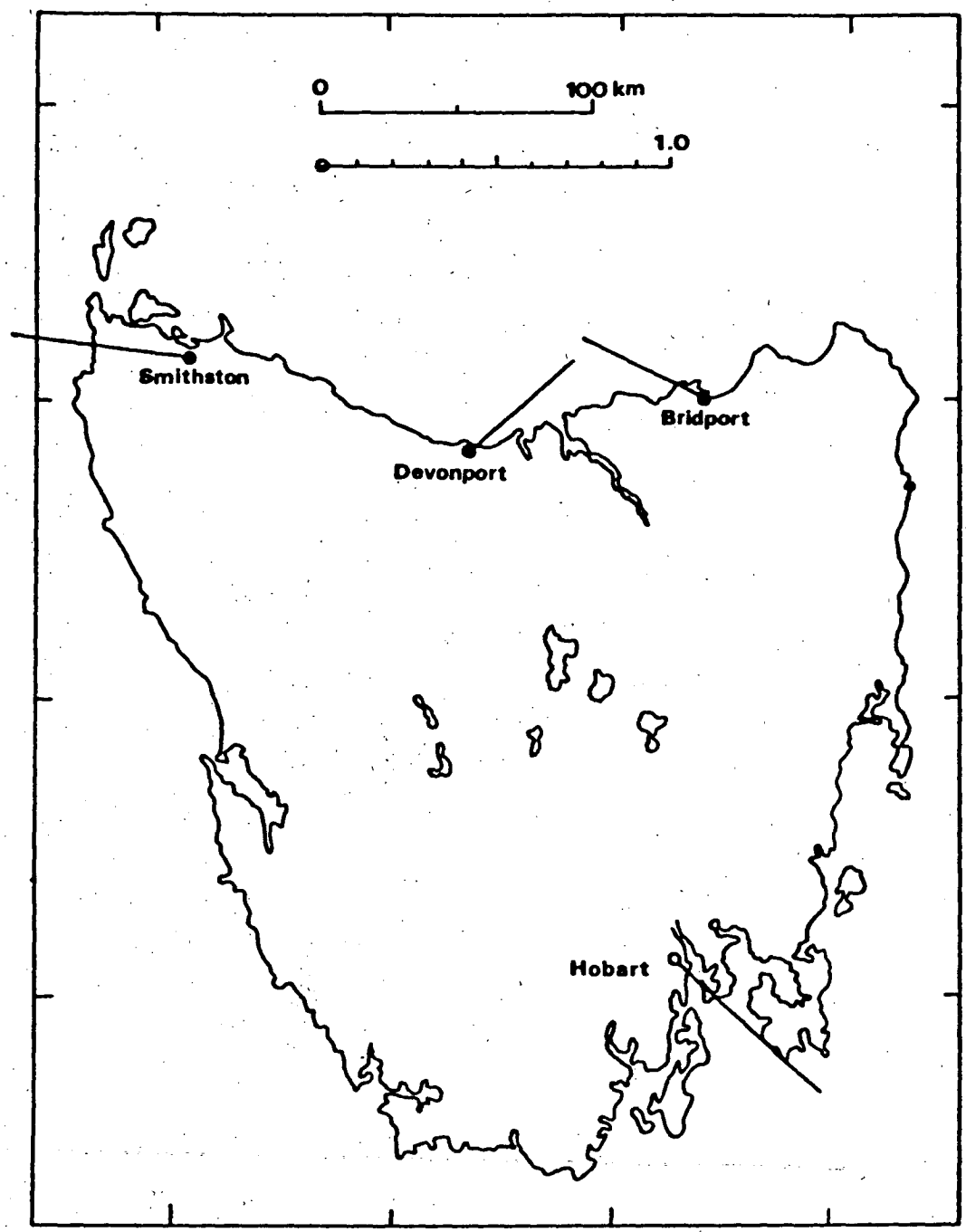

Fig.1.1: Induction vectors around Tasmania. Hobart vector is for 40 minutes period, and Smithton, Devonport and Bridport vectors are for 5 - 20 minutes period.

● Lilley (1973 - 1974)

O Parkinson (1962)

(From Buyung, 1980)

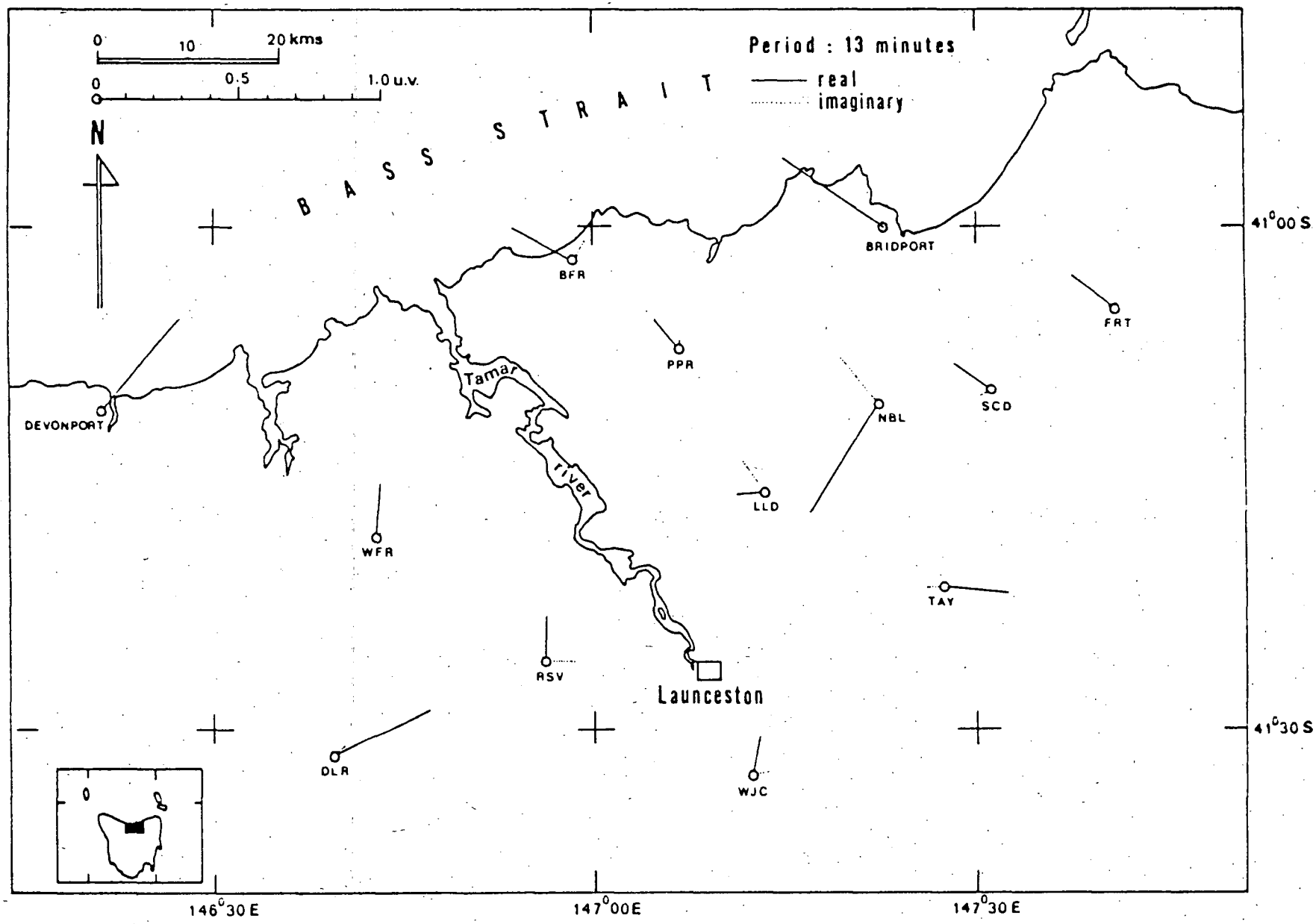

Fig. 1.2 Induction vectors at period of 13 minutes and location of Buyung's m-v stations.

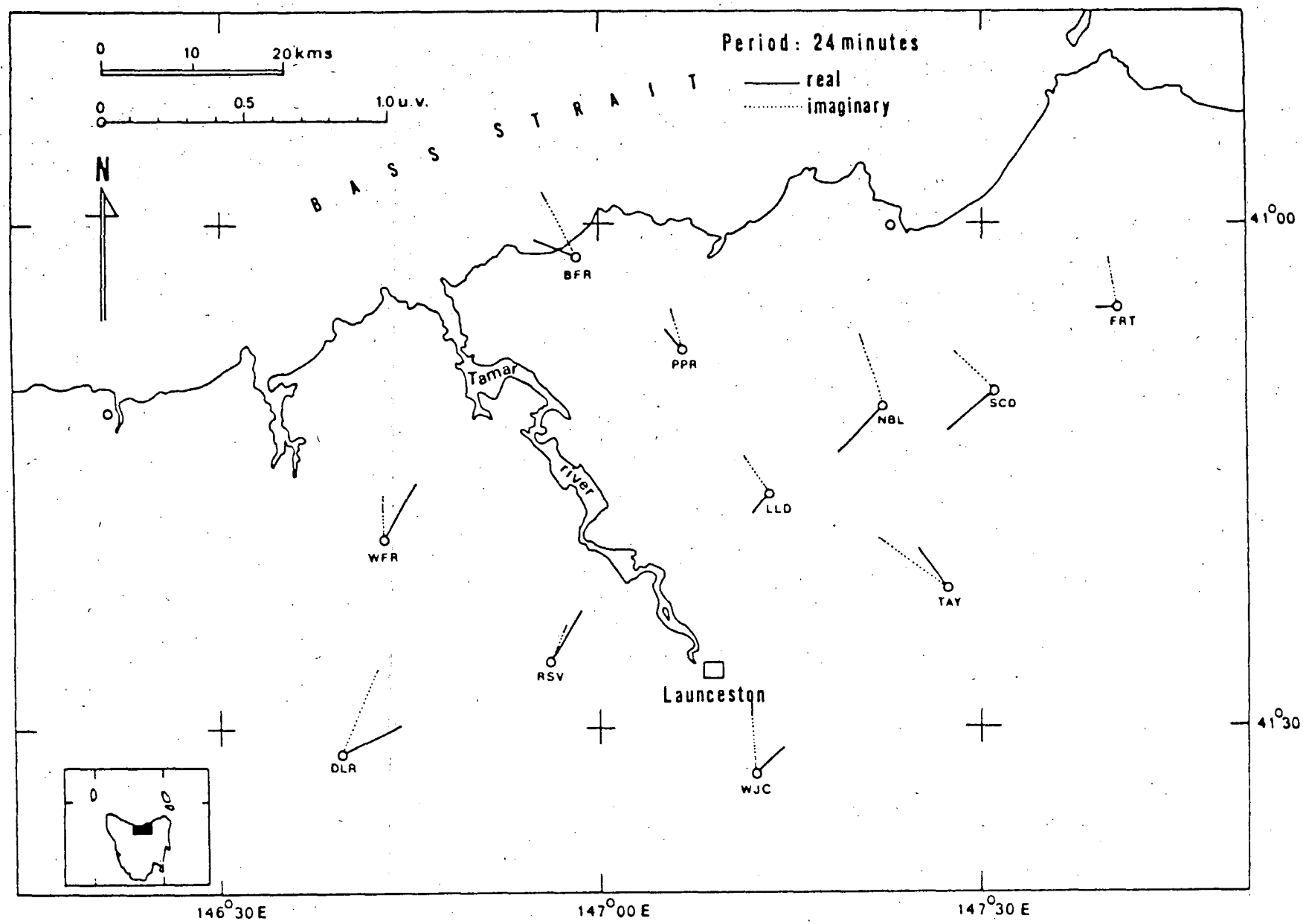

Fig. 1.3 Induction vectors at period of 24 minutes and location of Buyung's m-v stations.

1.1.2 MAGNETO-TELLURIC METHOD

The magneto-telluric method (m-t) can be used to investigate the electrical conductivity structure of the interior of the earth. The principal difference between this and the magneto-variational method is that it determines conductivity as a function of depth while m-v observes lateral conductivity inhomogeneities. In practice both of these methods complement each other. Lewis (1965) first used the method in Tasmania to study the conductivity of the crust in the Hobart area. Some other early observations of local conductivity contrast were made in the north of Tasmania. A magneto-telluric survey in the Longford area was carried out by Asten (1972) who postulated a deep structure striking at approximately N30^{o}E below the Tertiary structure. Magneto-telluric surveys at Lilydale (LIL) and North Scottsdale (NTS) in the north-east of Tasmania were made by Bindoff (1983). A two-dimensional model interpretation of the results from LIL showed a conductive region having resistivities of 2 - 50 Ω m and a thickness in excess of 11 km. Another m-t survey was made by Sayers (1984) at Vaucluse (VAU) where a highly conductive anomaly was interpreted as due to an extensive fracture zone. This zone, which has a resistivity of between 0.5 and 1 Ω m and a thickness of about 2 - 5 km, is located only 2 km from the surface. Figure 5.2 shows the locations of the magneto-telluric surveys.

1.1.3 OTHER GEOPHYSICAL RESULTS

A seismic refraction profile from Savage River to Binalong Bay was conducted by Richardson (1980). Results from this work showed that the Tamar Fracture Zone coincides with a thickening of the crust and this thickening is also observed on regional gravity surveys (see fig. 5.10).

CHAPTER 2

MAGNETO-VARIATIONAL THEORY

2.1 INTRODUCTION

The primary electromagnetic field that is utilised by the magneto-variational method to study lateral conductivity inhomogeneities is assumed to be almost uniform. This assumption is most nearly true in mid-latitudes. It fails at high latitudes near the auroral electrojet and at very low magnetic latitudes near the equatorial electrojet (W.D. Parkinson, personal communication).

A theory that assumes the field is uniform was developed by Cagniard (1952) and was applied to the magneto-telluric method in the investigation of large sedimentary basins. The case of non-uniform source fields was discussed by Wait (1954). Weaver (1970) extended the theory of electromagnetic induction by considering three specific sources, namely; a periodic magnetic dipole normal to the surface of the conductor, a periodic magnetic dipole parallel to the surface of the conductor and a periodic line current flowing parallel to the surface of the conductor.

Starting with the classic paper on the general theory of electromagnetic induction by Price (1950), the theory has now been developed analytically and numerically by many authors and has been used to interpret electrical conductivity anomalies in the earth's crust and upper mantle.

At present the theory is best developed for a two-dimensional model structure. Some of the aspects which have been studied include : the effect of faults (d'Erceville and Kunetz, 1962); the effect of a dyke (Rankin, 1962); the perturbation of alternating geomagnetic fields by conductivity anomalies (Jones and Price, 1970); the effect of a non-horizontally stratified two-layered conductor (Jones,1970); the effect of vertical, sloping and shelving discontinuities (Jones and Price, 1971a); the effect of two-dimensional conductivity inhomogeneities at different depths (Jones and Price, 1971b); the effect of an asymmetric two-layered

conductor (Jones, 1971); the electromagnetic induction in two thin half-sheets (Weidelt, 1971); the effect of a dipping interface (Geyer, 1972), and the effect of discontinuities with high conductivity contrast (Jones and Ainslie, 1973).

Few problems in magneto-variational or magneto-telluric studies have been solved by three-dimensional models. Some of these include: the perturbation of an alternating geomagnetic field by three-dimensional conductivity inhomogeneities (Jones and Pascoe, 1972); the perturbation of alternating geomagnetic fields by an island near a coastline (Lines and Jones, 1973); the effect of an island and bay structure on alternating geomagnetic fields at three periods (Jones, 1974); and the effect of an irregular coastline and channelling effects (Jones and Lokken, 1975).

Analogue models can also be used in laboratory studies of three-dimensional conductivity structures. For example, an analogue model of electromagnetic induction in the oceans in the Tasmanian region has been investigated by Dosso and his collaborators at the University of Victoria, British-Columbia, Canada, (Dosso et al., in press). Numerous other studies of analogue models have been carried out for different regions, e.g. an analogue model of electromagnetic induction in the Vancouver Island region (Nienaber et al., 1979); numerical and analogue model results for electromagnetic induction for an island situated near a coastline (Ramaswamy et al., 1975); and an electromagnetic scale model study of the Rhine Graben anomaly (Ramaswamy et al., 1983).

2.2 TWO-DIMENSIONAL MODEL.

2.2.1 MAXWELL'S EQUATIONS

Maxwell's equations which describe electromagnetic theory express the relationship between the vectors of the electromagnetic field. The equations are as follows

$$\text{CURL } \underline{E} = -\frac{\partial \underline{B}}{\partial t} \qquad \ldots\ldots\ldots\ldots\ldots\ldots (2.1)$$

$$\text{CURL } \underline{H} = \underline{J} + \frac{\partial \underline{D}}{\partial t} \qquad \ldots\ldots\ldots\ldots\ldots\ldots (2.2)$$

$$\text{DIV } \underline{D} = \rho \qquad \ldots\ldots\ldots\ldots\ldots\ldots (2.3)$$

$$\text{DIV } \underline{B} = 0 \qquad \ldots\ldots\ldots\ldots\ldots\ldots (2.4)$$

together with

$$\underline{J} = \sigma \underline{E} \qquad \ldots\ldots\ldots\ldots\ldots\ldots (2.5)$$

$$\underline{D} = \varepsilon \underline{E} \qquad \ldots\ldots\ldots\ldots\ldots\ldots (2.6)$$

$$\underline{B} = \mu_0 \underline{H} \qquad \ldots\ldots\ldots\ldots\ldots\ldots (2.7)$$

where; $\underline{E}$ is electric field strength, $\underline{B}$ is magnetic induction, $\underline{H}$ is magnetic field strength, $\underline{D}$ is electric displacement, $\underline{J}$ is current density, ρ is charge density and μ_0 is permeability constant. In general $\underline{B} = \mu \underline{H}$; $\mu = \mu_0$ only for non-magnetic materials. In m-v theory we generally ignore the few parts of the earth that have μ slightly different from μ_0. All quantities are measured in MKS units.

As an example of the application of these equations (Jones and Price, 1970), let us consider a two-dimensional model with a vertical contact that

separates region 1 (resistive block) having conductivity σ_1, from region 2 (conductive block) having conductivity σ_2 (see figure 2.1).

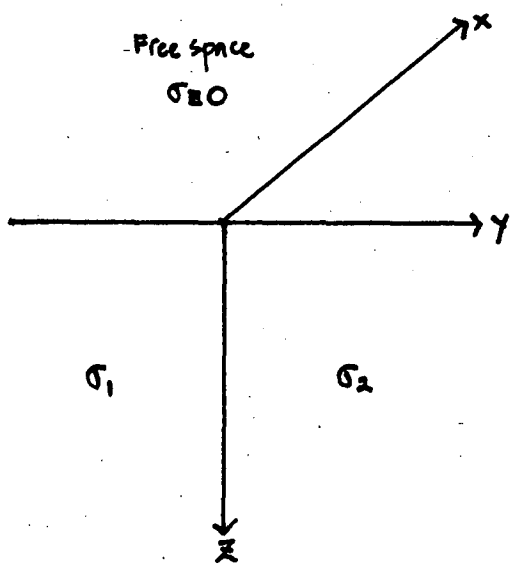

Fig. 2.1 Vertical contact model
and co-ordinate system.

In the following treatment the conductivity $\sigma = \sigma(y,z)$ and all quantities are constant in the x direction, i.e. $\frac{\partial}{\partial x} = 0$. The fields oscillate harmonically as a function of time. It is normally assumed that the oscillation of the fields is very slow thus permitting the

displacement current $\frac{\partial \underline{D}}{\partial t}$, in the right hand side of equation (2.2), to be ignored. Conditions under which this is valid have been specified by Price (1973). The equation (2.2) thus becomes

$$\nabla \times \underline{H} = \sigma(y,z)\ \underline{E} \qquad \ldots\ldots\ldots\ (2.8)$$

using the vector operator, $\nabla = \frac{\partial}{\partial x}\hat{i} + \frac{\partial}{\partial y}\hat{j} + \frac{\partial}{\partial z}\hat{k}$ ..... (2.8′)

and if $\underline{H} = Hx\,\hat{i} + Hy\,\hat{j} + Hz\,\hat{k}$, we get

$$\nabla \times \underline{H} = \left[\frac{\partial Hz}{\partial y} - \frac{\partial Hy}{\partial z}\right]\hat{i} + \left[\frac{\partial Hx}{\partial z} - \frac{\partial Hz}{\partial x}\right]\hat{j} + \left[\frac{\partial Hy}{\partial x} - \frac{\partial Hx}{\partial y}\right]\hat{k}$$

$$= \sigma(y,z)\ \underline{E} \qquad \ldots\ldots\ldots\ldots (2.9)$$

Since in the two-dimensional model all quantities are independent of the x direction, equation (2.9) reduces to

$$\nabla \times \underline{H} = \left[\frac{\partial Hz}{\partial y} - \frac{\partial Hy}{\partial z}\right]\hat{i} + \left[\frac{\partial Hx}{\partial z}\right]\hat{j} + \left[-\frac{\partial Hx}{\partial y}\right]\hat{k} = \sigma(y,z)\underline{E} \;..\; (2.10)$$

and if $\underline{E} = Ex\,\hat{i} + Ey\,\hat{j} + Ez\,\hat{k}$, then

i.e.

$$\frac{\partial Hz}{\partial y} - \frac{\partial Hy}{\partial z} = \sigma(y,z)Ex \;.\; (2.11)$$

$$\frac{\partial Hx}{\partial z} = \sigma(y,z)Ey \;.\; (2.12)$$

$$-\frac{\partial Hx}{\partial y} = \sigma(y,z)Ez \;.\; (2.13)$$

From (2.1) we also get

$$\nabla \times \underline{E} = -\mu_0 \frac{\partial H}{\partial t} \qquad \ldots\ldots\ldots (2.14)$$

in cartesian coordinates equation (2.14) can be written as

$$\left[\frac{\partial E_z}{\partial y} - \frac{\partial E_y}{\partial z}\right]\hat{i} + \left[\frac{\partial E_x}{\partial z} - \frac{\partial E_z}{\partial x}\right]\hat{j} + \left[\frac{\partial E_y}{\partial x} - \frac{\partial E_x}{\partial y}\right]\hat{k} = -\mu_o \frac{\partial H}{\partial t} \quad .. (2.15)$$

assume for wave solution $H = Ho\, e^{jwt}$ ..... (2.16)

substitute (2.16) into (2.15) then

$$\left[\frac{\partial E_z}{\partial y} - \frac{\partial E_y}{\partial z}\right]\hat{i} + \left[\frac{\partial E_x}{\partial z}\right]\hat{j} + \left[-\frac{\partial E_x}{\partial y}\right]\hat{k} = -j\,\mu_o w\, H \quad ..... (2.17)$$

i.e.

$$\frac{\partial E_z}{\partial y} - \frac{\partial E_y}{\partial z} = -j\,\mu_o w\, Hx \quad ..... (2.18)$$

$$\frac{\partial E_x}{\partial z} = -j\,\mu_o w\, Hy \quad ..... (2.19)$$

$$-\frac{\partial E_x}{\partial y} = -j\,\mu_o w\, Hz \quad .... (2.20)$$

The equations (2.11), (2.19) and (2.20) contain only Ex, Hy and Hz. They can be considered apart from equations (2.12), (2.13), (2.18), and describe a condition known as E-polarization, i.e. electric field parallel to the strike direction. Similarly, equations (2.12) ,(2.13) and (2.18) contain only Hx, Ey and Ez and describe a condition known as H-polarization, i.e. magnetic field parallel to the strike direction. By eliminating Hz and Hy from equation (2.11) by using equations (2.19) and (2.20) the E-polarization equations can be written as

$$\frac{\partial^2 E_x}{\partial y^2} + \frac{\partial^2 E_x}{\partial z^2} = j\,\mu_o w\,\sigma(y,z)\,Ex \quad ..... (2.21)$$

or

$$\frac{\partial^2 E_x}{\partial y^2} + \frac{\partial^2 E_x}{\partial z^2} - j\,\eta^2\,Ex = 0 \quad ..... (2.22)$$

where $\eta^2 = \mu_0 w \sigma(y,z)$ is the propagation constant.

Similarly by eliminating Ez and Ey from equation (2.18) by using equations (2.12) and (2.13) the H-polarization can be written as

$$\frac{\partial^2 Hx}{\partial y^2} + \frac{\partial^2 Hx}{\partial z^2} = j \mu_0 w \sigma(y,z)\, Hx \quad \ldots\ldots (2.23)$$

or

$$\frac{\partial^2 Hx}{\partial y^2} + \frac{\partial^2 Hx}{\partial z^2} - j \eta^2 Hx = 0 \quad \ldots\ldots (2.24)$$

If we take $F = Hx$ or Ex, equations (2.22) and (2.24) now become

$$\frac{\partial^2 F}{\partial y^2} + \frac{\partial^2 F}{\partial z^2} - j \eta^2 F = 0 \quad \ldots\ldots (2.25)$$

this equation is known as the diffusion equation (Patra and Mallick, 1980, p. 254).

Equations (2.22) and (2.24) can be solved separately, depending on which case is considered, by inserting the appropriate value of σ in each region and suitable boundary conditions.

2.2.2. BOUNDARY CONDITIONS

The general boundary condition for E- and H-polarizations which were outlined by Jones and Price (1970) are as follows;

a. All components of $\underline{H}$ are continuous.

b. The tangential components of $\underline{E}$ are continuous.

c. The normal component of $\underline{J}$ must be continuous across the interface between two different conductivities, i.e. at y = 0.

d. The normal component of $\underline{J}$ = 0 across z = 0 , therefore, Ez (inside the conductor) equals zero, at z = 0.

Let us consider first the case of E-polarization. For E-polarization the field components that are considered are Ex , Hy and Hz .

At very large positive values of z, i.e. at great depth, the field Ex will be zero, thus as z approaches infinity Ex = Hy = Hz = 0.

For large positive or negative values of y the field approaches that for a one-dimensional structure. ~~It can be seen from equation (2.20) that~~ For this reason $\frac{\partial E}{\partial y}$ approaches zero as y approaches $\pm$ infinity, provided the primary field is uniform.

Equation (2.21) then reduces to

$$\frac{\partial^2 E_x}{\partial z^2} = j \mu_o w \sigma(y,z)\, Ex \qquad \ldots\ldots\ldots (2.26)$$

or

$$\frac{\partial^2 E_x}{\partial z^2} = j \eta^2 Ex \qquad \ldots\ldots\ldots (2.27)$$

where $\eta^2 = \mu_o w \sigma$ ..... (2.28)

The solution for equation (2.27) is of the form,

$$Ex = Eo\, e^{-\sqrt{j}\,\eta z} \qquad \ldots\ldots\ldots (2.29)$$

if $\eta \neq 0$

Define constant electric fields E1 and E2 and also η_1 and η_2 for different σ i.e. σ_1 and σ_2 , so that

as , $y \longrightarrow -\infty$, $Ex = E1\, e^{-\sqrt{j}\,\eta_1 z}$ ..... (2.30)

and as, $y \longrightarrow +\infty$, $Ex = E2\, e^{-\sqrt{j}\,\eta_2 z}$ ..... (2.31)

with $Ex = E1$ or $E2$ at $z = 0$.

In the non-conducting region, i.e. at $z < 0$, where $\sigma \equiv 0$, equation (2.21) can immediately be written as

$$\frac{\partial^2 Ex}{\partial y^2} + \frac{\partial^2 Ex}{\partial z^2} = 0 \qquad \text{..... (2.32)}$$

From equation (2.11) we have $\frac{\partial Hy}{\partial z} = 0$, as y approaches $\pm$ infinity, for $H_z = 0$ in a one-dimensional model. Then for large y values, Hy must be a constant (say Ho) w.r.t. $z < 0$, i.e. $Hy = Ho$. From equations (2.19) and (2.29) we also have that for $z > 0$,

$$\frac{\partial}{\partial z} Eo\, e^{-\sqrt{j}\,\eta z} = -j\,\mu_o\, w\, Hy \qquad \text{..... (2.33)}$$

i.e. $$-\sqrt{j}\,\eta\, Eo\, e^{-\sqrt{j}\,\eta z} = -j\,\mu_o\, w\, Hy \qquad \text{..... (2.34)}$$

$$-\sqrt{j}\,\eta\, Eo = -j\,\mu_o\, w\, Hy \quad , \text{at } z = 0, \qquad \text{..... (2.35)}$$

Equation (2.19) thus can be written, at $z = 0$, as

$$\frac{\partial Ex}{\partial z} = -j\,\mu_o\, w\, Hy = -\sqrt{j}\,\eta\, Eo \qquad \text{..... (2.36)}$$

And because Hy is constant with respect to z for large $|y|$ this applies throughout $z < 0$. Taking the integral

$$Ex = - \int \sqrt{j}\, \eta\, Eo\, dz \qquad \ldots\ldots\ldots (2.37)$$

$$Ex = Eo - \sqrt{j}\, \eta\, Eo\, z \qquad \ldots\ldots (2.38)$$

and taking constant electric fields E1 and E2 and η_1 and η_2 for different values of σ then

at $y \longrightarrow -\infty$, $Ex = E1 (1 - \sqrt{j}\, \eta_1 z)$ $\ldots\ldots (2.39)$

and at $y \longrightarrow +\infty$, $Ex = E2 (1 - \sqrt{j}\, \eta_2 z)$ $\ldots\ldots (2.40)$

Another boundary condition for E-polarization is that the field components of Ex , Hy , and Hz are continuous across the vertical contact, i.e. at $y = 0$ and $z = 0$.

To complete the necessary boundary conditions for the E-polarization case Jones and Price (1970) took for Ex a linear interpolation between the asymptotic values given by equations (2.39) and (2.40) at some great height, i.e. at $z = - h$. Others have taken more elaborate boundary conditions, e.g. Brewitt-Taylor and Weaver (1976).

Figure 2.2 shows diagramatically the boundary conditions for E-polarization.

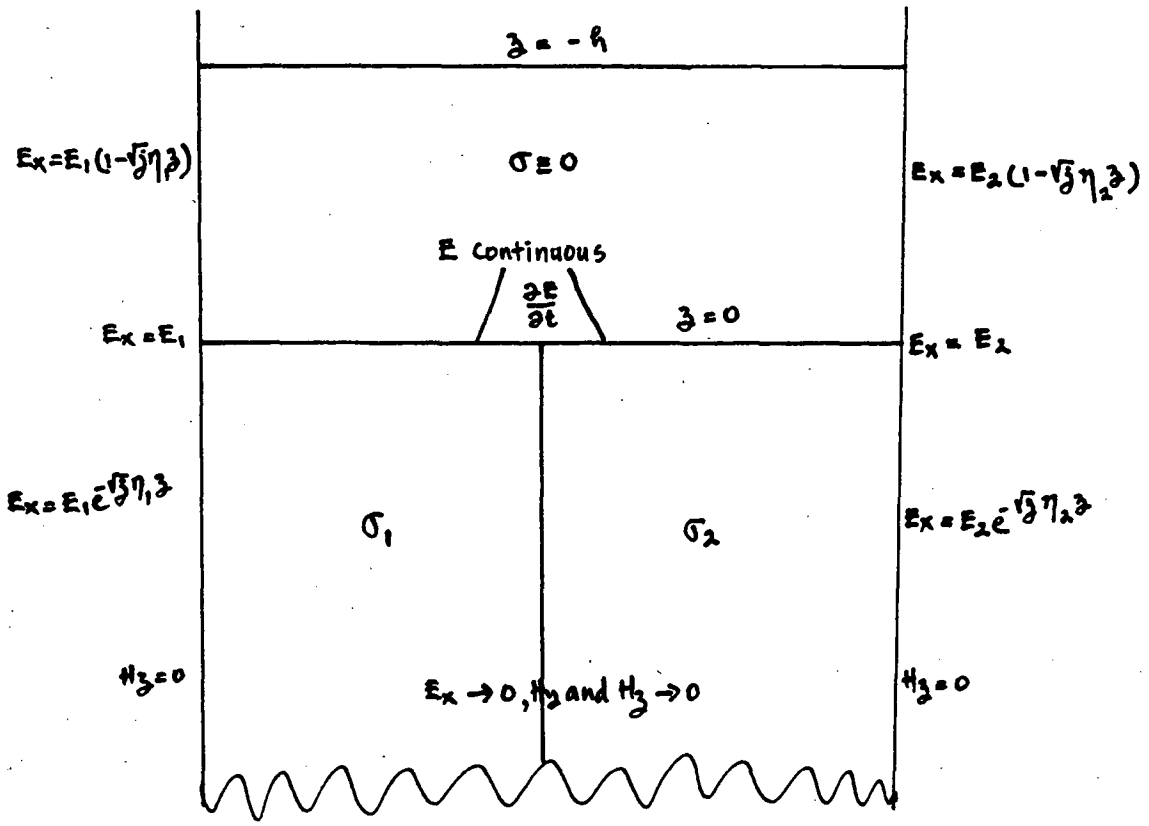

Fig. 2.2. Boundary conditions for E-polarization.

Consider now the case for H-polarization. In the region outside the conductor, i.e. at $z < 0$ where $\sigma \equiv 0$, equations (2.12) and (2.13) show that Hx is independent of y and z, therefore Hx is constant throughout this region. Because Hx is continuous, it is the same constant at $z = 0$, i.e. just below the surface.

At large positive values of z, i.e. at great depth, the field Hx is assumed to be zero. It is also assumed that $\frac{\partial}{\partial y}$ is equal to zero as y approaches ± infinity. Equation (2.23) then reduces to

$$\frac{\partial^2 Hx}{\partial z^2} = j \mu_0 w \sigma (y,z) Hx \qquad \ldots\ldots (2.41)$$

or

$$\frac{\partial^2 Hx}{\partial z^2} = j \eta^2 Hx \qquad \ldots\ldots (2.42)$$

where $\eta^2 = (\mu_0 w \sigma)$, and $y \longrightarrow \pm \infty$

The appropriate solution of equations (2.41) and (2.42) is then of the form

$$Hx = Ho\, e^{-\sqrt{j}\,\eta\, z} \qquad \ldots\ldots\ldots (2.43)$$

Taking η_1 and η_2 for different σ values, so that at

$$y \longrightarrow -\infty \quad , \; Hx = H1\, e^{-\sqrt{j}\,\eta_1\, z} \qquad \ldots\ldots\ldots (2.44)$$

and $$y \longrightarrow +\infty \quad , \; Hx = H2\, e^{-\sqrt{j}\,\eta_2\, z} \qquad \ldots\ldots\ldots (2.45)$$

Another boundary condition for the H-polarization is that the field $\underline{H}$ is continuous across the boundary, i.e. at $y = 0$. It can also be seen from equation (2.12) that because the normal current density σ Ey is continuous, then $\frac{\partial Hx}{\partial z}$ is also continuous.

The boundary conditions for Hx in the case of H-polarization are thus complete, $Hx \longrightarrow 0$, as $z \longrightarrow \infty$, Hx is given by equations (2.44) and (2.45) at the left and right hand edges of the model and $Hx = Ho$ for all $z < 0$.

Figure 2.3 shows diagramatically the boundary conditions for H-polarization.

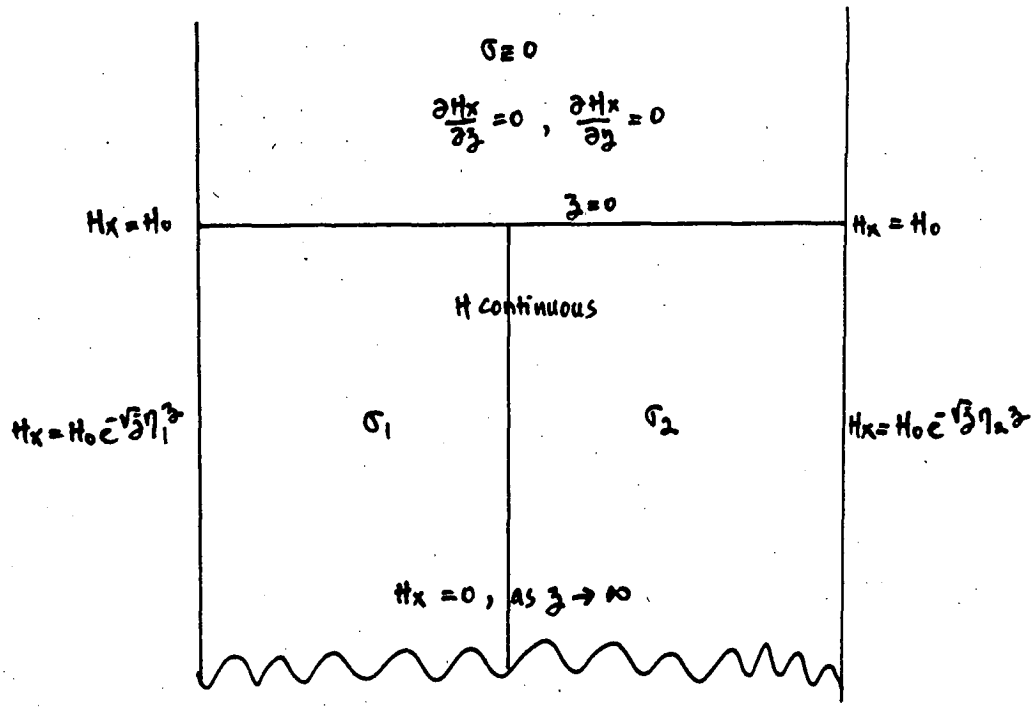

Fig. 2.3. Boundary conditions for H-polarization.

The model discussed here (two quarter-spaces) is comparatively simple, but it shows the principle of boundary conditions as applied to most two-dimensional modelling. If the structures at the left and right hand boundaries are stratified, then in place of equations (2.30), (2.31), (2.44) and (2.45) a one-dimensional solution, such as that of Schmucker (1970), must be used.

CHAPTER 3

EQUIPMENT AND PROCEDURES

The m-v observations conducted by the author were made at 32 temporary magnetograph sites. Figures 3.1 and 3.2 show the location and distribution of the observation sites, and table 1 lists the sites together with their geographical coordinates.

Two three-component EDA FM100 B fluxgate magnetometers were employed during these observations to record geomagnetic variations. The main components of the magnetometers are a sensor head containing a three-component fluxgate magnetometer, a multiplexer, an analog-to-digital converter (A/D), channel switch, tape drive, DC-DC inverter, battery, solar panel and cable. Except for the sensor head, battery, solar panel and cable which are separate the others components are placed together in a watertight box (see figures 3.3 and 3.4). The magnetometers were modified at the Geology Department University of Tasmania to interface to a Memodyne digital cassette recorder. One of the magnetometers is fitted with four telluric channels for magneto-telluric observations. Both magnetometers have several advantages over those used by previous observers. The magnetometers now record digitally to allow more data to be processed quickly and give correspondingly more accurate results. Two temperature sensors have also been fitted to the two magnetometers and the sensor heads to allow better temperature corrections to be made and to avoid the necessity of burying the detectors, although they are still temperature-dependent. Since experience shows that the equipment has very good peformance no calibrations were done. Instead the calibrations of Sayers (1984) and Buyung (1980) were used. These workers obtained calibrations very close to those specified by the manufacturer. Temperature calibration, on the other hand, was carried out at Lauderdale (east of Hobart) to determine the temperature coefficients of both the sensor head and control circuits of both magnetometers. Although the experiment was not completely successful, because the field variations were contaminated by an artificial source, satisfactory temperature coefficients were

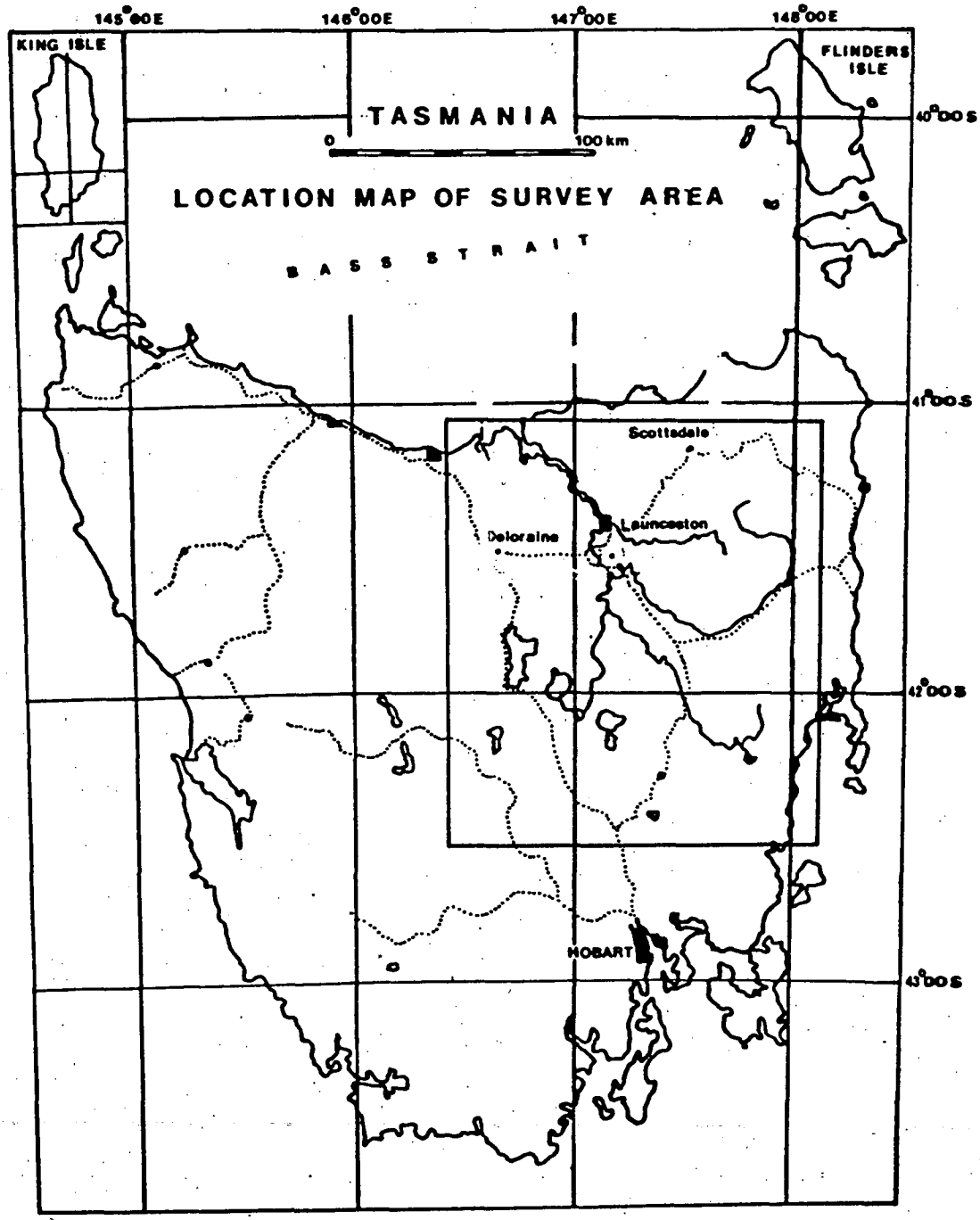

Fig. 3.1 Location map

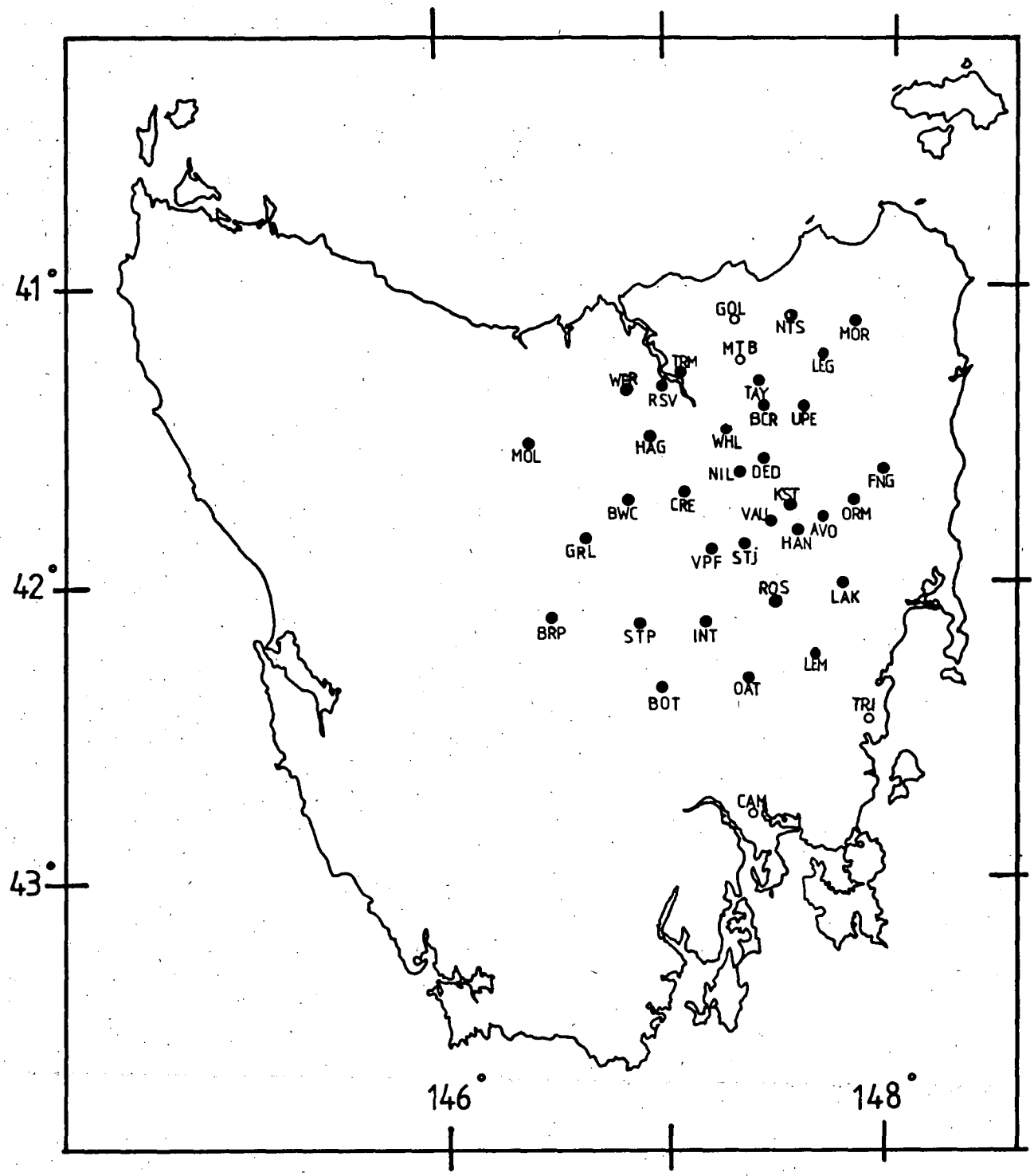

Fig. 3.2 Distribution of m-v stations

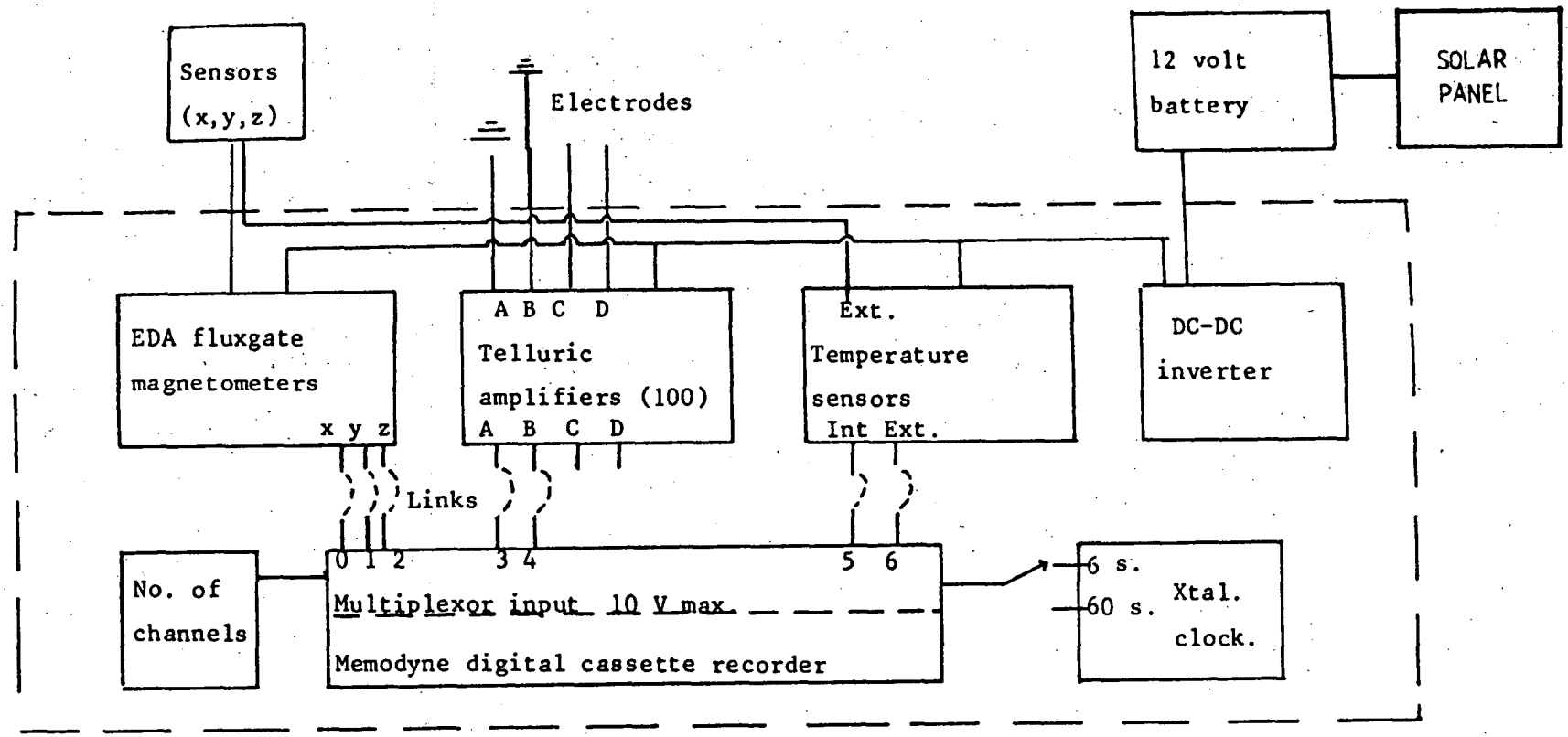

Fig. 3.3 Functional units of field equipment. All components inside dashed line are enclosed in a single watertight box.

(From Bindoff, 1983).

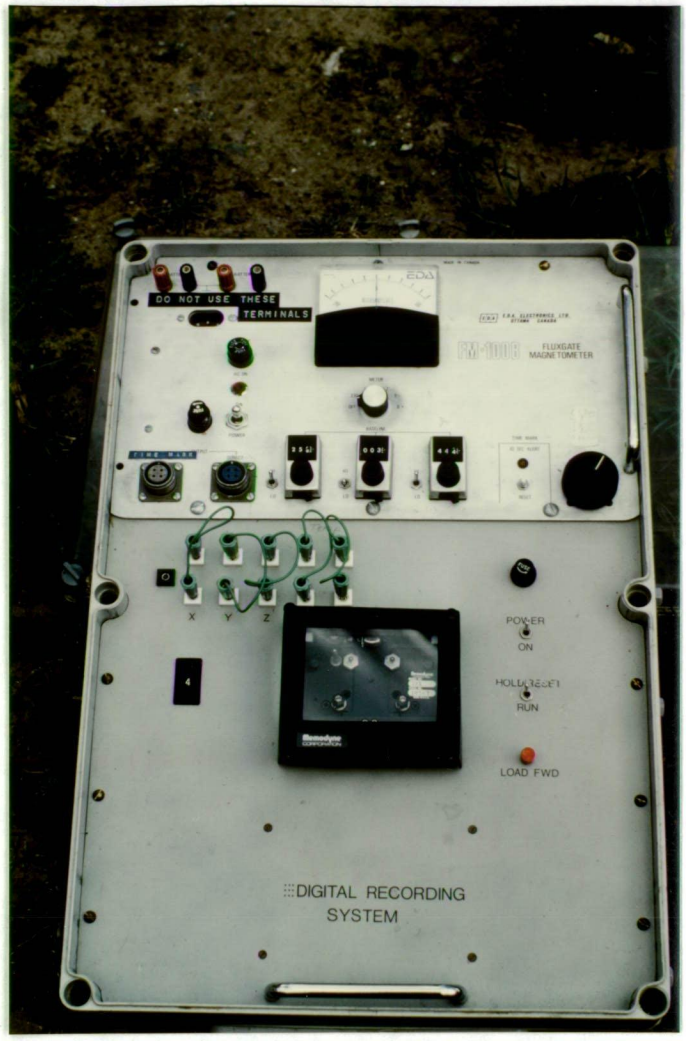

Fig. 3.4a EDA FM100B fluxgate magnetometer.

Fig. 3.4b Sensor head.

determined. The temperature corrections are usually made to the data in the first analysis (program EMMTEE 1).

In practice both of the magnetometers were operated at 30 seconds reading interval. Only at Ross (ROS) the magnetometer was set at 6 seconds reading rate. During the observations most of the sites were occupied for about 2 weeks.

TABLE 1

List of stations and geographic coordinates.

NO	STATIONS	CODE	LONGITUDE	LATITUDE
1.	WHITE HILLS	WHL	147° 14′ 52"	41° 29′ 27"
2.	BURNS CREEK	BCR	28′ 00	26′ 29"
3.	UPPER ESK	UPE	42′ 36"	25′ 57"
4.	HANLETH	HAN	36′ 18"	50′ 55"
5.	AVOCA	AVO	41′ 54"	46′ 28"
6.	ORMLEY	ORM	47′ 51"	43′ 05"
7.	FINGAL	FNG	56′ 15"	36′ 45"
8.	ST.JOHNSON	STJ	24′ 30"	51′ 03"
9.	VIEW POINT FARM	FRM	13′ 28"	53′ 13"
10.	VAUCLUSE	VAU	26′ 15"	45′ 47"
11.	KINGSTON	KNG	34′ 12"	42′ 41"
12.	TAYENE	TAY	26′ 36"	20′ 55"
13.	TURNERS MARSH	TRM	06′ 39"	16′ 44"
14.	ROSEVEAR	RSV	01′ 03"	19′ 26"
15.	CRESSY	CRE	07′ 42"	11′ 48"
16.	LEGERWOOD	LEG	41′ 38"	11′ 13"
17.	NILE	NIL	18′ 15"	37′ 26"
18.	DEDINGTON	DED	23′ 28"	36′ 00"
19.	MOORINA	MOR	49′ 14"	05′ 56"
20.	INTERLAKEN	INT	10′ 51"	42° 08′ 22"
21.	BOTHWELL	BOT	00′ 00"	20′ 00"
22.	LEMONT	LEM	13′ 18"	11′ 37"
23.	LAKE LEAKE	LAK	41′ 55"	00′ 00"
24.	ROSENEATH	ROS	57′ 55"	02′ 16"
25.	OATLANDS	OAT	22′ 00"	17′ 56"
26.	HAGLEY	HAG	146° 54′ 51"	41° 30′ 32"
27.	MOLE CREEK	MOL	25′ 27"	32′ 42"
28.	WEST FRANKFORD	WFR	07′ 42"	11′ 48"
29.	BLACKWOOD CREEK	BCR	55′ 25"	42′ 58"

30.	GREAT LAKE	GRL		40′	50"		50′ 08"
31.	STEPPES	STP		56′	07"	42°	05′ 20"
32.	BRONTE PARK	BRP		30′	00"		06′ 29"
33.	GOLCONDA	GOL	147°	17′	00"	41°	12′ 00"
34.	MYRTLE BANK	MTB		21′	00"		18′ 00"
35.	NORTH SCOTTSDALE	NTS		32′	00"		07′ 00"

CHAPTER 4

DATA REDUCTION AND ANALYSIS

4.1 INTRODUCTION

Several steps in the analysis of the data were carried out on the Geology Department's Interdata 7/16 computer before further interpretations were undertaken. The analysis uses three main programs: EMMTEE 1, TASIGMA 1, and TASIGMA 2. The programs which were already available were written by Dr. W.D. Parkinson to match the field format. These programs are given in Appendices 1, 2 and 3.

4.2 STEPS IN THE ANALYSIS

4.2.1 EMMTEE 1

EMMTEE 1 was written to read the recorded geomagnetic variation data from a digital Memodyne cassette and then to display them on a TV screen according to interactive commands. The displays consist of three-components, i.e. X (northward component), Y (eastward component), and Z (upward component), of the geomagnetic field and two temperature variation channels. Typical variations that are of interest in this study are those that are associated with magnetic substorms or similar types of bays with period ranges from several minutes to a few hours. An example of an analogue record of typical variations is shown in figure 4.1. Occasional reading errors occur during play-back. Most of these are automatically corrected by interpolating the mean of the previous and next values for all values that differ from the previous value by more than a predetermined amount. From such displays on the TV screen, between 50 and 100 events were chosen for further analysis. These events contain slightly less than 512, 256, 128, or 64 consecutive readings. For a 30 second reading rate, for example, these numbers correspond to interval periods of approximately 240, 120, 60, and 30 minutes respectively, while for a 6 second reading rate these numbers correspond to periods of approximately 60, 30, 15, and 8

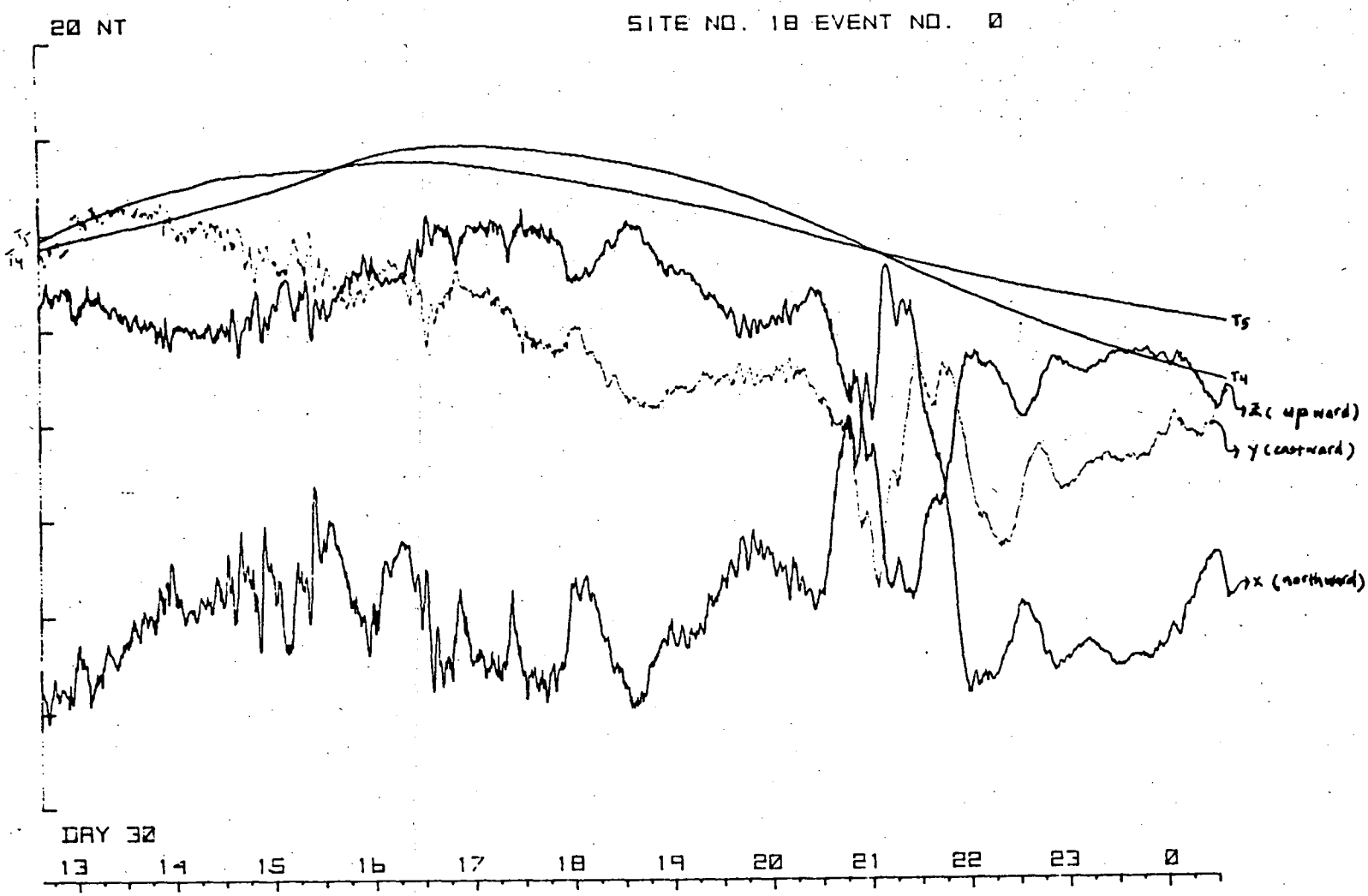

Fig. 4.1 Digital record of typical geomagnetic variations X (northward), Y (eastward) and Z (upward). T4 and T5 are temperature variations.

minutes respectively. Temperature corrections are then applied to the magnetic components for all of the selected events before they are stored on magnetic tape for further analysis.

4.2.2 TASIGMA 1

TASIGMA 1 uses the fast Fourier transform algorithm which converts the time domain data, selected in the first analysis (EMMTEE 1), into the frequency domain. Before transformation linear drift is removed from every event, and the number of data points is padded by zeros up to the next power of 2. Every Fourier coefficient, calculated at various periods, up to the 12th harmonic of the data length, is punched and stored on paper tape.

4.2.3 TASIGMA 2

With the aid of TASIGMA 2 the Fourier transforms for groups of 6 to 10 events of equal length, determined from the second analysis (TASIGMA 1), are used to calculate the transfer functions at each station for various periods. The calculation is based on the least-square method developed by Everett and Hyndman (1967) to obtain the best fit relation between the vertical and horizontal components. Equation (4.1) expresses a linear relationship between the three-components of the geomagnetic field

$$Z = AX + BY \qquad \ldots\ldots\ldots\ldots (4.1)$$

Where Z, X, Y are Fourier transforms of the vertical, north, and east magnetic components and A and B are complex functions of frequency. This relationship is also called a single-site transfer function as it can be calculated from observations at only one site (Gough and Ingham, 1983). The process of calculation consists of choosing A and B to minimize the sum of squared residuals over an ensemble of geomagnetic events. Note that the summations are made over the ensemble of events not over frequency bands. In this way each frequency is treated independently. Some equations used in the calculations are as follows (Parkinson, 1983, pp. 332-333)

$$|\delta j|^2 = (Z - AX - BY) (Z^* - A^*X^* - B^*Y^*) \quad \ldots\ldots (4.2)$$

where δj is the difference between the LHS and RHS of equation (4.1) for the jth event and * denotes the complex conjugate. After differentiating and minimizing $\Sigma|\delta j|^2$ with respect to in-phase and quadrature components of A and B this gives

$$A = \frac{(\Sigma X^*Z \times \Sigma Y^*Y) - (\Sigma Y^*Z \times \Sigma X^*Y)}{(\Sigma X^*X \times \Sigma Y Y^*) - (\Sigma X Y^* \times \Sigma X^*Y)} \quad .. (4.3)$$

and

$$B = \frac{(\Sigma X^*X \times \Sigma Y^*Z) - (\Sigma X Y^* \times \Sigma X^*Z)}{(\Sigma X^*X \times \Sigma Y Y^*) - (\Sigma X Y^* \times \Sigma X^*Y)} \quad .. (4.4)$$

4.3 TRANSFER FUNCTION AND INDUCTION VECTORS ANALYSIS

4.3.1 INTRODUCTION

The A and B transfer functions which were derived from the third analysis (TASIGMA 2) were plotted against periods ranging from 4 to 128 minutes and are shown in figures 4.2 to 4.9. The error bars were determined by calculating the standard error of the mean (i.e. the standard deviation divided by the square root of the number of points calculated) and then adding and substracting this from the median. Since it is clear from the figures that at different locations the trends of the transfer functions exhibit different characteristics and behaviour, it is worthwhile to divide them into three different regions: western, eastern and central. In figure 4.10, these regions, which represent the locations of a group of stations to the west, east and approximately along the Tamar Fracture Zone, are divided by broken lines. The transfer functions, expressed by A and B, can be considered as vectors and hence they will point in a certain direction. In this case A and B have directions of magnetic north and east, for positive amplitudes, and magnetic south and west, for negative amplitudes, respectively. In the following analysis the A and B transfer functions are used to determine the orientation and length of the induction vectors or Parkinson vectors.

The lengths (L) of the in-phase and quadrature vectors, which indicate the ratio of vertical to horizontal components, and their directions (θ), which indicate the horizontal direction which correlates positively with upward vertical change (Parkinson, 1959, 1962, 1964), are determined by

$$Li = \sqrt{Ai^2 + Bi^2} \qquad \ldots\ldots\ldots (4.5)$$

$$\tan \theta = \frac{Bi}{Ai} \qquad \ldots\ldots\ldots (4.6)$$

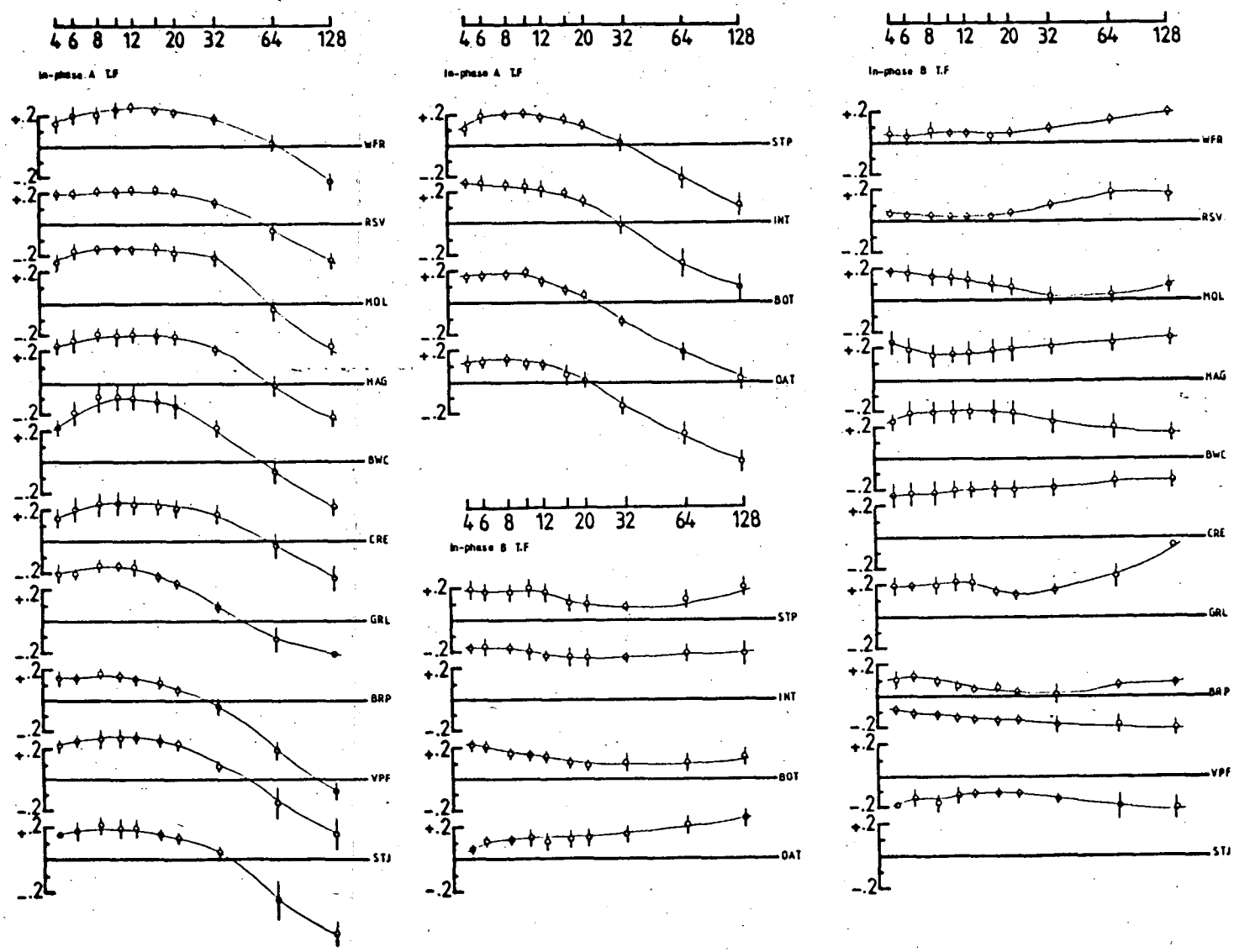

Fig. 4.2 In-phase components of the A and B transfer function in the western region.

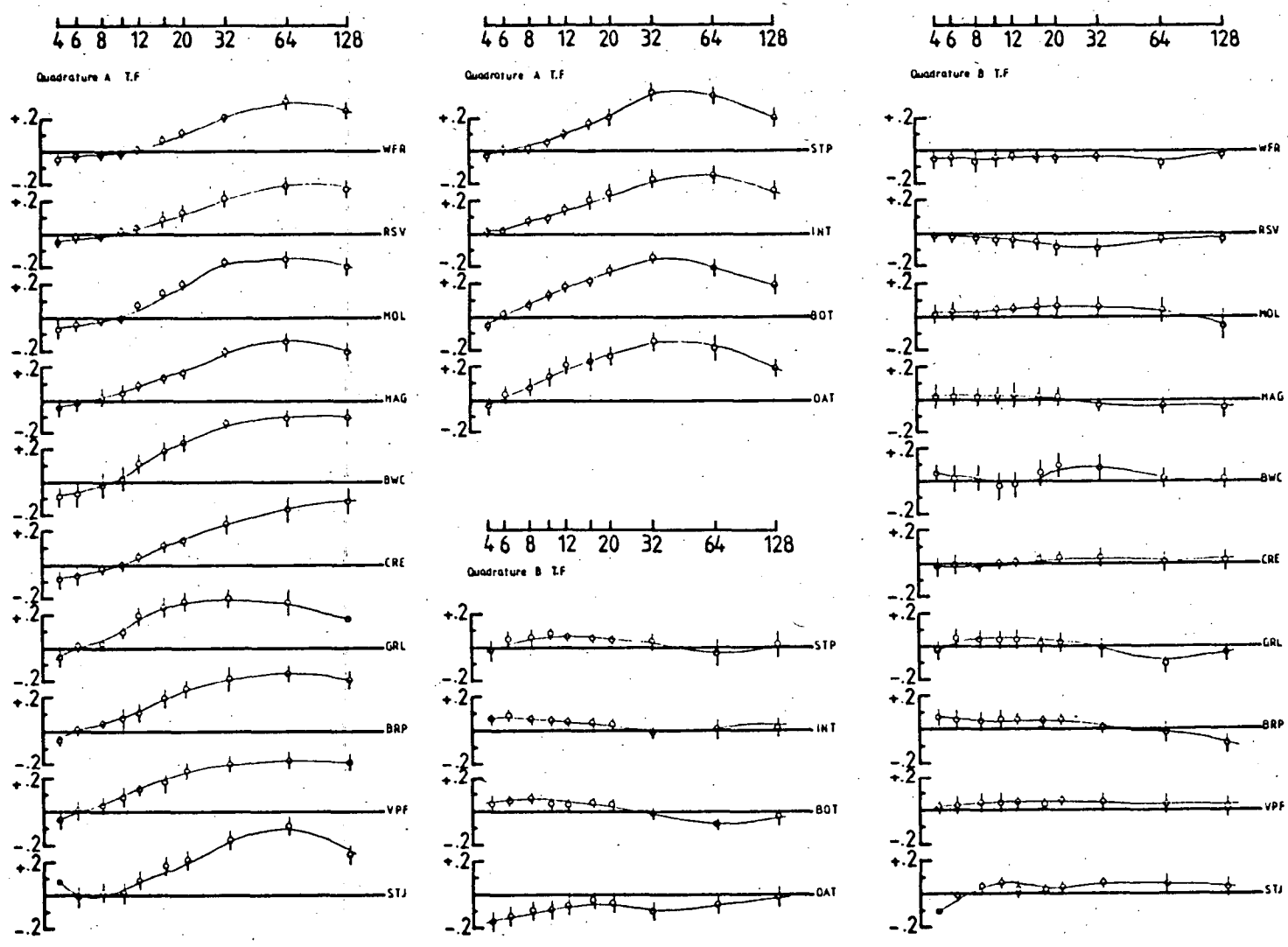

Fig. 4.3 Quadrature components of the A and B transfer function in the western region.

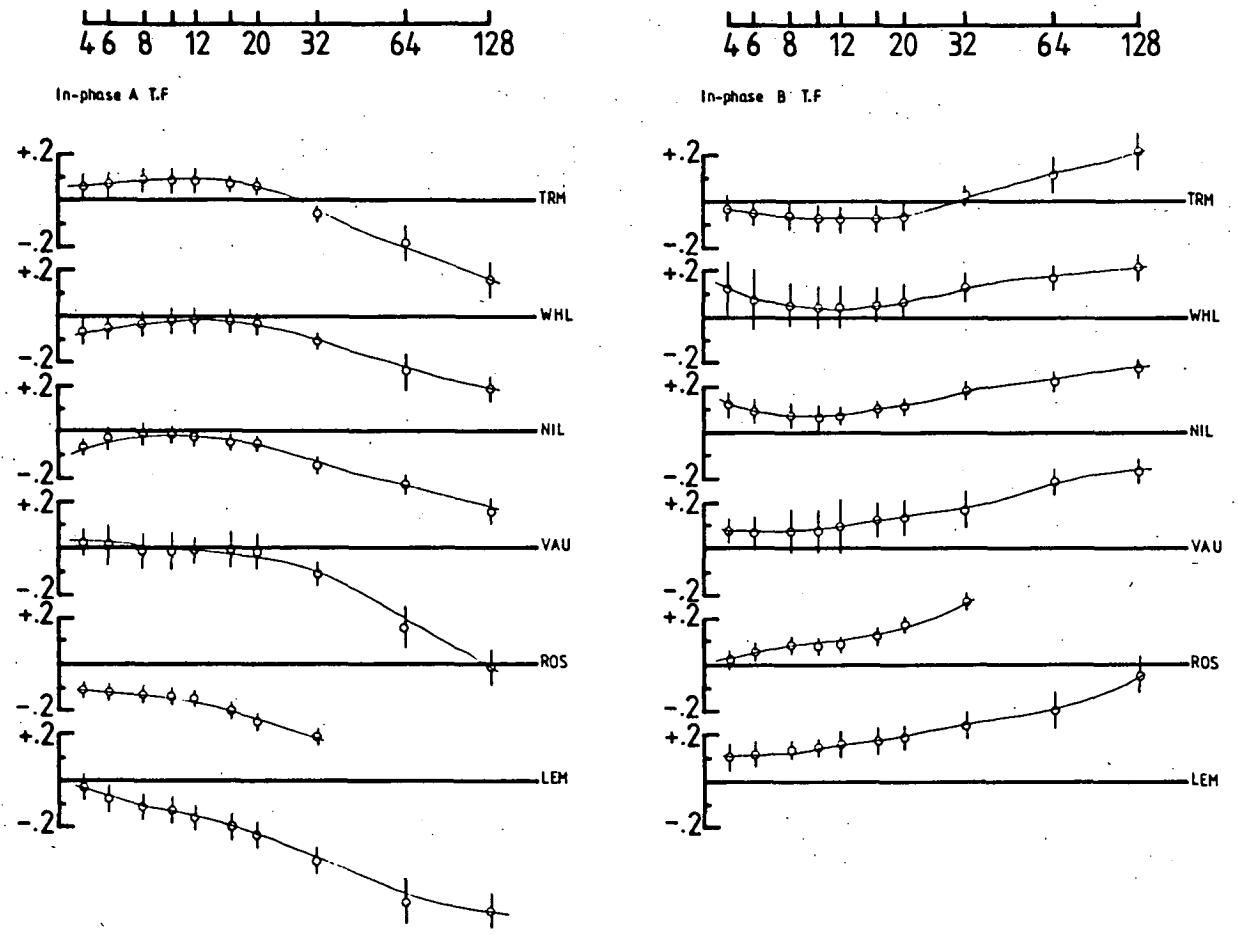

Fig. 4.4 In-phase components of the A and B transfer function in the central region.

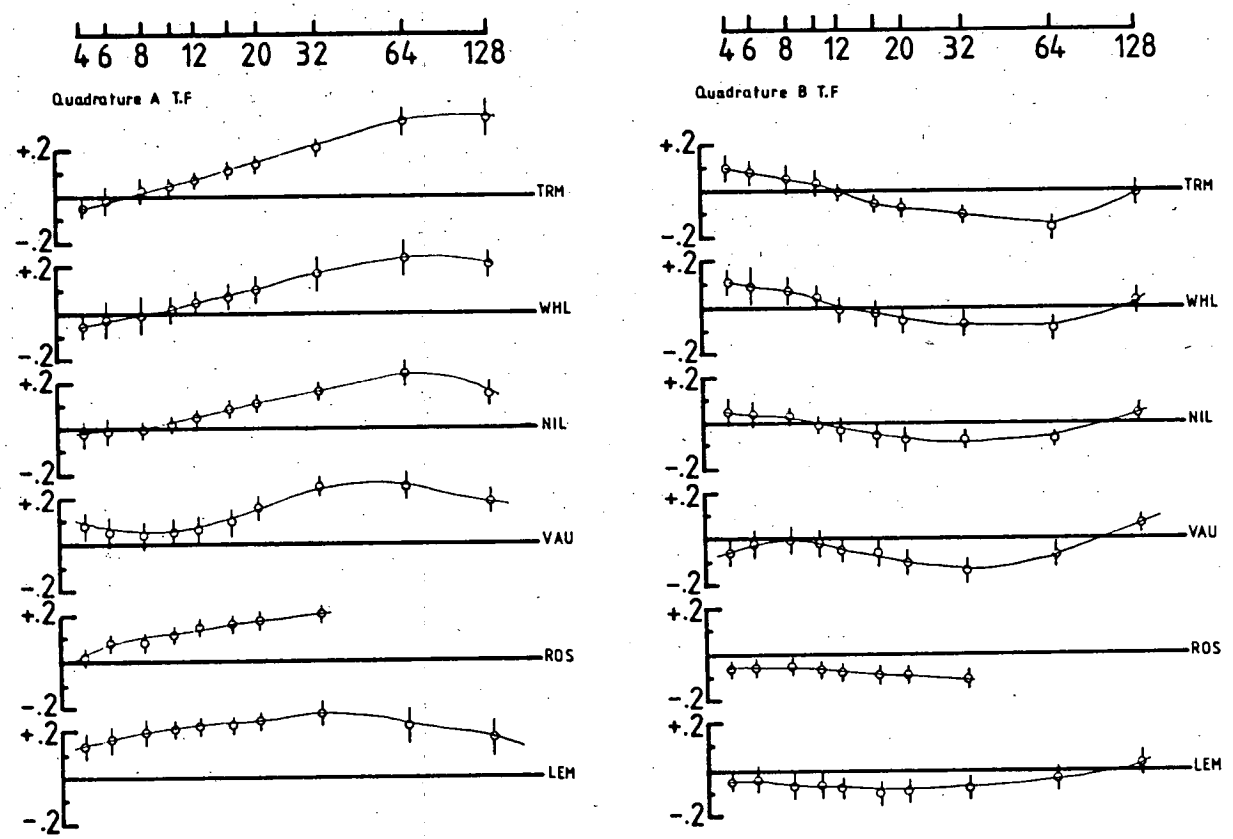

Fig. 4.5 Quadrature components of the A and B transfer function in the central region.

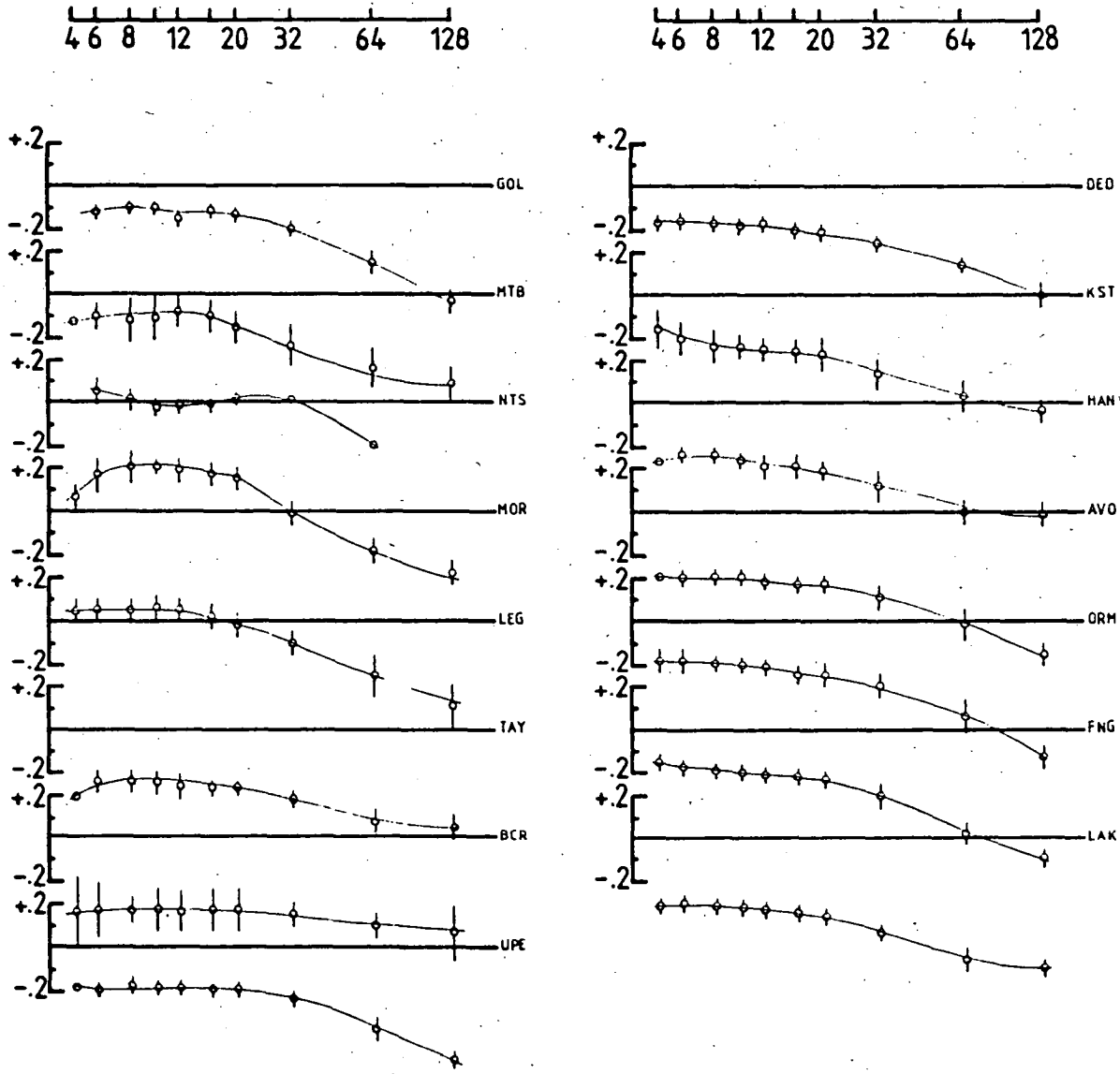

Fig. 4.6 In-phase components of the A transfer function in the eastern region.

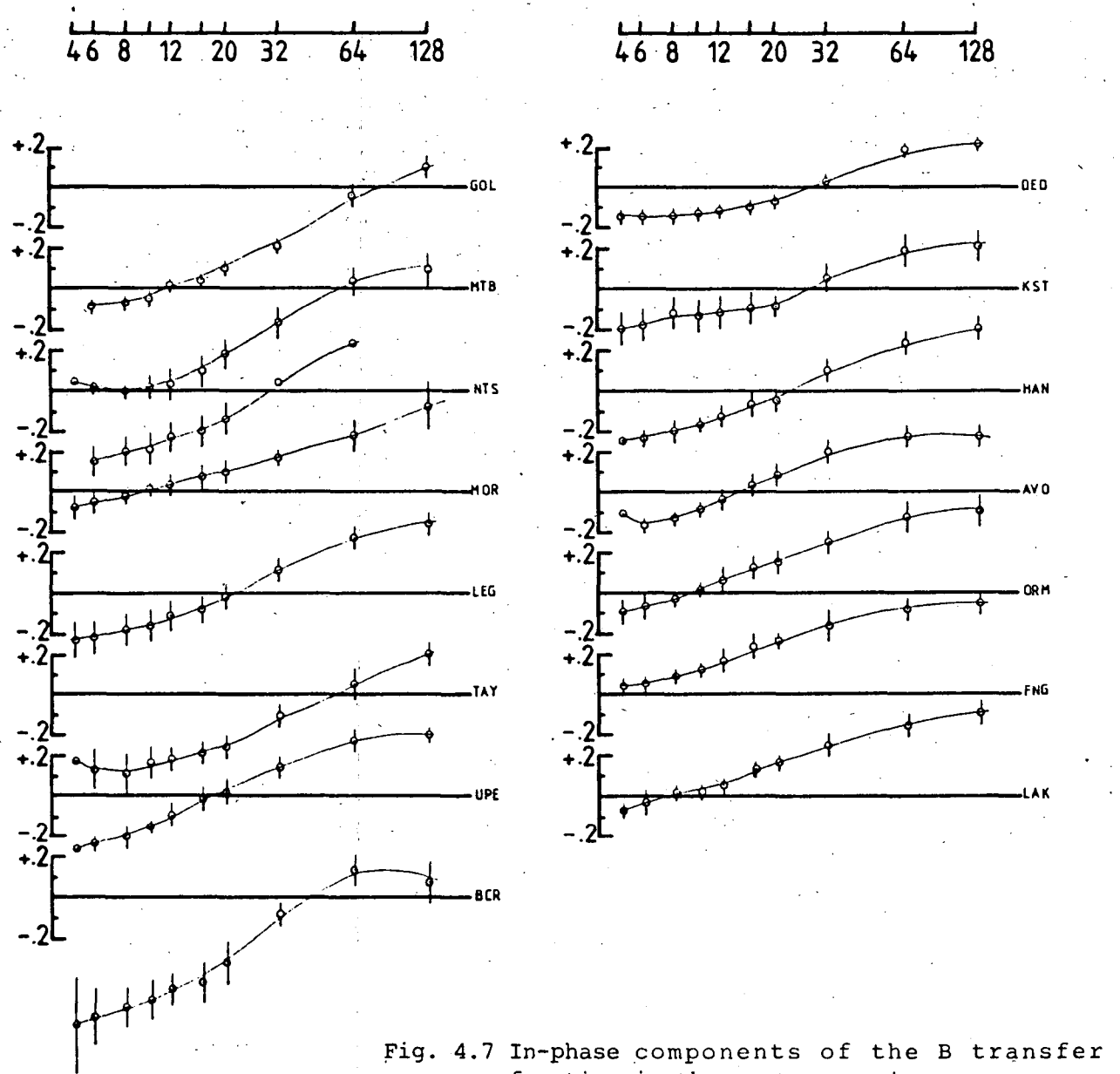

Fig. 4.7 In-phase components of the B transfer function in the eastern region.

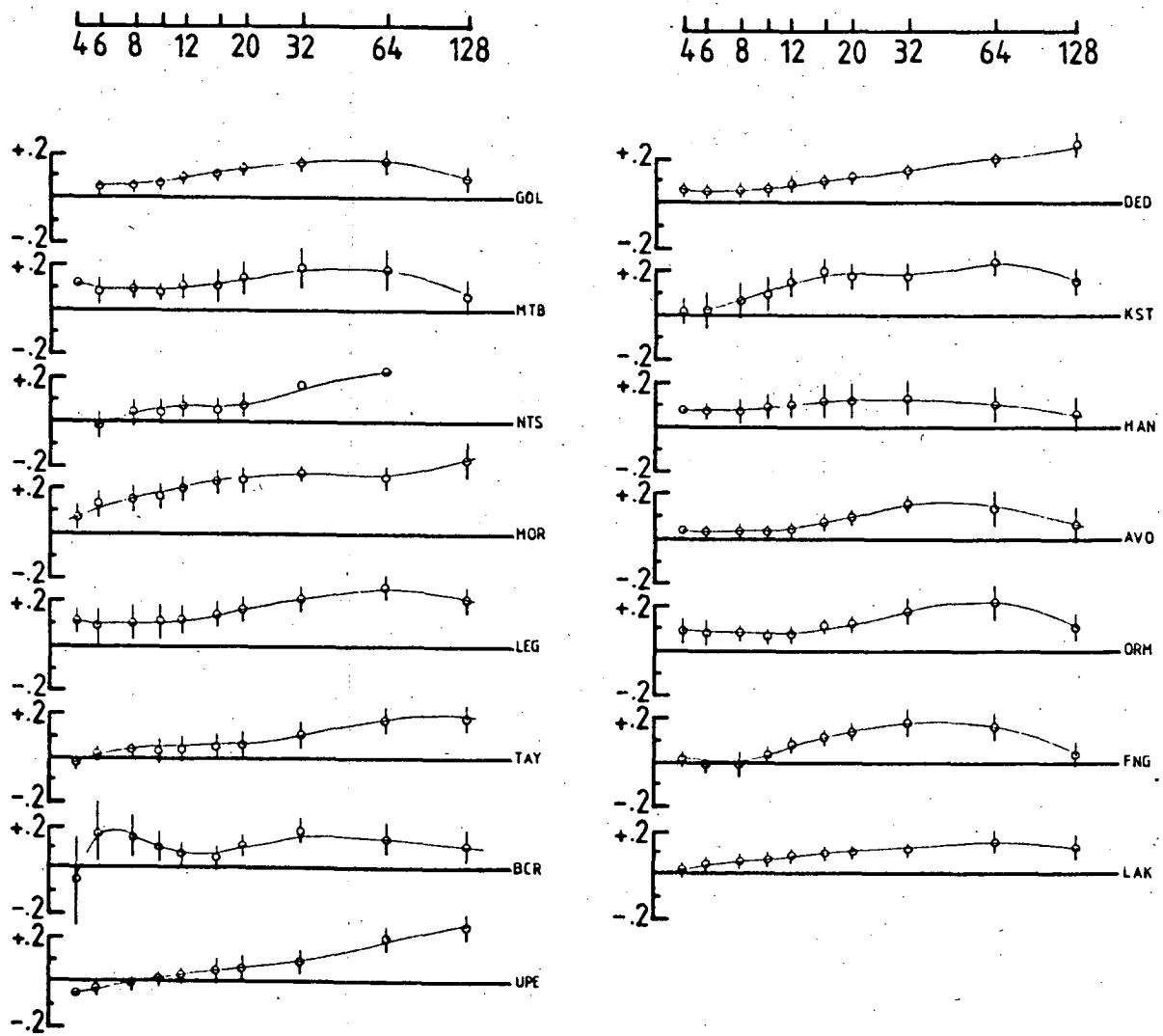

Fig. 4.8 Quadrature components of the A transfer function in the eastern region.

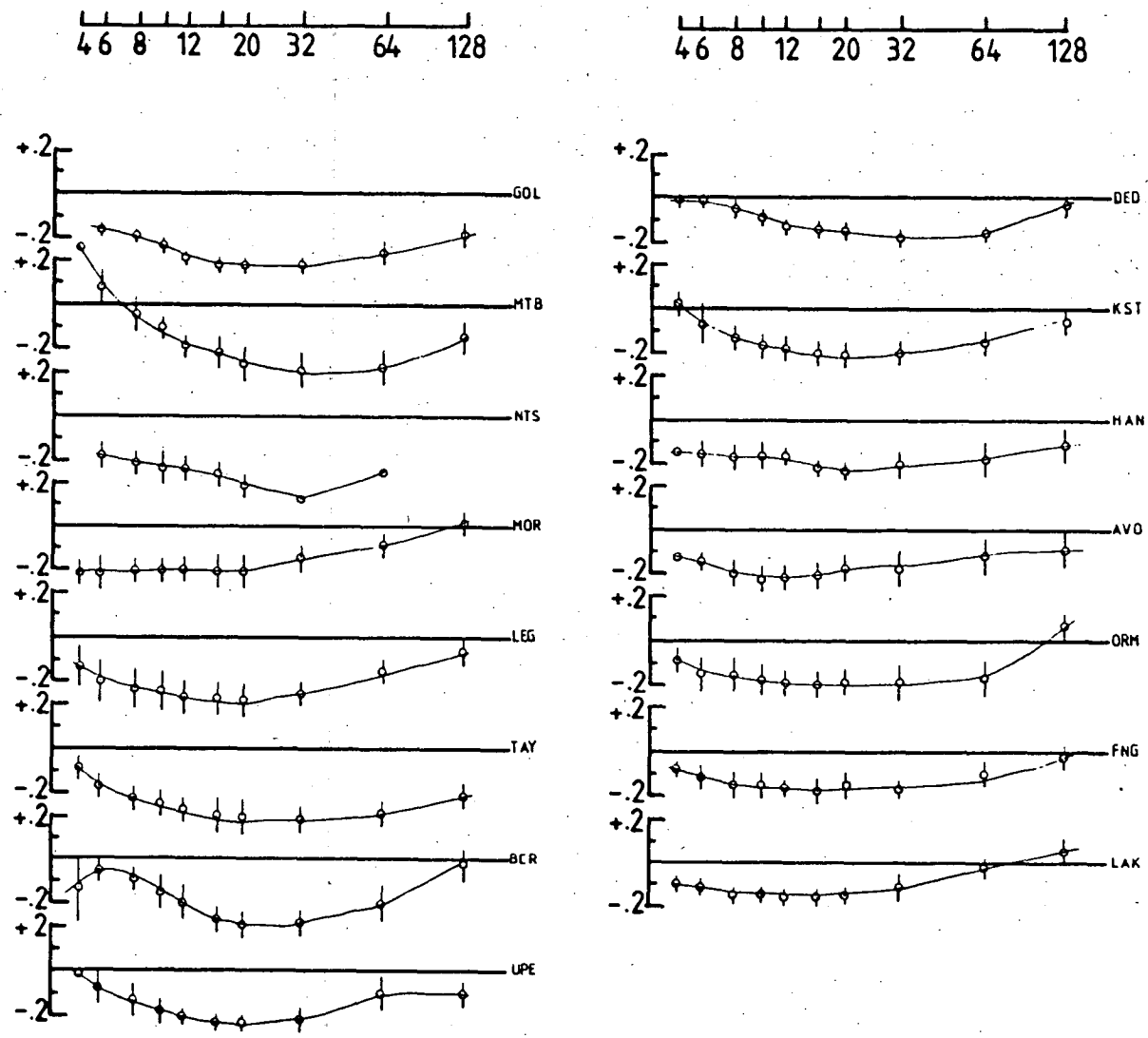

Fig. 4.9 Quadrature components of the B transfer function in the eastern region.

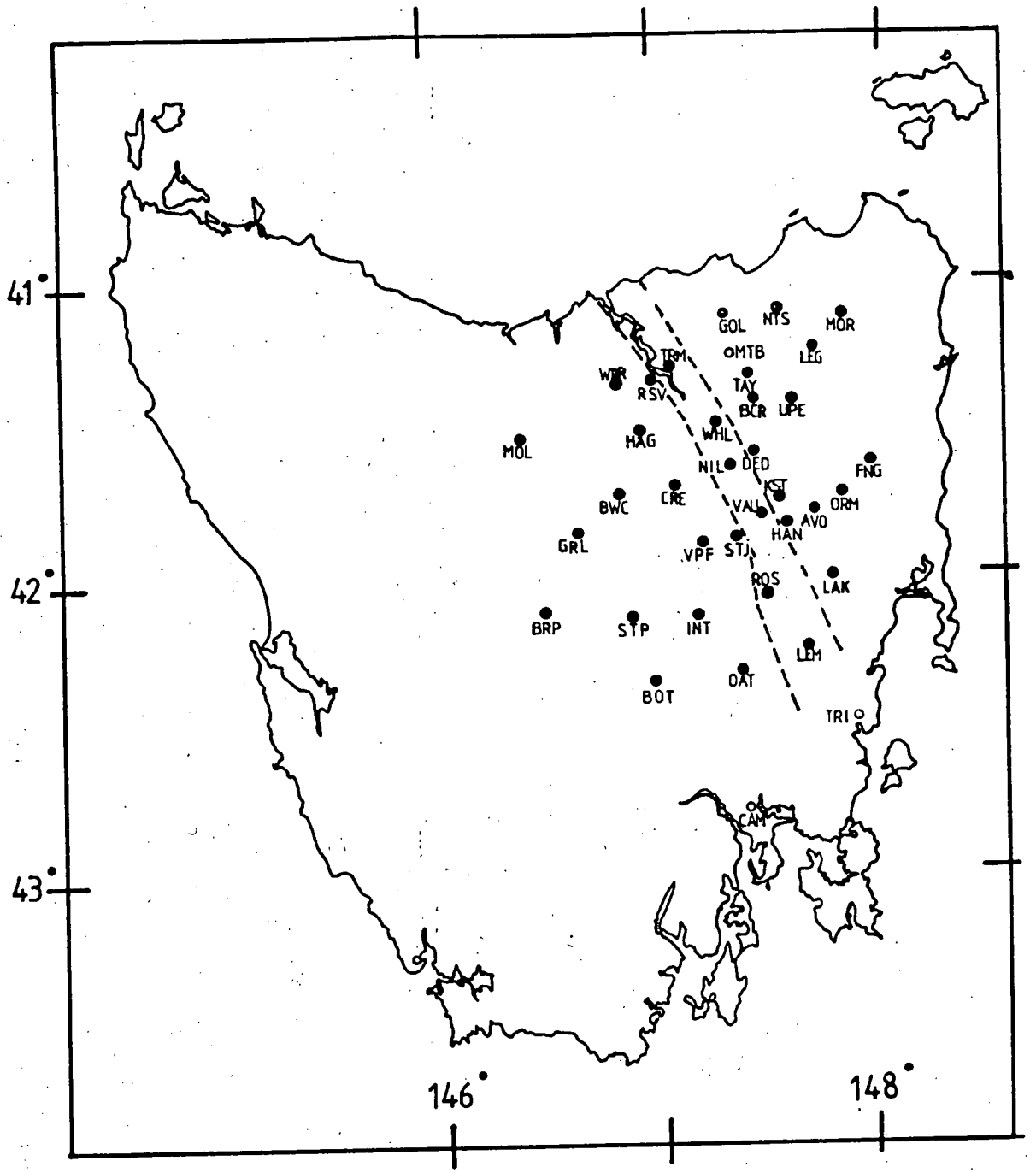

Fig. 4.10 Separation of stations into three different regions.

where subscript i denotes the in-phase component of the induction vectors and θ denotes the angle of the vectors measured clockwise from magnetic north. Similar formulae also apply to the quadrature component simply by changing the subscript i to q which denotes the quadrature. Figures 4.11 to 4.20 show the in-phase and quadrature components of the induction vectors for periods from 4 to 128 minutes. All of the vectors were plotted with respect to true north and, since the magnetic declination in Tasmania is approximately 13° east of north, all of the θ values determined by formula (4.6) have had 13° added so that they are true geographic directions. The in-phase and quadrature components were drawn in solid and broken lines, respectively.

The vectors, which are known as the Parkinson vectors, are normally plotted from the observation stations to point toward a zone of anomalously high conductivity (Parkinson, 1962). Because Z is taken as the upward component of the field, reversal of the direction of the induction arrows is not necessary.

4.3.2 IN-PHASE VECTORS

Generally, the trends of the in-phase vectors can be divided into two different groups, namely the short period induction vectors (< 20 min.) and the long periods induction vectors (> 32 min.). These two groups of vectors are distinguished by different orientations which are clearly shown in figures 4.11 to 4.20. The differences in orientation between these groups imply that they are affected by different anomalies. However, the most remarkable feature of these short period vectors is that the vectors in the western region have different characteristics to those in the eastern region. For example, in the western region all of the vectors point almost to the north-east. In general, the lengths of these vectors tend to increase smoothly with increasing period and appear to be at a maximum at periods between 8 and 12 minutes. The lengths of the vectors appear to decrease gradually at periods greater than 16 minutes but recover and tend to increase again beyond periods of 64 minutes. The ~~signs~~ directions of the vectors tend to change at some of the most southern stations at periods of 32 minutes and become uniformly distributed at periods greater than 64 minutes. This feature can also be seen very clearly from ~~the~~ change of sign of the in-phase

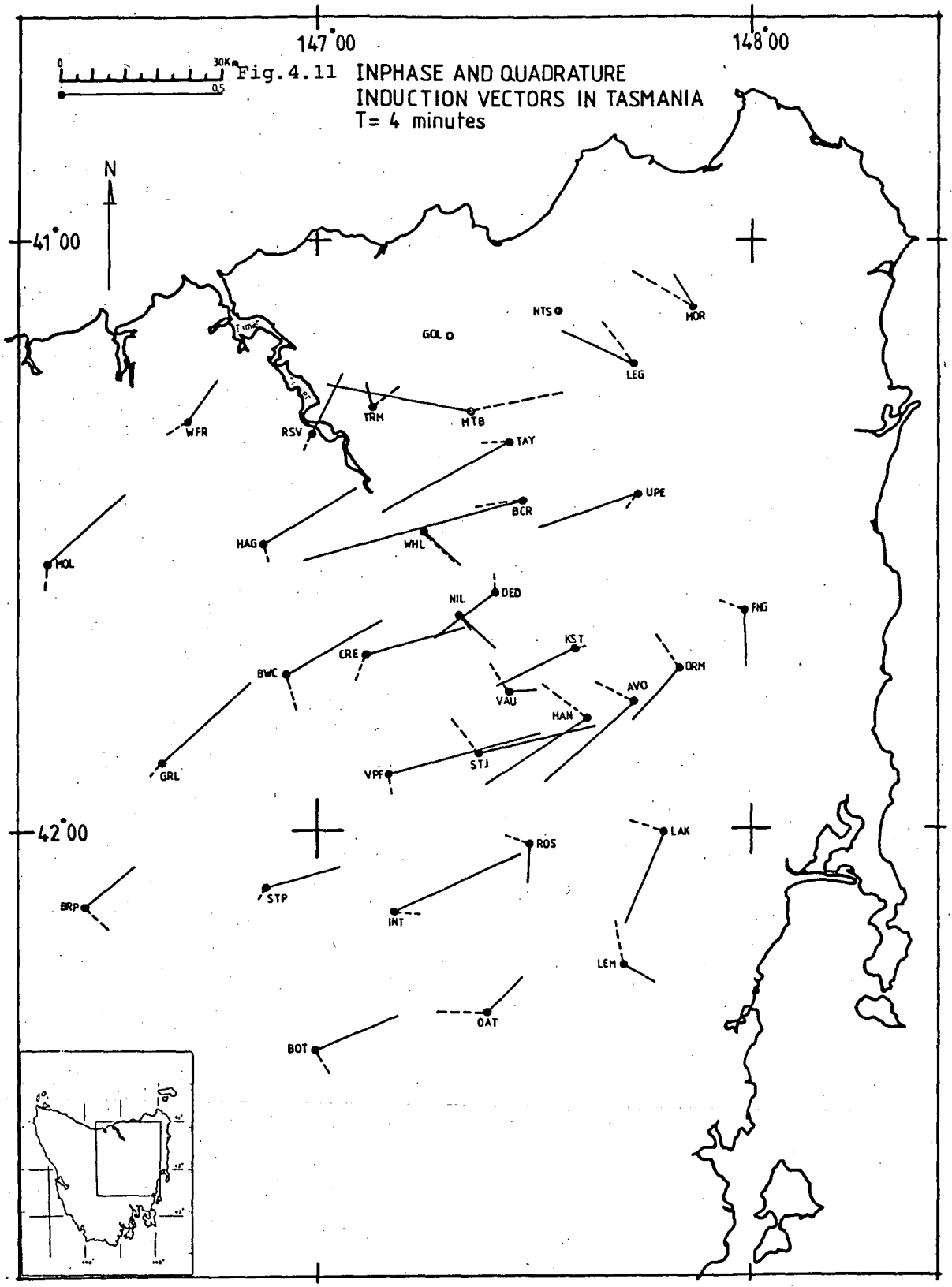

Fig.4.11 INPHASE AND QUADRATURE INDUCTION VECTORS IN TASMANIA T= 4 minutes

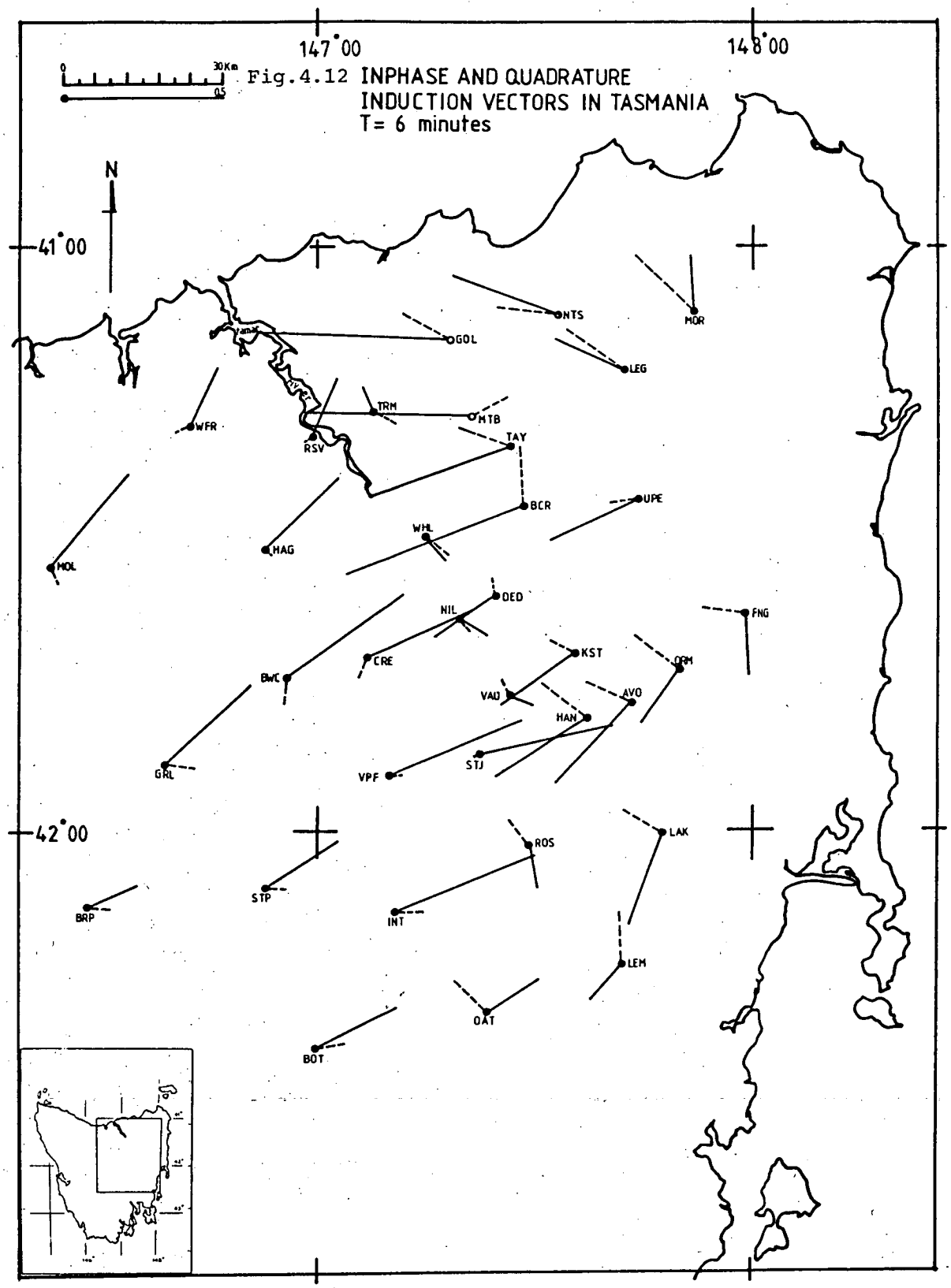
147°00
148°00
0
30Km
0.5
Fig.4.12 INPHASE AND QUADRATURE
INDUCTION VECTORS IN TASMANIA
T= 6 minutes
N
41°00
42°00
NTS
MOR
GOL
LEG
TRM
MTB
WFR
RSV
TAY
BCR
UPE
WHL
HAG
MOL
OED
NIL
FNG
CRE
KST
ORM
BWC
VAU
AVO
HAN
GRL
VPF
STJ
ROS
LAK
STP
BRP
INT
LEM
OAT
BOT

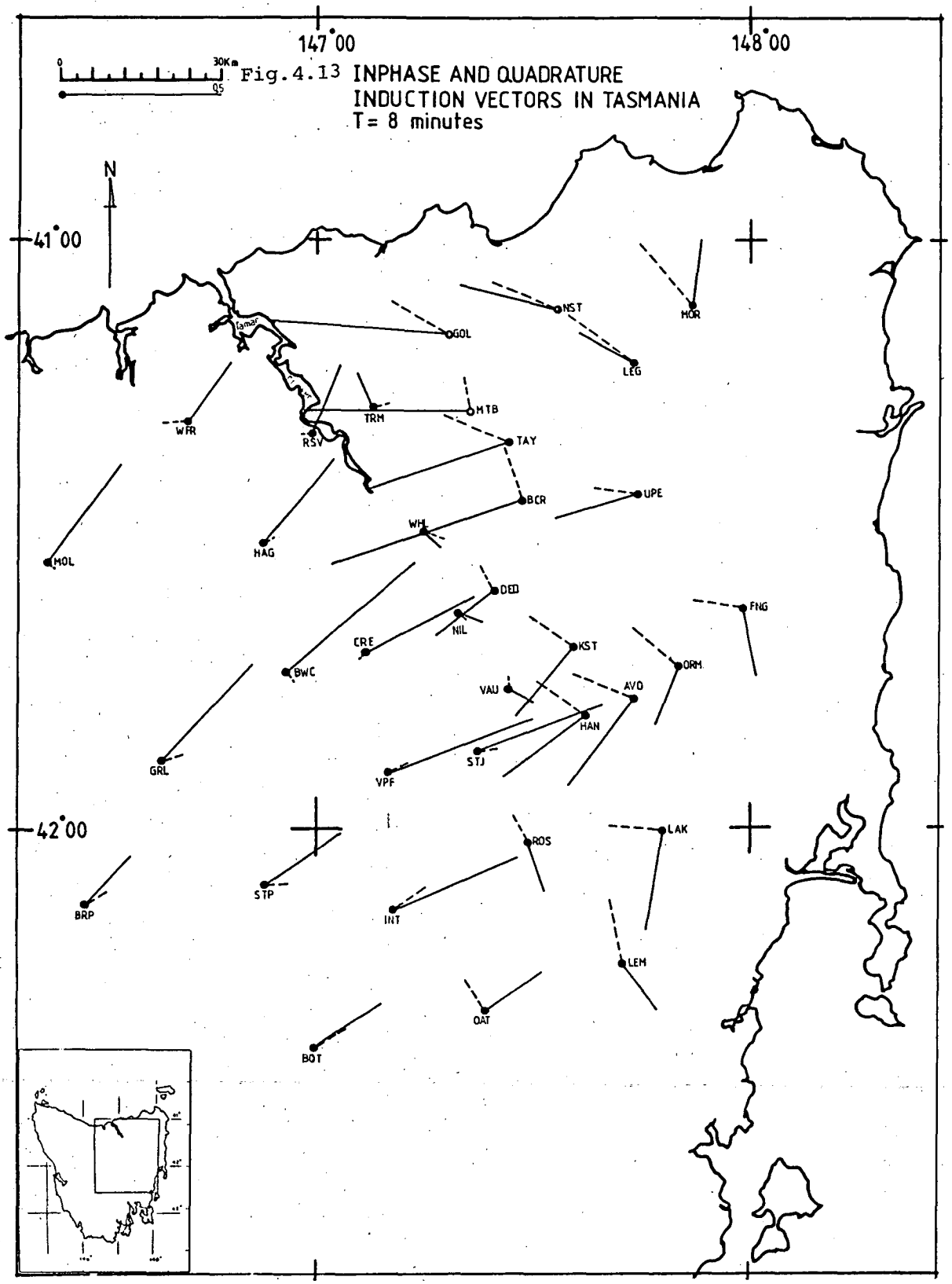

Fig.4.13 INPHASE AND QUADRATURE INDUCTION VECTORS IN TASMANIA T= 8 minutes

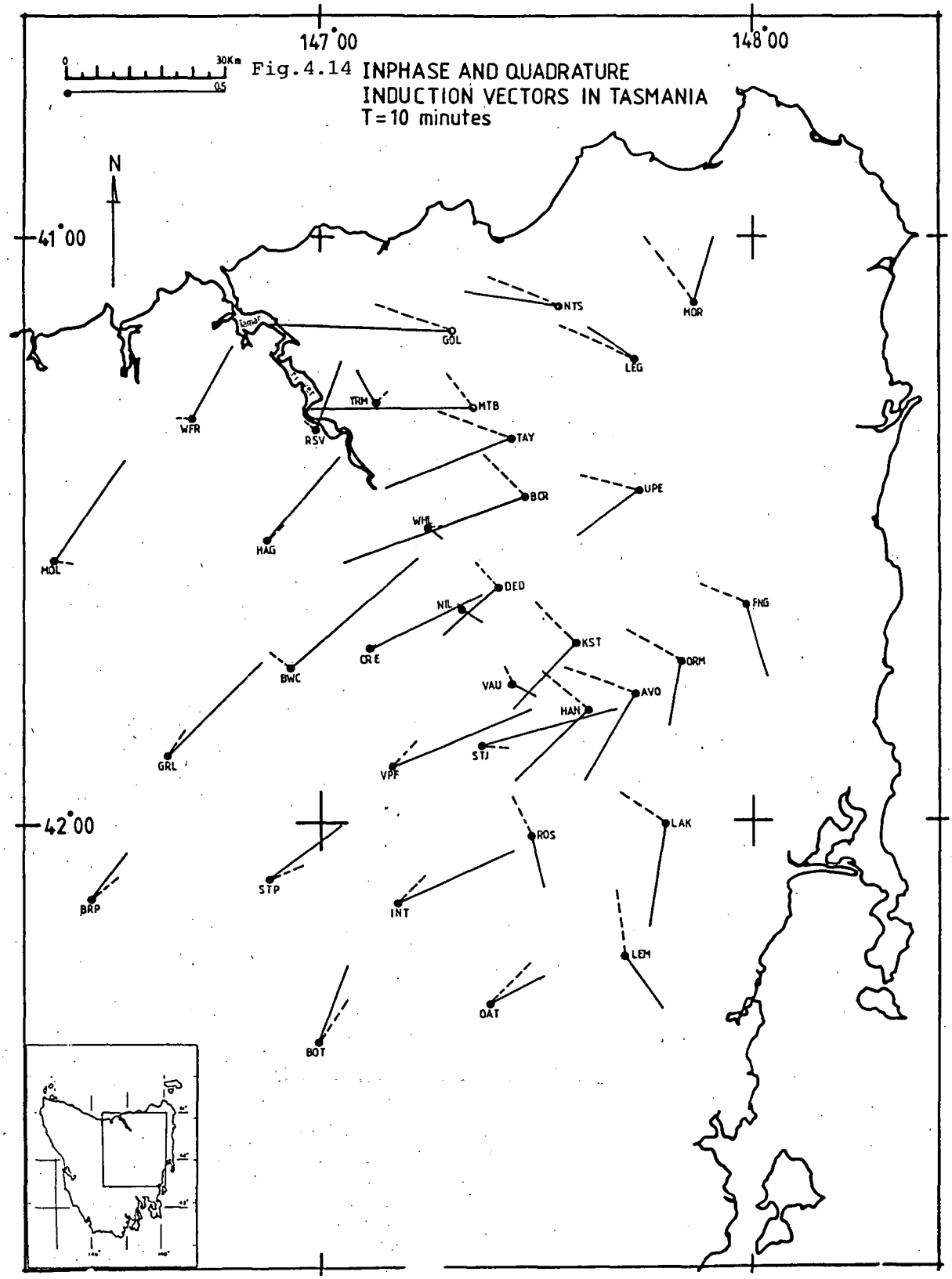

Fig.4.14 INPHASE AND QUADRATURE INDUCTION VECTORS IN TASMANIA T=10 minutes

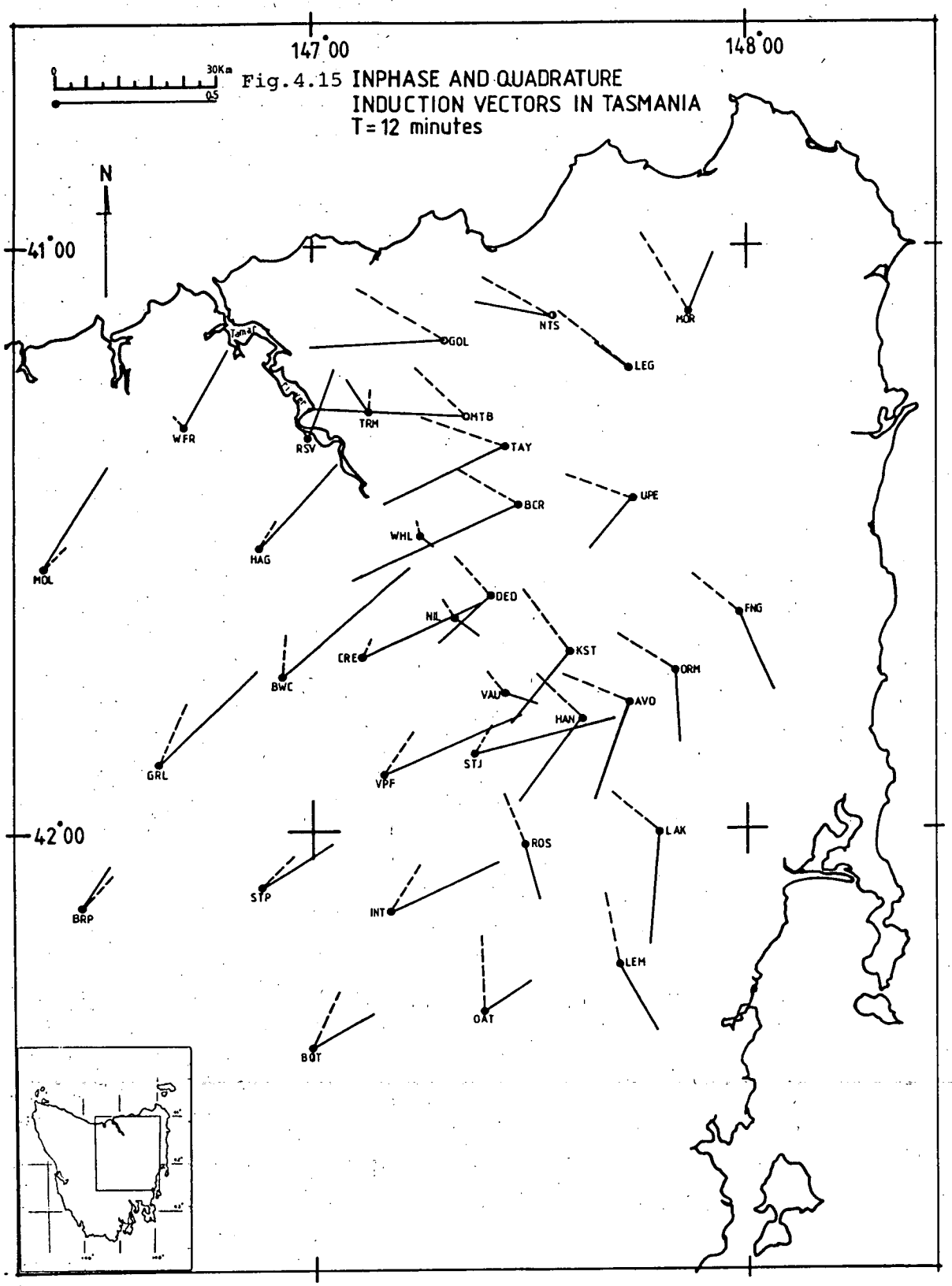
147°00
148°00
41°00
42°00
N
0
30Km
0.5
Fig.4.15 INPHASE AND QUADRATURE
INDUCTION VECTORS IN TASMANIA
T = 12 minutes
GOL
NTS
MOR
LEG
WFR
RSV
TRM
OMTB
TAY
BCR
UPE
WHL
HAG
MOL
DED
NIL
FNG
CRE
KST
ORM
BWC
VAL
AVO
HAN
GRL
STJ
VPF
ROS
LAK
STP
INT
BRP
LEM
OAT
BOT

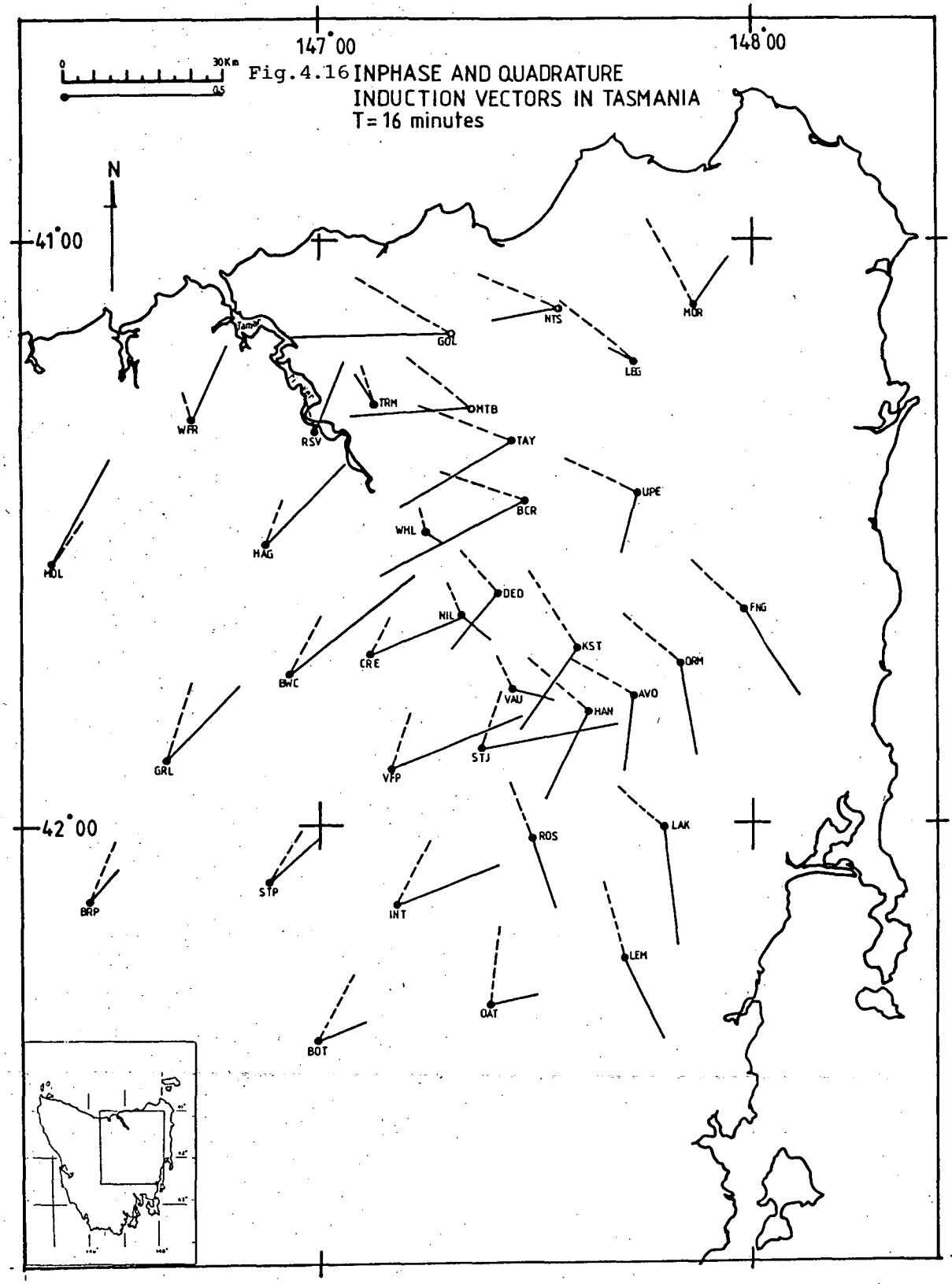

Fig.4.16 INPHASE AND QUADRATURE INDUCTION VECTORS IN TASMANIA
T = 16 minutes

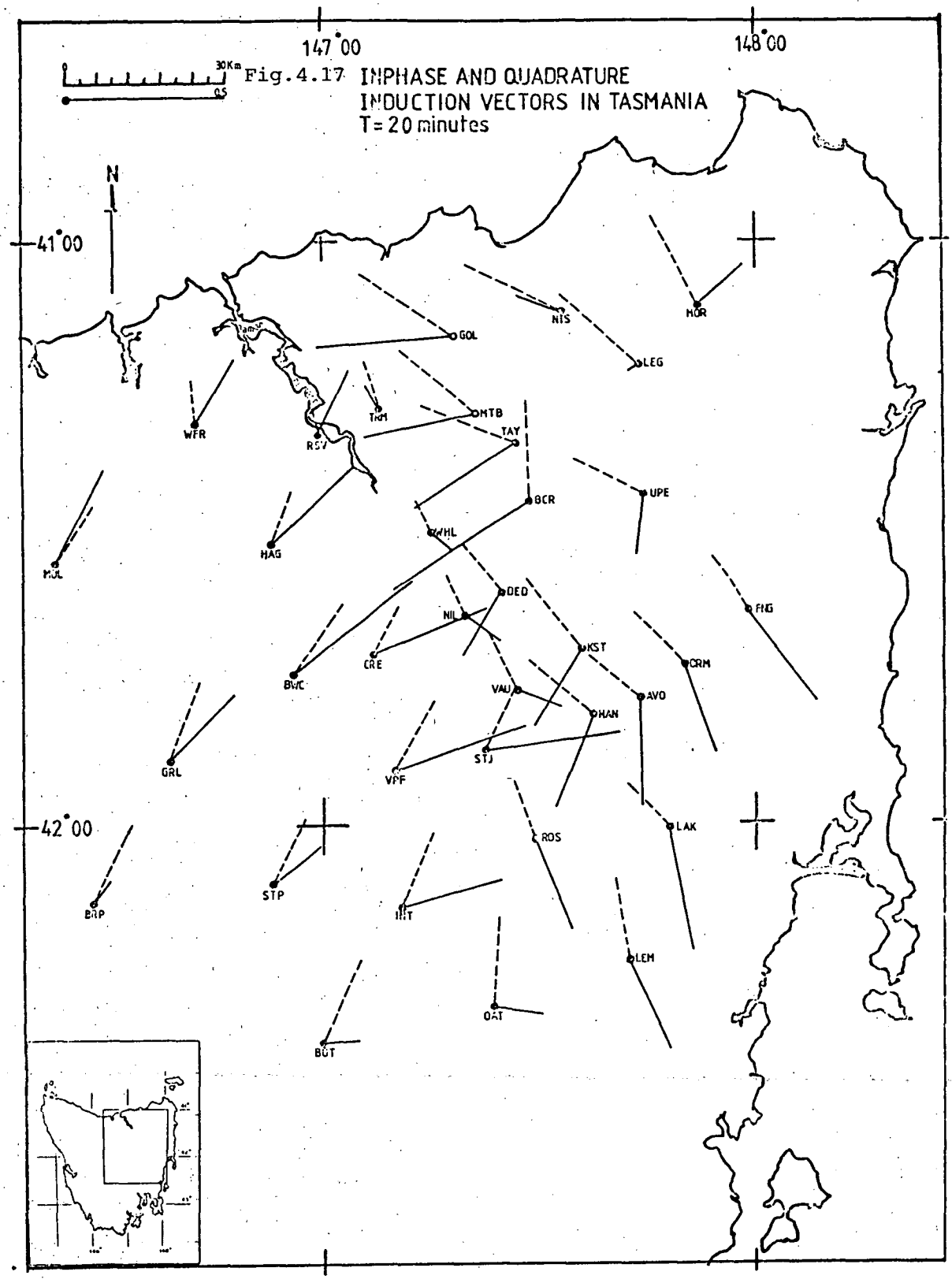
147°00
148°00
41°00
42°00
N
30Km
GS
Fig.4.17 INPHASE AND QUADRATURE
INDUCTION VECTORS IN TASMANIA
T=20 minutes
GOL
NIS
MOR
LEG
WFR
RSV
TAM
MTB
TAY
BCR
UPE
WHL
HAG
MOL
DED
NIL
FNG
CRE
KST
CRM
BWC
VAU
AVO
OHAN
STJ
GRL
VPF
LAK
ROS
STP
BRP
LEM
OAT
BOT

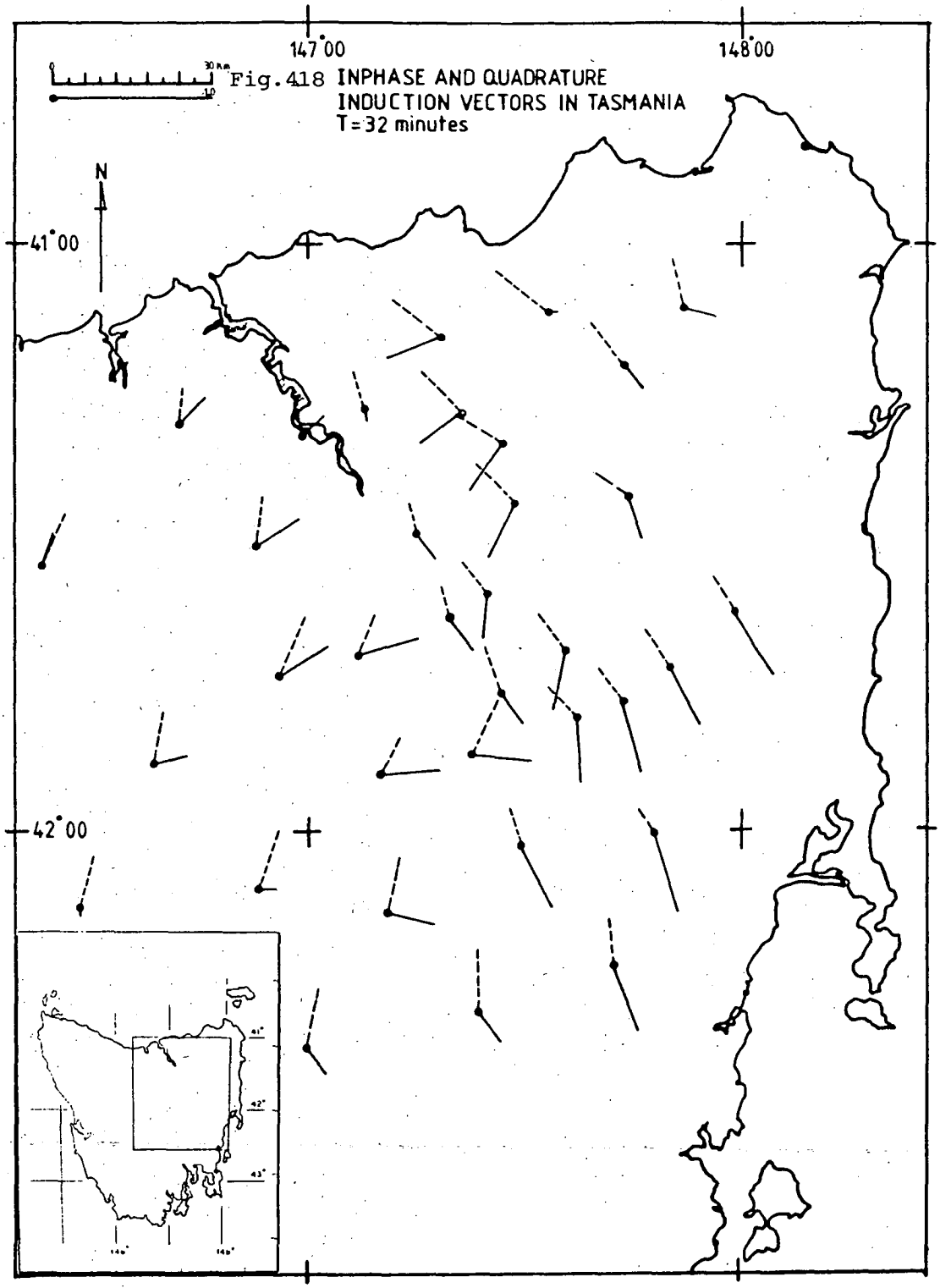

Fig.418 INPHASE AND QUADRATURE INDUCTION VECTORS IN TASMANIA T=32 minutes

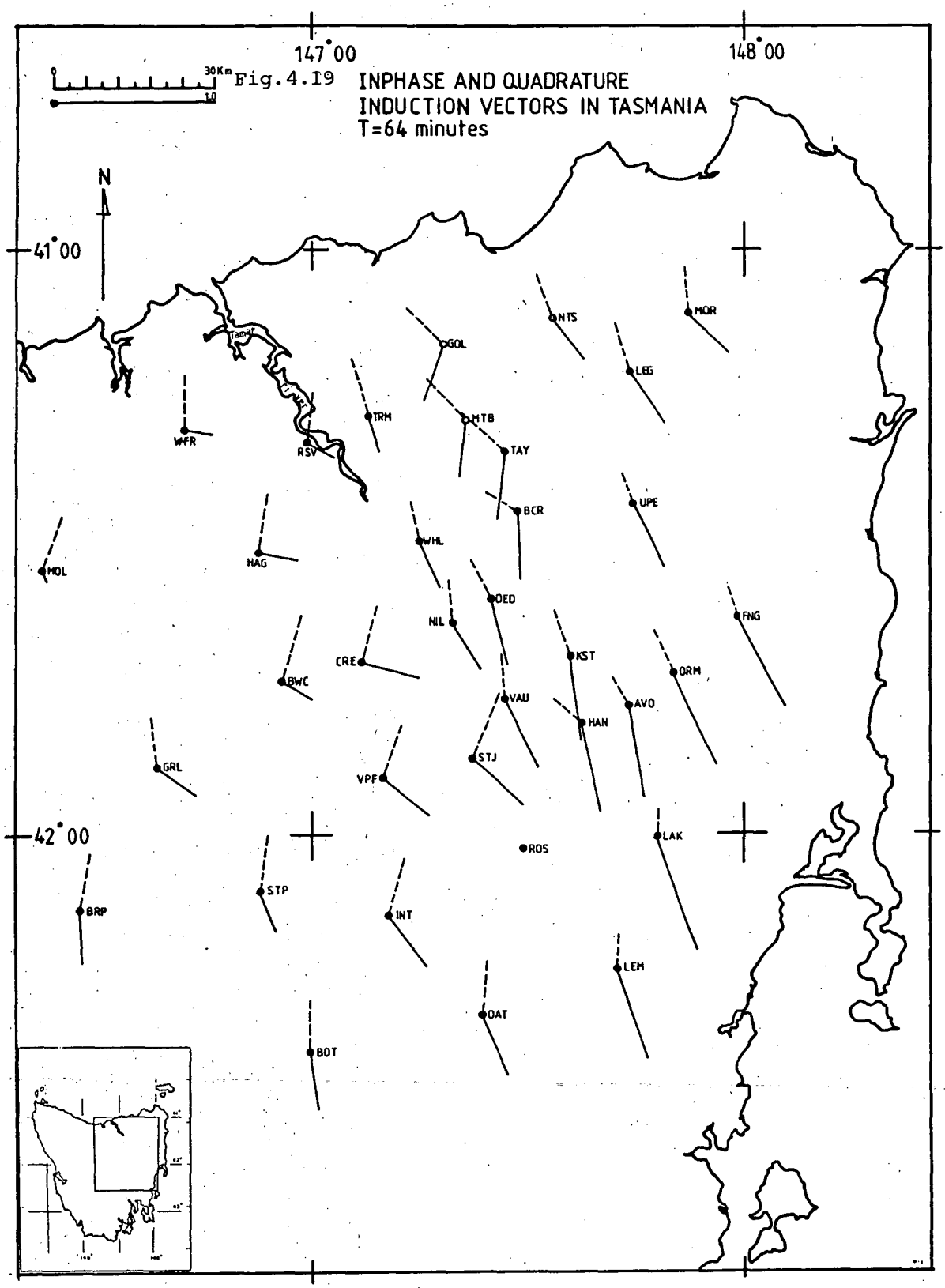
147°00
148°00
41°00
42°00
N
30Km
1.0
INPHASE AND QUADRATURE
INDUCTION VECTORS IN TASMANIA
T=64 minutes
NTS
MQR
GOL
LEG
TRM
MTB
WFR
RSV
TAY
BCR
UPE
WHL
HAG
MOL
OED
FNG
NIL
KST
CRE
ORM
BWC
VAU
AVO
HAN
GRL
STJ
VPF
LAK
ROS
STP
BRP
INT
LEM
DAT
BOT

Fig.4.19

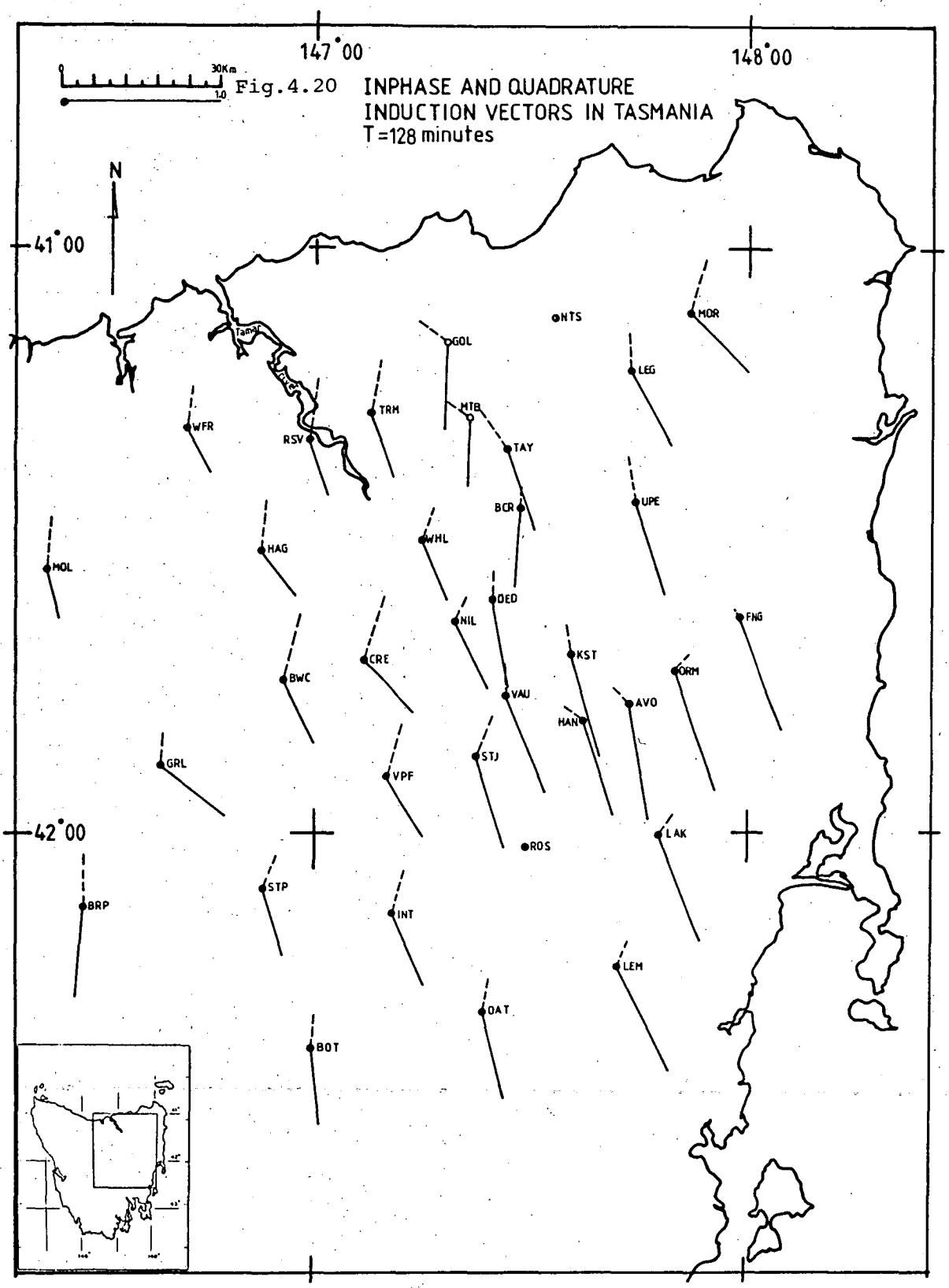
147°00
148°00
41°00
42°00
N
30Km
1.0
Fig.4.20 INPHASE AND QUADRATURE
INDUCTION VECTORS IN TASMANIA
T=128 minutes
Tamar
River
NTS
MOR
GOL
LEG
TRM
MTB
WFR
RSV
TAY
UPE
BCR
WHL
HAG
MOL
DED
NIL
FNG
KST
CRE
BWC
ORM
VAU
AVO
HAN
GRL
VPF
STJ
LAK
ROS
STP
BRP
INT
LEM
OAT
BOT

transfer function values, from which the induction vectors were derived (see figure 4.2). The gradual increase in the lengths of the vectors from the western stations (e.g. BRP) toward the central stations, implies that the effect of a lateral conductivity inhomogeneity becomes important. The lengths of the vectors, which appear to be at a maximum at around BWC and VPF suggests that these stations are probably on the edge of a good conductor. The orientations of the vectors in this region at periods between 4 and 20 minutes do not change as much with period as those in the eastern region. This is probably due to the fact that the western region is relatively more distant from the oceans and thus is almost free of the ocean effect. Apparently, the effect of the good conductor, which lies approximately along the line of the central stations, is recorded at BRP (the most westerly station) (see figures 4.11 to 4.17). On the other hand, in the eastern region most of the vectors point in the opposite direction to that of the vectors in the western region. As in the western region, the lengths of the vectors in the eastern region also show a progressive increase with increasing period and appear to be at a maximum at the same period as those in the western region. This feature can also be seen from the transfer function values (see figure 4.4). Unlike the transfer function values in the western region, which show very little period dependence, the transfer functions in the eastern region, especially the B values, show large period dependence. The orientations of the vectors in the middle of this region (i.e. for stations TAY, BCR, UPE, DED, KST, HAN, and AVO) are slightly different from those of the stations in the north-east (i.e. GOL, MTB, NTS, LEG, and MOR) and the stations in the south-east (FNG, LAK, and LEM) (see figures 4.11 to 4.17). The effect of electric current flow in the good conductor is very obvious in the first-mentioned group of stations. At some of these stations the vectors point almost perpendicular to the anomaly. On the other hand, in the north-east and south-east the vectors, which point slightly away from the anomaly at the shortest period and ~~become more significant~~ further away at longer periods, are more likely to be affected by the electric current flow in Bass Strait and the Southern Ocean, respectively. At GOL, MTB, TAY, and BCR (at periods less than 20 minutes) much longer vectors than those at neighbouring stations indicate that these stations are probably located on the eastern edge of the anomaly. The relatively small values of the A and

B transfer functions at some of the central stations, such as TRM, WHL, NIL, and VAU (at periods less than 20 minutes) result in very short induction vectors at these stations (see figures 4.11 to 4.17). This indicates that they are presumably very close to or on the axis of the anomaly. In contrast, at periods longer than 20 minutes, the directions of the vectors swing gradually from the north-east in the western region and south-west in the eastern region to south or south-east at almost all sites (see figures 4.18 to 4.20). The lengths of the vectors also show a decrease at the inland stations and a progressive increase toward the nearest coastline. [Note that the scale length of the vectors in figures 4.18 to 4.20 is different to that in figures 4.11 to 4.17 (see the scale length in the above figures).] These signs could be considered as due to the coast effect, which becomes dominant at these periods. This effect is probably either due to a conductivity contrast between the rocks beneath the continents and oceans (Parkinson and Jones, 1979), or due to induced electric currents flowing in the ocean (Honkura, 1978). Probably one of the best example of the ocean effect can be seen at the stations along the Fingal Valley Road, namely FNG, ORM, AVO, and HAN (see figures 4.18, 4.19, and 4.20). The orientation of the vectors at FNG, which points to the south at periods between 4 and 6 minutes, shows clearly that this station is more affected by the ocean (east of this station) than the stations further inland. The gradual increase in the lengths of the vectors toward inland stations accompanied by a gradual change in the direction of the vectors from almost south at FNG to west-south-west at HAN indicates that at short periods the effect of the ocean disappears further inland. This is in agreement with the Dosso's analogue model results (Dosso et al., in press), which suggest that for E-polarization (electric field of the source in the N-S direction) the coastal anomaly at short periods does not extend far inland.

4.3.3 QUADRATURE VECTORS

Generally, the lengths of the quadrature vectors are much less than those of the in-phase vectors. The directions of the vectors at periods less than 10 minutes are distributed erratically and show remarkably large period dependence (see figures 4.11 to 4.14). At periods between 4 and 10 minutes, for instance, the vectors in the western region point in different

directions. The fact that they do not point toward the coast suggests that the electric currents flowing in the ocean are in-phase with the magnetic variations (Gough and Ingham, 1983). Except at WFR and RSV, where they rotate clockwise as the period increases, the vectors at the other stations in this region tend to rotate anticlockwise. At some stations the lengths of the vectors show a slight decrease at periods between 4 and 8 minutes and becomes very short at the 8 minutes period. However, at periods longer than 8 minutes the lengths of the vectors tend to increase again with increasing periods. At some stations the orientation of the quadrature vectors, at a period of 10 minutes, are roughly in the same direction as the in-phase components. In fact these orientations, which become almost uniform at most stations in this region at a period of 12 minutes (see figure 4.15), can be accounted for by a two-dimensional structure (Parkinson, 1983, p. 333). At periods between 12 and 20 minutes the orientations of the vectors change very smoothly with increasing period.

In the eastern region, on the other hand, the vectors tend to rotate very gently with increasing periods. A reversal of signs between the in-phase and quadrature components, which is shown at GRL and RSV (in the western region) at period of 4 minutes (see figure 4.11), can also be seen at MTB (in the eastern region). It is not understood what causes this effect. However, since the vectors in the neighbouring stations point in different directions, it is assumed that they are probably due to a local anomaly. It is known that at the period at which the amplitude $\sqrt{A^2 + B^2}$ of the transfer function reaches a maximum, the phases change sign, which makes the quadrature function change sign. This applies to two-dimensional models (see e.g. Rokityansky 1975; and 1982, section 6.2.1). Note that the vectors at MTB and GRL change direction dramatically between periods of 4 and 10 minutes (see figures 4.11 to 4.14).

In general, the lengths of the vectors at the stations in the eastern region are much greater than those in the western region. Similar results are also shown by the quadrature difference vectors at a period of 10 minutes obtained from the analogue model study of the Tasmania region (Dosso et al., in press). These differences are probably due to the fact that the stations in the eastern region are much closer to the ocean, thus recording much greater ocean effect, than the stations in the western

region. The reversal of the vectors, similar to that at GRL, RSV and MTB, at a period of 4 minutes, becomes a general feature of stations in the eastern region at periods longer than 32 minutes.

The quadrature vectors in the central region are characterised by moderate period dependence. In general, the lengths of the vectors are relatively small at periods less than 20 minutes but become progressively larger at periods longer than 20 minutes. The orientations of the vectors at TRM, WHL and NIL, at periods less than 10 minutes, change more erratically than those at VAU, ROS and LEM. These orientations, however, change very smoothly at much longer periods.

It is concluded, therefore, that the scatter in orientations of the quadrature vectors at periods less than 8 minutes are probably due to a local anomaly. Meanwhile, the almost constant vector orientations at all stations at periods greater than 20 minutes, which point almost to the north, appear likely to be due to the effect of electric current flowing in the shallow water of Bass Strait.

CHAPTER 5

INTERPRETATION OF DATA

5.1 DATA

The data used in the interpretation are based on the in-phase part of the induction vectors at periods less than 20 minutes (see figures 4.11 to 4.17). As mentioned in section 4.3.2 they clearly show an electrical conductivity anomaly running across the area surveyed, e.g. at RVR, TRM, GOL, MTB, TAY, HAG, BCR, WHL, BWC, CRE, NIL, DED, VPF, STJ, VAU, HAN, AVO, INT, ROS and LEM. Taking into account the fact that the quadrature as well as the in-phase induction vectors at periods between 10 and 20 minutes, especially at stations in the western region (see figures 4.14 to 4.17), point in roughly the same direction, the underground conductivity structure at those sites can be considered to have a two-dimensional structure (Parkinson, 1983, p. 333). In the eastern region, however, the in-phase and quadrature induction vectors are more scattered in direction thus implying that a more complex structure is involved. A two-dimensional structure was also deduced from the magneto-telluric observations at Vaucluse (Sayers, 1984). The apparent resistivity plot for the Vaucluse site (see figure 5.1) (Sayers, 1984) shows ~~that the~~ a divergence of the two apparent resistivity curves at periods greater than $10^{2.6}$ seconds which is likely to be due to an inhomogeneity, i.e. possibly a two-dimensional structure. In contrast the curves at periods less than $10^{2.6}$ seconds which coincide, imply that the upper layers are one-dimensional and are approximately 2 km thick (Sayers, 1984). The curve $\hat{\rho}_{yx}$ which always gives a better estimate of the conductivity configuration (Swift, 1967), ~~shows~~ indicates the presence of a high conductivity zone with a resistivity of less than 1 Ωm underneath the 2 km of overburden.

The strike of the conducting zone is approximately 38^{o} west of magnetic north or 25^{o} west of true north. The bearing of the structure can be deduced from the pattern of the electrical conductivity anomaly marked by anti-parallel induction arrows at stations in the western and eastern regions that lie close to the central stations. Stations at which

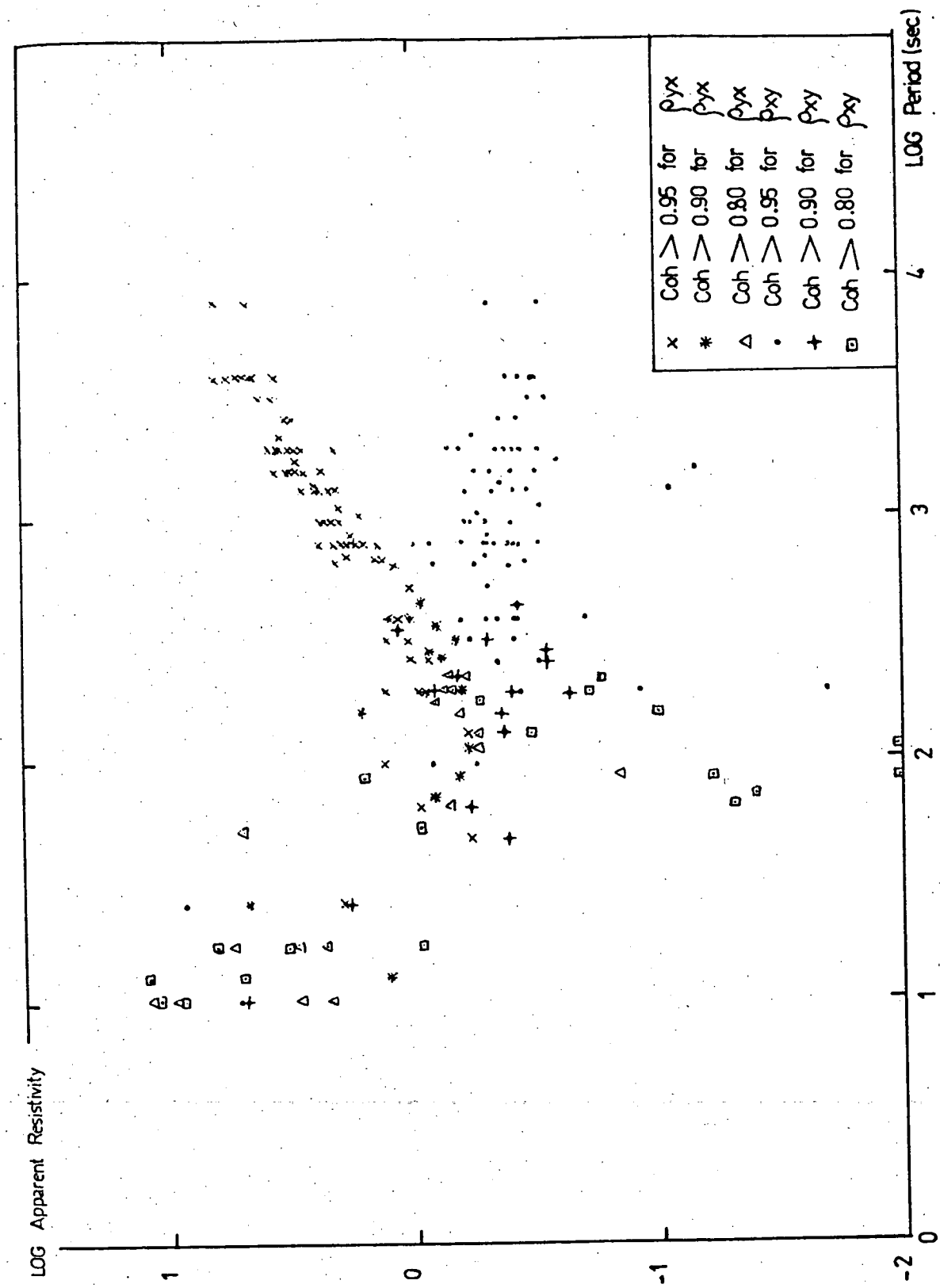

Fig. 5.1 . Apparent resistivity plot for the Vaucluse site.

(From Sayers,1984)

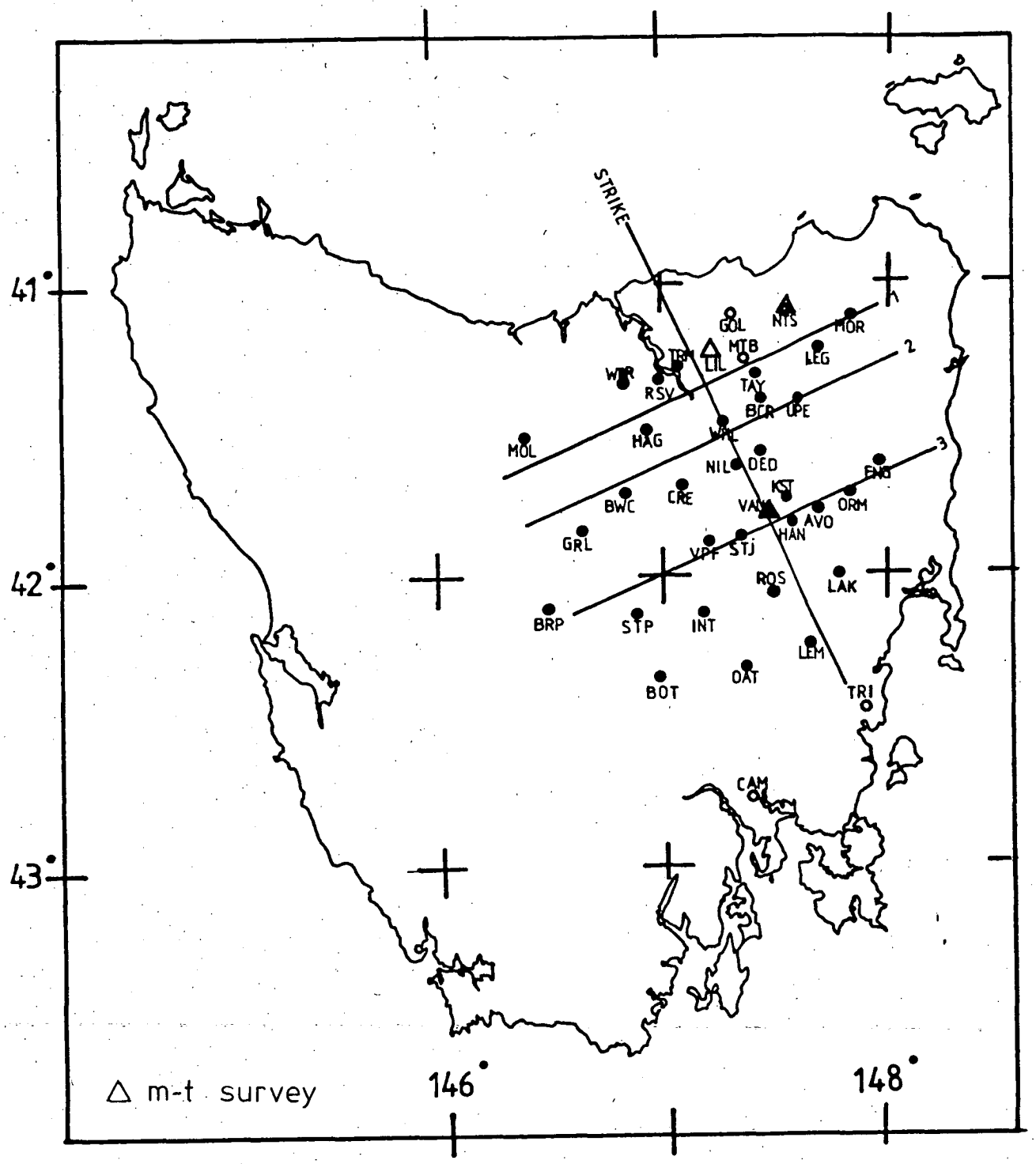

Fig. 5.2 Plots of traverses 1,2,and 3 drawn perpendicular to the approximate strike of the anomaly.

the induction vector is small, i.e. TRM, WHL, NIL and VAU, are considered to lie on the axis of the anomaly (see figures 4.11 to 4.14). The strike correlates very well with the strike determined from magneto-telluric observations at Vaucluse (VAU), e.g. 142°east of magnetic north (Sayers, 1984, p. 76). Three traverses (1,2,3 in figure 5.2) were drawn perpendicular to the strike. The components of the observed induction vectors that were used in the two-dimensional interpretation were those resolved parallel to these traverses. The components in this direction were calculated by using

$$F = \cos (\theta - 65^{\circ}) \times L \qquad \ldots\ldots\ldots (5.1)$$

where F is the component of the induction vector along the traverse. L and θ are the length and direction of the induction vector defined by equations (4.5 and 4.6) and 65° is the angle of the traverse perpendicular to the strike measured from true north. F is positive for $(\theta - 65) < 90^{\circ}$ and $(\theta - 65) > 270^{\circ}$ and negative for $90^{\circ} < (\theta - 65) < 270^{\circ}$. All of the resolved components are then plotted with respect to position along the traverses. The plots of the observed in-phase components for periods of 4, 8, 10, 20, 32 and 128 minutes, for traverses 1, 2 and 3, are shown in figures 5.3, 5.4 and 5.5, respectively.

Analogue modelling of electromagnetic induction in Tasmania was carried out by Dosso and his collaborators at the University of Victoria, British Columbia (Dosso et al., in press). The results obtained from the study have been used to obtain difference transfer functions, i.e. by vector subtraction of Dosso's results from the observed transfer functions. The difference components were also resolved along the traverses by using formula (5.1). The plots of the in-phase difference components for traverses 1, 2 and 3 at periods of 5, 10 and 20 minutes are given in figure 5.6. Both the observed and difference components are used in the following section to find the best fitting results from two-dimensional modelling by using the Jones and Pascoe (1971) and Pascoe and Jones (1972) programs. However, due to time limitations and very limited data to control the western side of the Tamar River, traverse 1 was not included in the modelling.

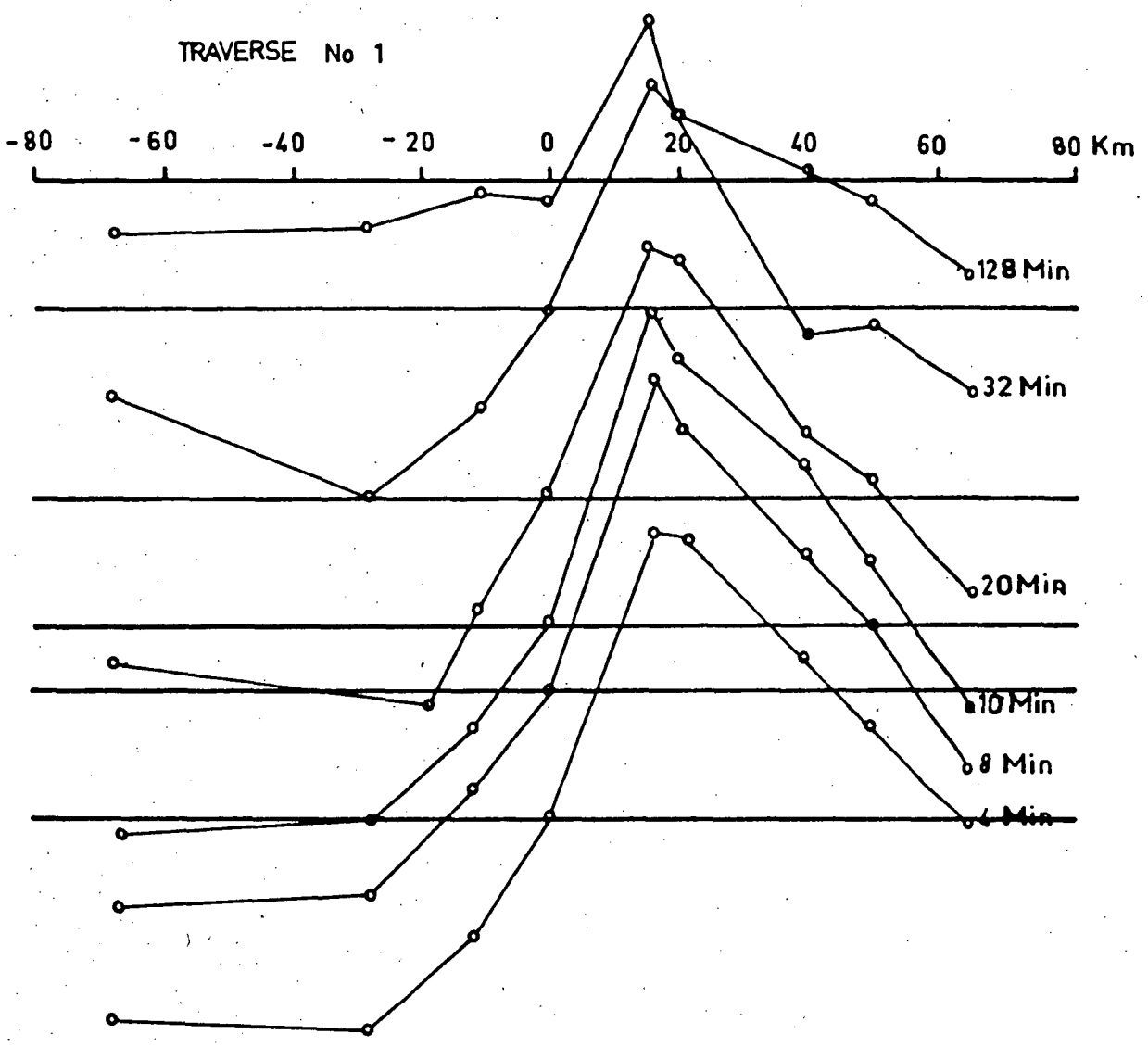

Fig. 5.3 Plots of the observed in-phase components for traverse 1 at periods of 4,8,10,20,32,and 128 minutes.

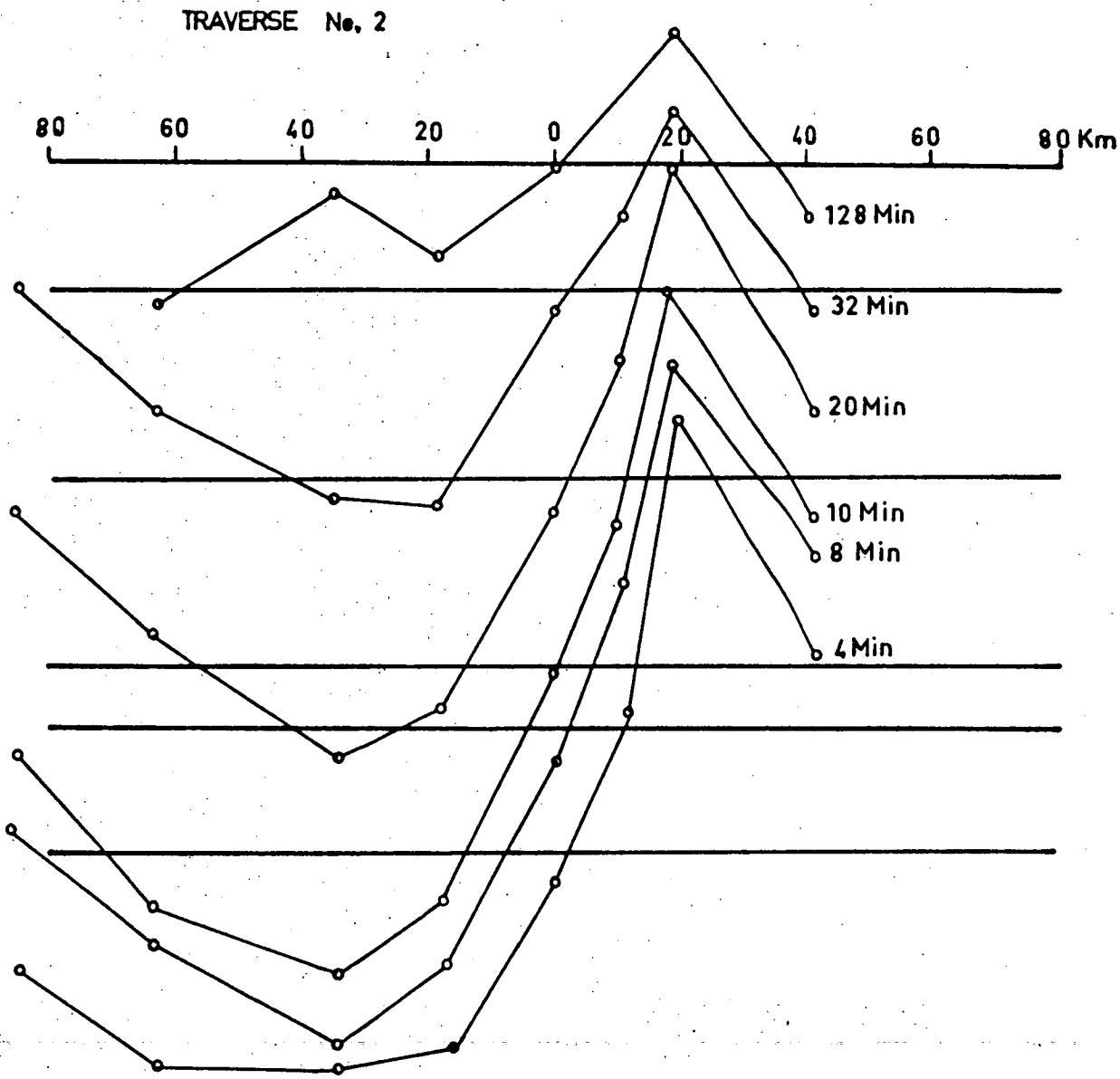

Fig. 5.4 Plots of the observed in-phase components for traverse 2 at periods of 4,8,10,20,32,and 128 minutes.

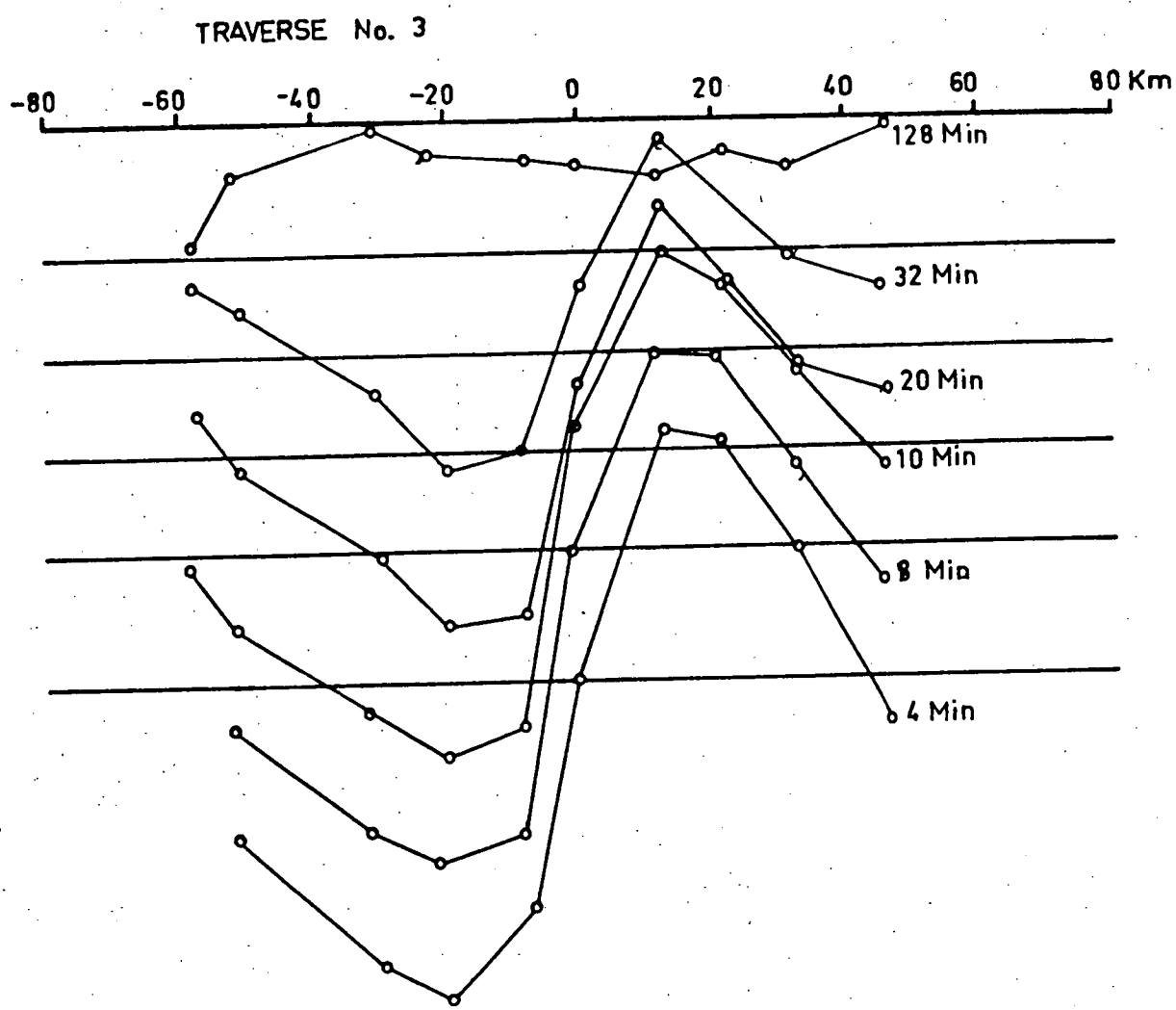

Fig. 5.5 Plots of the observed in-phase components for traverse 3 at periods of 4,8,10,20,32,and 128 minutes.

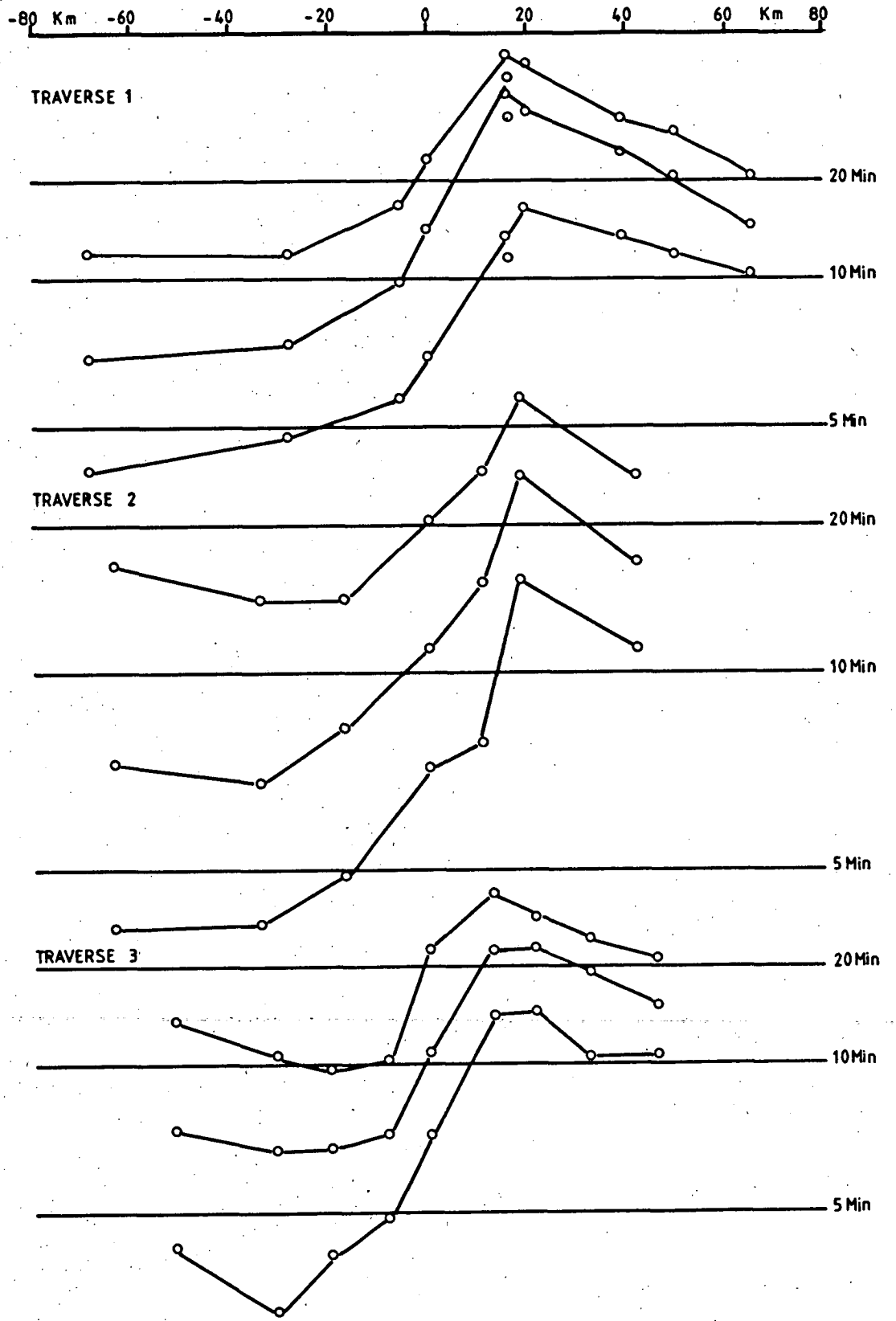

Fig. 5.6 Plots of the difference in-phase components for traverses 1,2,and 3 at periods of 5,10,and 20 minutes.

5.2 TWO-DIMENSIONAL MODELLING

Models including oceans were compared with the observed transfer functions (resolved along traverses) and models without oceans were compared with the difference transfer functions obtained as described above. For brevity these models are called Type I and Type II, respectively.

The programs, using the finite difference method, written by Jones and Pascoe (1971) and Pascoe and Jones (1972) were used to determine the most likely underground electrical conductivity structure under the study area. In view of limitations in the Jones and Pascoe (1971) program pointed out by Williamson et al. (1974) the program was modified as suggested by Jones and Thompson (1974). Some modifications to the program for E-polarisation were also made by W.D. Parkinson (Parkinson et al., in preparation), e.g. subroutines were added to the program to calculate the components of induction vectors so that a comparison of the observed and calculated components could be made directly. The modified version of the Jones and Pascoe program is given in Appendix 4.

Taking into account the two models of electrical conductivity distribution proposed by Sayers (1984) for the Vaucluse site (see figures 5.7 and 5.8) on the basis of magneto-telluric results, several models were tried and the resulting induction coefficients calculated. Apparent resistivity curves for one of these models and data are given in figure 5.9. At least two important constraints, namely the depth to the top of the good conductor and the resistivity of the good conductor, can be obtained from the magneto-telluric results, and are used throughout the modelling. However, the thickness of the conductive zone was varied during modelling to find the result best fitting the observed and difference data. In the first attempt for traverse 3 (see figure 5.11), a model ~~almost~~ similar to that proposed by Sayers (1984) was tried. The conductive zone which has a thickness of 5 km is assumed to dip, and may be broadening, to the north-west especially at traverses 1 and 2 . Such an assumption is justified by the broad minimum of the observed and difference in-phase components to the west of those traverses as can be seen in figures 5.3, 5.4, 5.5, and 5.6. It is also in agreement with the crustal structure model obtained from gravity and with a seismic refraction survey

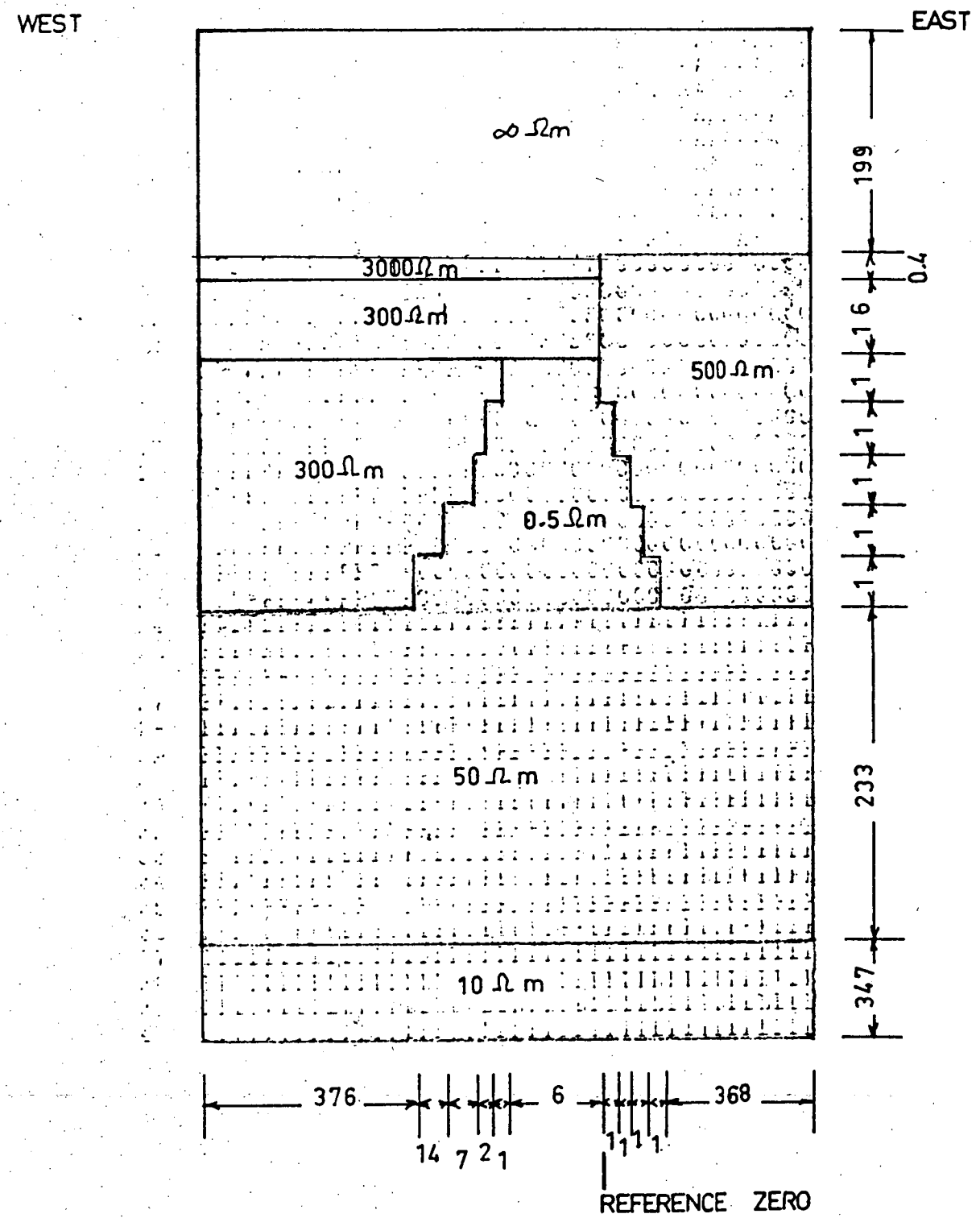

Fig. 5.7 . The conductive configuration for model E. The distances are in kilometers.

(From Sayers, 1984)

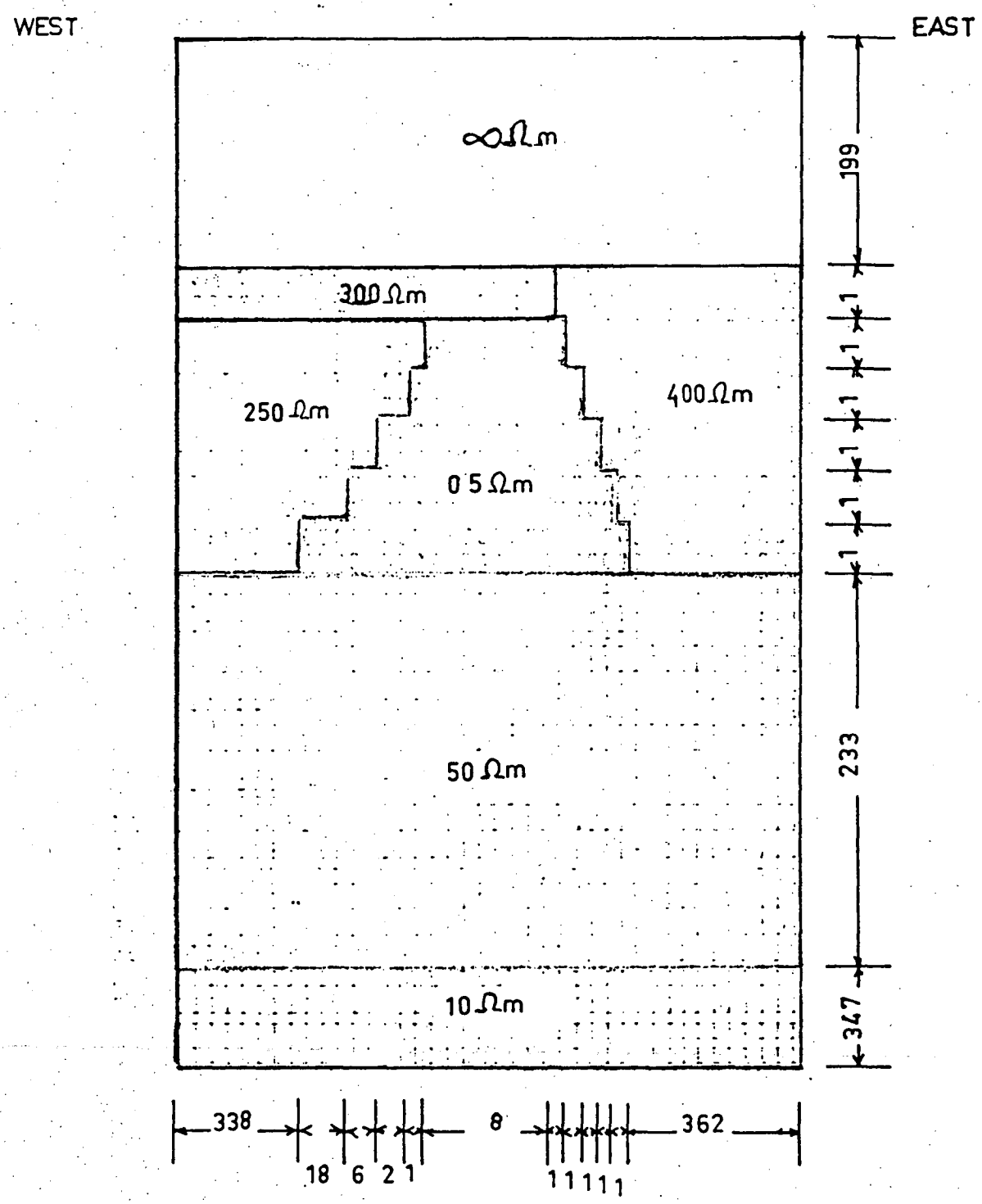

Fig. 5.8 . The conductive configuration for model F. The distances are in kilometers.

(From Sayers, 1984)

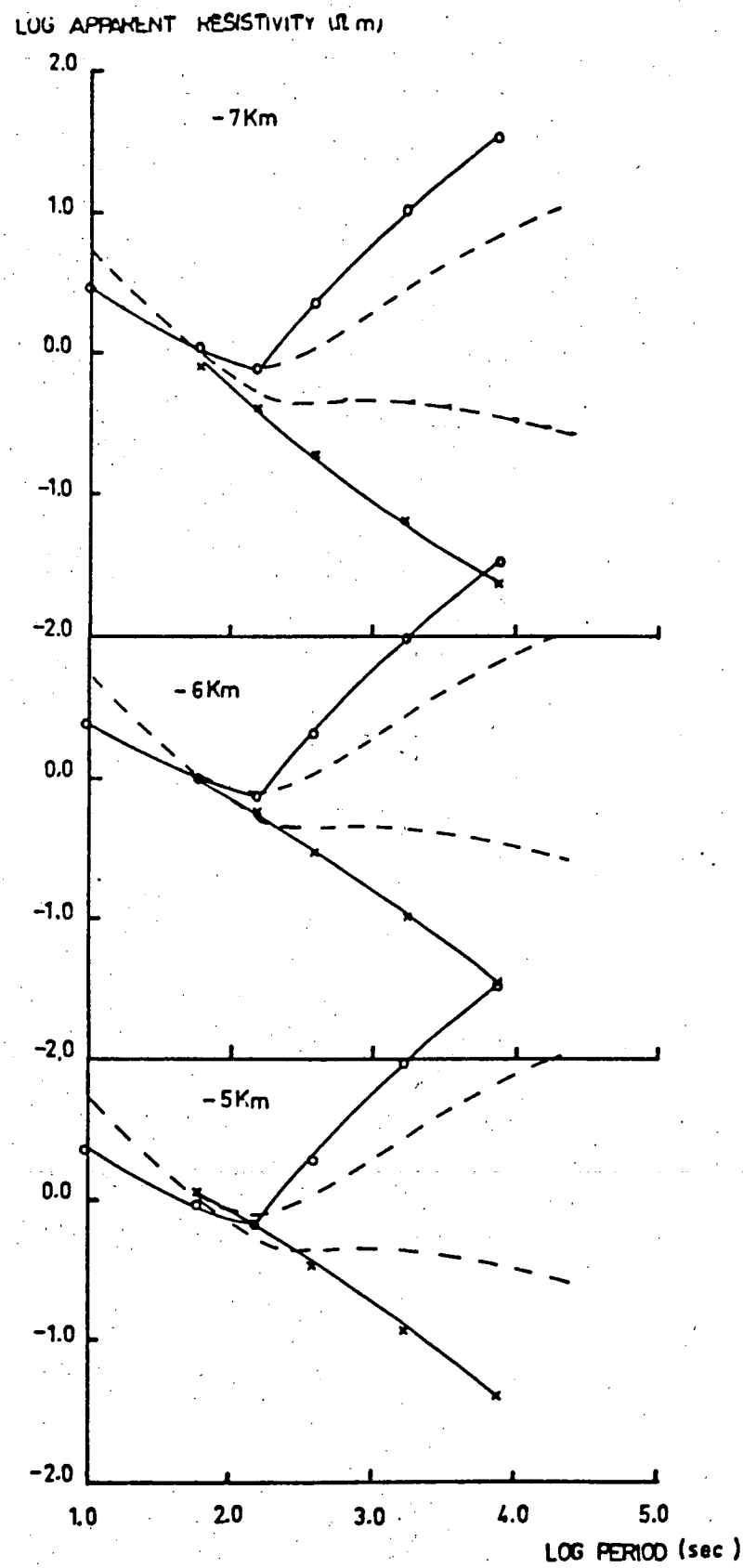

Fig. 5.9. Comparaison of the model and data apparent resistivities for Model F.The Vaucluse site data curves are the dashed curves,the model curves are the full lines.

(From Sayers, 1984)

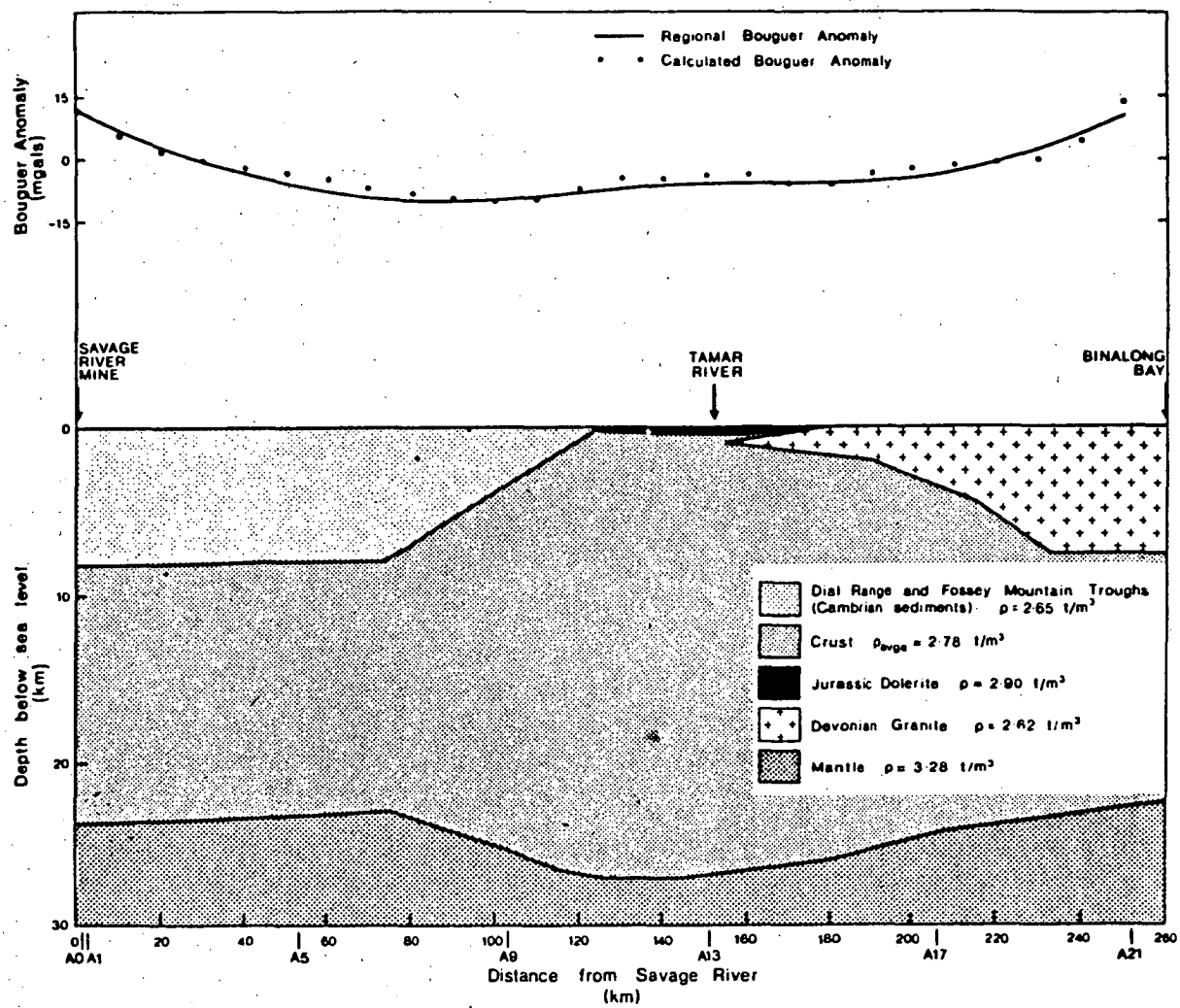

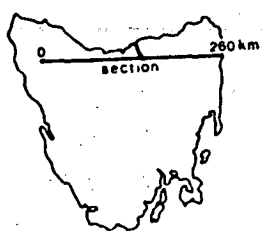

Figure 5.10 **CRUSTAL MODEL**
Gravity and seismic data
V/H = 4/1

(From Richardson, 1980)

across northern Tasmania (Richardson, 1980, see figure 5.10). To the east, however, a definite separation between conductive zone and the more resistive block is not obvious. Although it was suggested by Sayers (1984) that the eastern boundary of the conducting body could dip to the east, a vertical boundary was used throughout this modelling.

5.2.1 TRAVERSE 3

Figure 5.11 shows a structural view of model 1 including vertical and horizontal grid spacing, resistivities, and skin depth values to represent traverse 3, i.e. along the Fingal Valley Road from FNG to STP (see figure 4.11). The model has a similar structure to that of Sayers (1984) (see figures 5.7 and 5.8). The top ten rows of this model are assumed to represent the atmosphere including the magnetosphere and ionosphere where the source field is generated. It is assumed to have infinite resistivity. The conductive zone which is located 2 km below the earth's surface has a resistivity of 0.5 Ω m. The width of the top and base of the conductive zone is approximately 16 and 28 km, respectively. The zone is bounded to the east and west by resistive blocks having resistivity of 400 Ω m and 200 Ω m, respectively. On both sides of this model oceans having a resistivity of 0.3 Ω m and a thickness of 1 km are included. The oceans are located 88 km to the east and 279 km to the west of the centre of the traverse. To the west, however, the ocean is not seen as it is located outside the limit of the diagrams (see, for example, figure 5.12). These oceans are included in the modelling because their effect is clearly seen in the observed results (see section 4.3.2.). Figure 5.12 shows a comparison of the results of model 1 (the first approximation) and the observed in-phase components together with the positions of stations. Vaucluse (VAU), where the magneto-telluric survey was carried out by Sayers (1984), is located in the middle of the traverse. The lines joining the circles and crosses are the in-phase components for the observations and the model (Type I), respectively. The fit, however, is not very good. The response of the model is too small compared to the observed data . However, the comparison for the quadrature components of the same model (see figure 5.13) shows that the model results are far larger than the observed results . The depressed values of the in-phase components and

```
/* E-POLARIZATION */
```

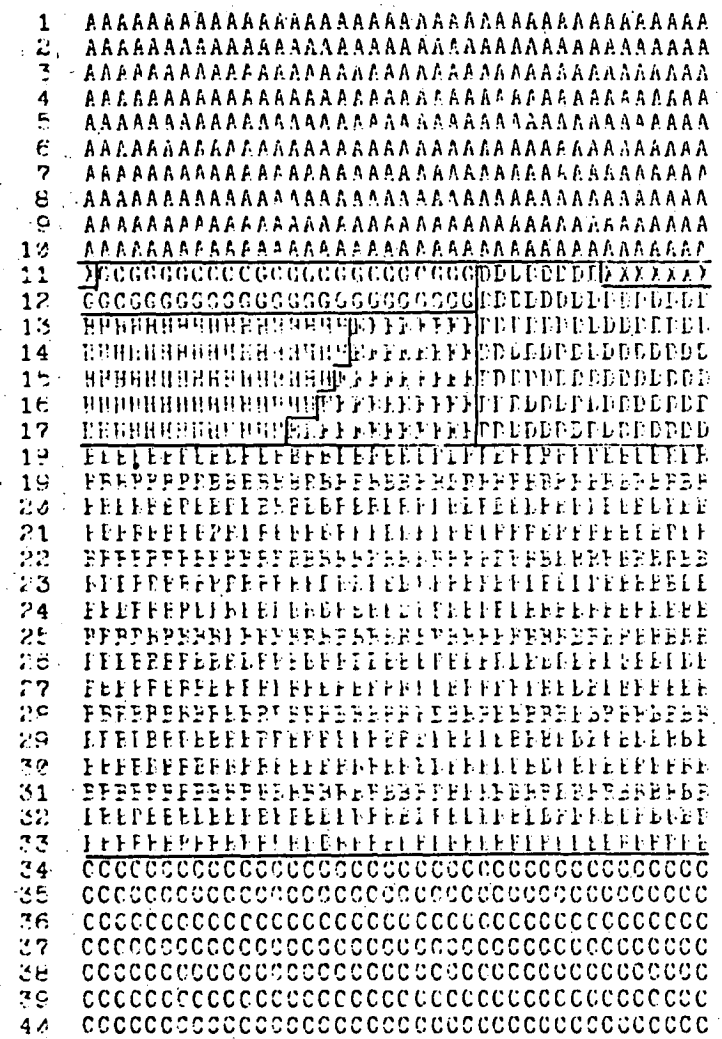

```
H VALUES   99.099.064.232.016.012.0 8.0 6.0 4.0 4.0 4.0 4.0 4.0 2.0 2.0 2.0 2.0 2.0 2.0 2.0 2.0
           2.0 2.0 2.0 2.0 4.0 4.0 4.0 4.0 6.012.016.024.032.064.099.099

K VALUES   99.064.032.016.012.0 8.0 6.0 4.0 2.0 1.0 1.0 1.0 1.0 1.0 1.0 1.0 2.0 2.0 2.0 2.0 2.0
           2.0 2.0 2.0 2.0 4.0 6.0 8.012.016.012.0 8.0 6.0 4.0 4.0 6.0 8.016.024.064.099
```

	SIGMA	SKIN DEPTH	RESIST
A	0.	*********	0.00
B	.20000E-12	87.17	50.00
C	.12000E-11	38.99	10.00
D	.25000E-13	246.56	400.00
F	.20000E-10	8.72	0.50
G	.50000E-13	174.35	200.00
H	.50000E-13	174.35	200.00
X	.33333E-10	8.75	0.33

Fig. 5.11 A structural view of model 1 (for traverse 3) including vertical and horizontal grid spacings, resistivities, and skin depth values.

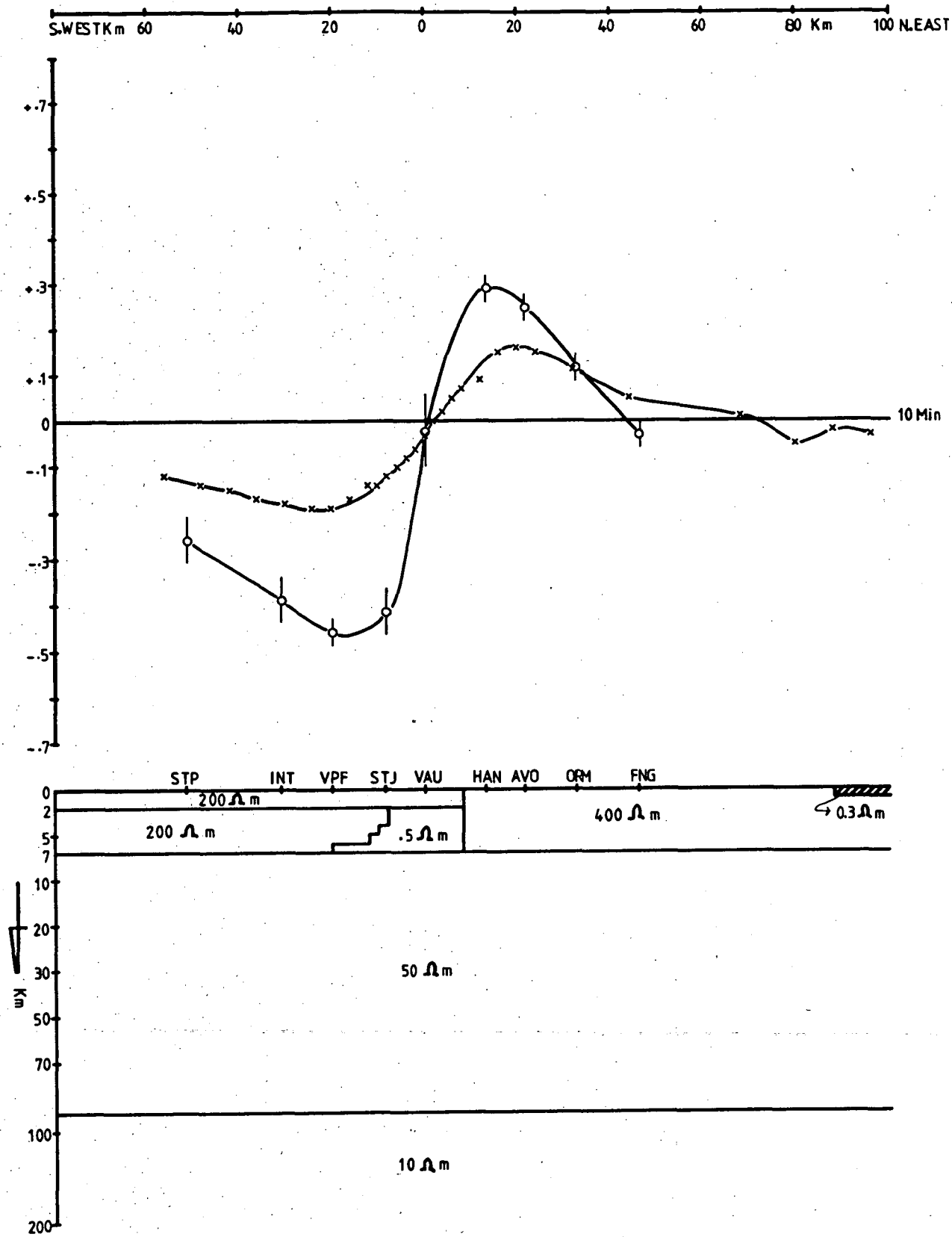

Fig. 5.12 Comparison of model (crosses) and observed (circles) in-phase results at period of 10 minutes and structural view of model 1 (type I).

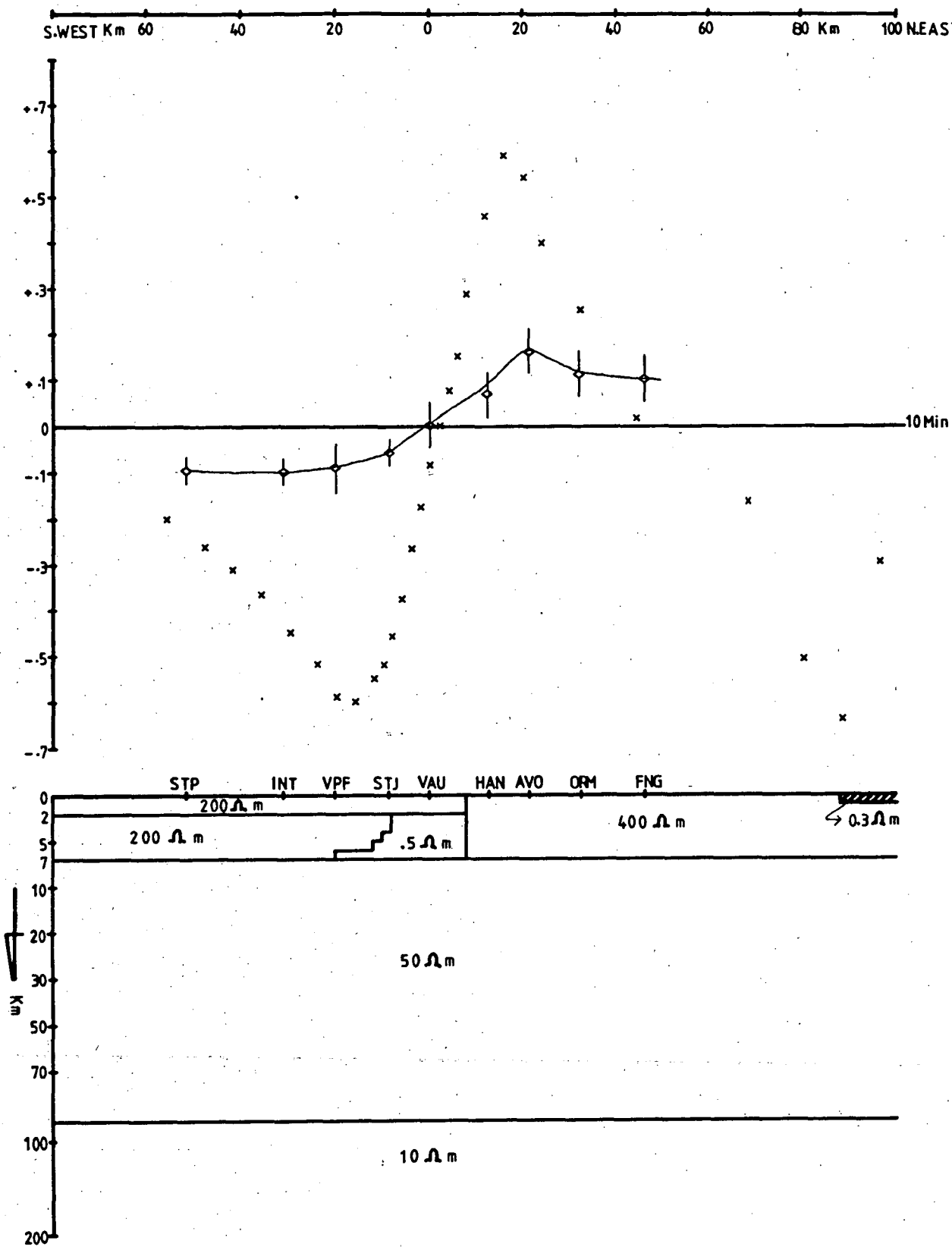

Fig. 5.13 Comparison of model (crosses) and observed (diamond symbols) quadrature results at period of 10 minutes and structural view of model 1 (type I).

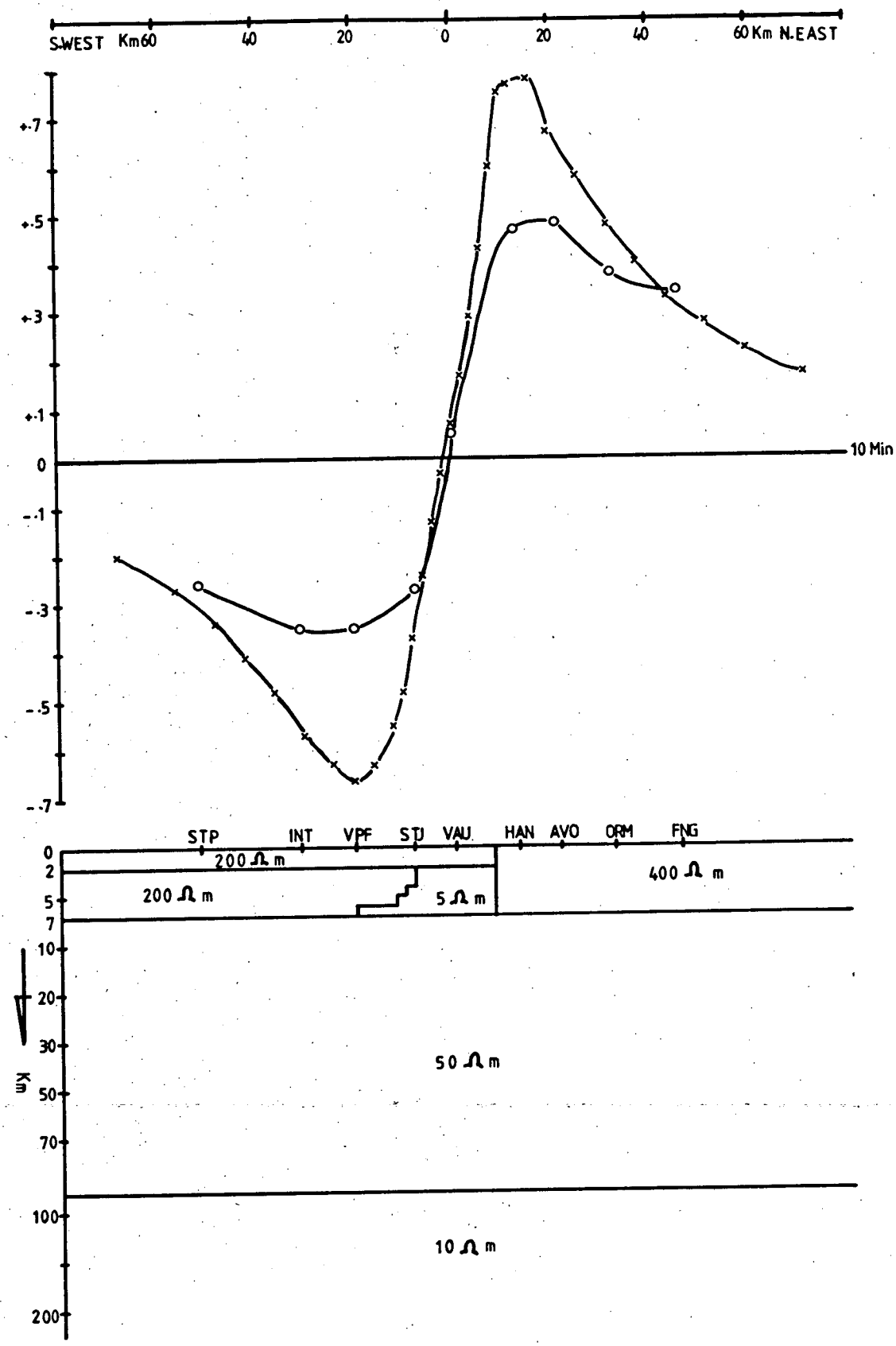

Fig. 5.14 Comparison of model (crosses) and difference (circles) in-phase results at period of 10 minutes and structural view of model 2 (type II).

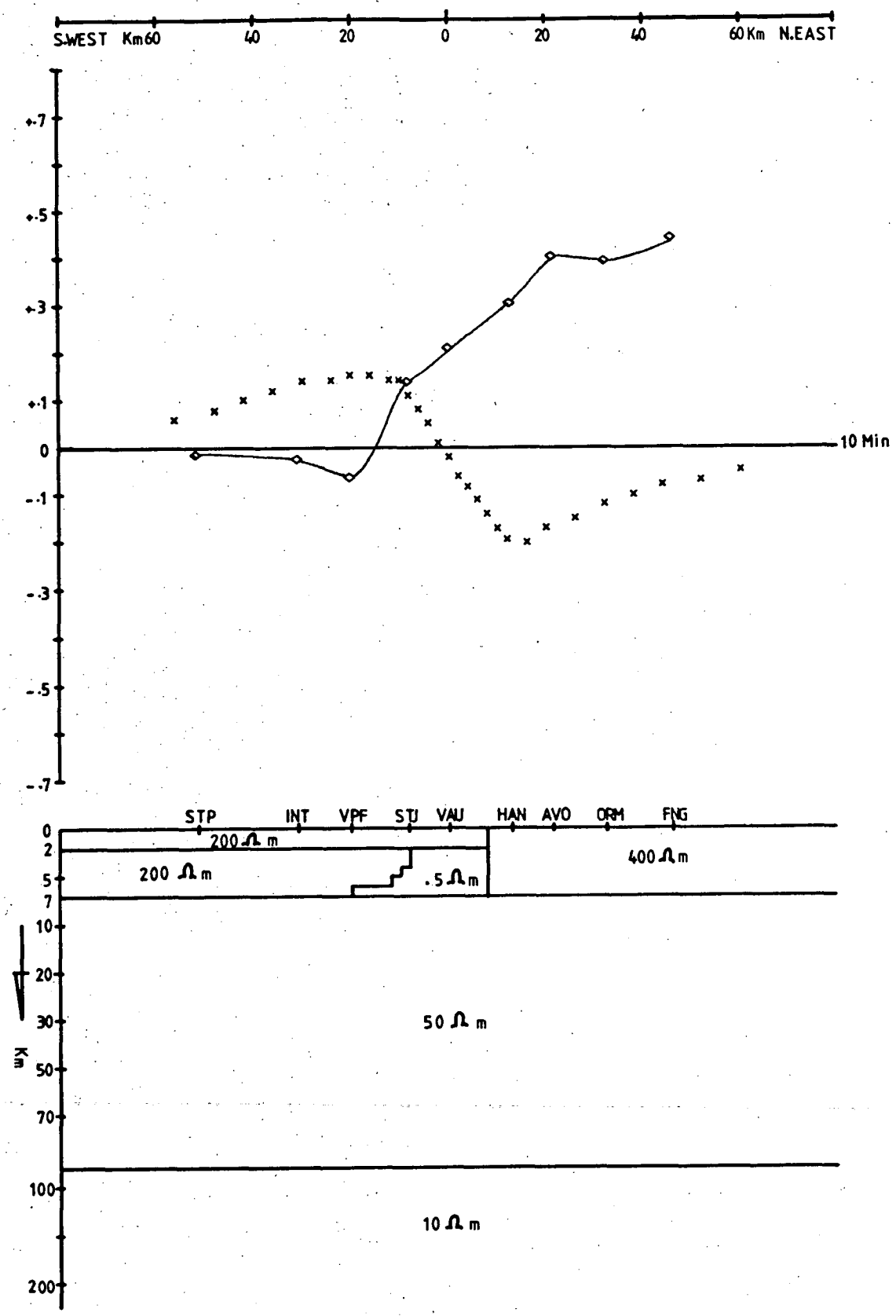

Fig. 5.15 Comparison of model (crosses) and difference (diamond symbols) quadrature results at period of 10 minutes and structural view of model 2 (type II).

the large values of the quadrature components of the model seem to be due to the presence of highly conducting oceans. To increase the in-phase and to decrease the quadrature components of the model it is necessary either to increase the thickness of the conductive zone or to increase the resistivity of the oceans. When the results for a similar model but with no oceans (model 2, Type II) (see figures 5.14 and 5.15) are calculated, the in-phase component is much larger and the quadrature component is of opposite sign. This suggests that a more realistic model would have oceans of higher resistivity. In other words, increasing the size or the thickness of the conductive zone will only satisfy the model for the observed components but not for the difference components. Therefore a model with an ocean of higher than true resistivity was tried. One justification for this is that the coastline is not parallel to the anomaly and therefore the oceans will have less effect than indicated by a strictly two-dimensional model.

Figures 5.16 and 5.17, show the in-phase and quadrature components for model 3 and the comparison between the observed and the model (Type I) results. In general the structure of the model is similar to that of previous models. The only difference between these models is that the resistivity of the oceans has been changed to 1 Ω m. Model 3 reveals that by changing the resistivity of the oceans significantly different results occur. Both the in-phase and quadrature components of the model change quite dramatically. The in-phase components are now slightly too large on the east side but fit reasonably well on the west side. The quadrature, on the other hand, almost fits the observed results. A better fit of the data to model Type I could have been obtained if the resistivity of the oceans had been changed to a value between 0.3 Ω m and 1 Ω m. However the difference data do not fit model 2 of Type II (see figures 5.14 and 5.15) which contains no oceans, so simply changing the ocean resistivity is not sufficient. These models imply, therefore, that the thickness of the conductive zone is probably less than 5 km.

The next models tried, i.e. models 4 and 5, are shown in figures 5.18 and 5.19 and figures 5.20 and 5.21 for the in-phase and quadrature components of the observed and difference components, respectively. The thickness of the conductive zone here is reduced to 3 km while the resistivities of the conductive zone and the surrounding regions are

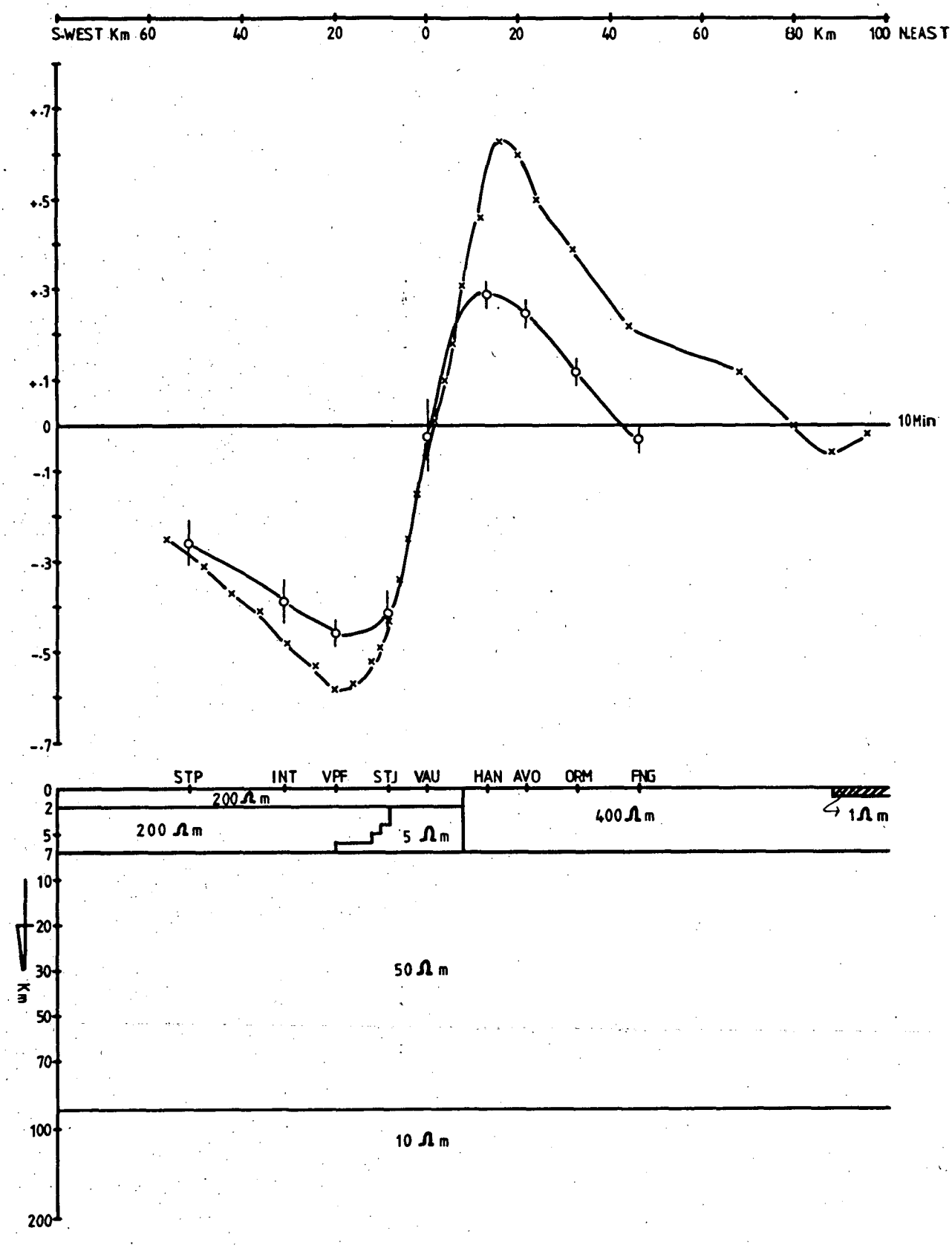

Fig. 5.16 Comparison of model (crosses) and observed (circles) in-phase results at period of 10 minutes and structural view of model 3 (type I).

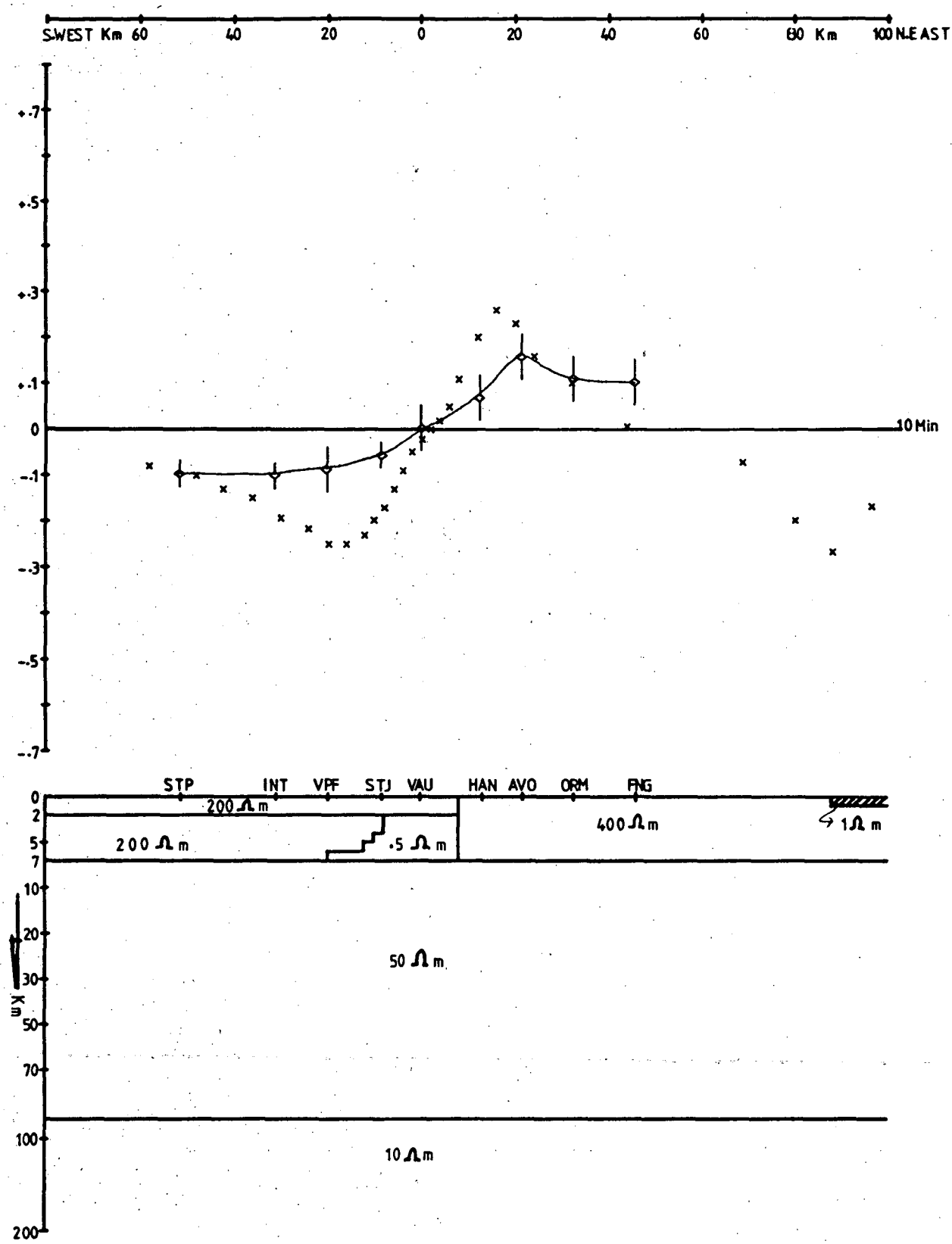

Fig. 5.17 Comparison of model (crosses) and observed (diamond symbols) quadrature results at period of 10 minutes and structural view of model 3 (type I).

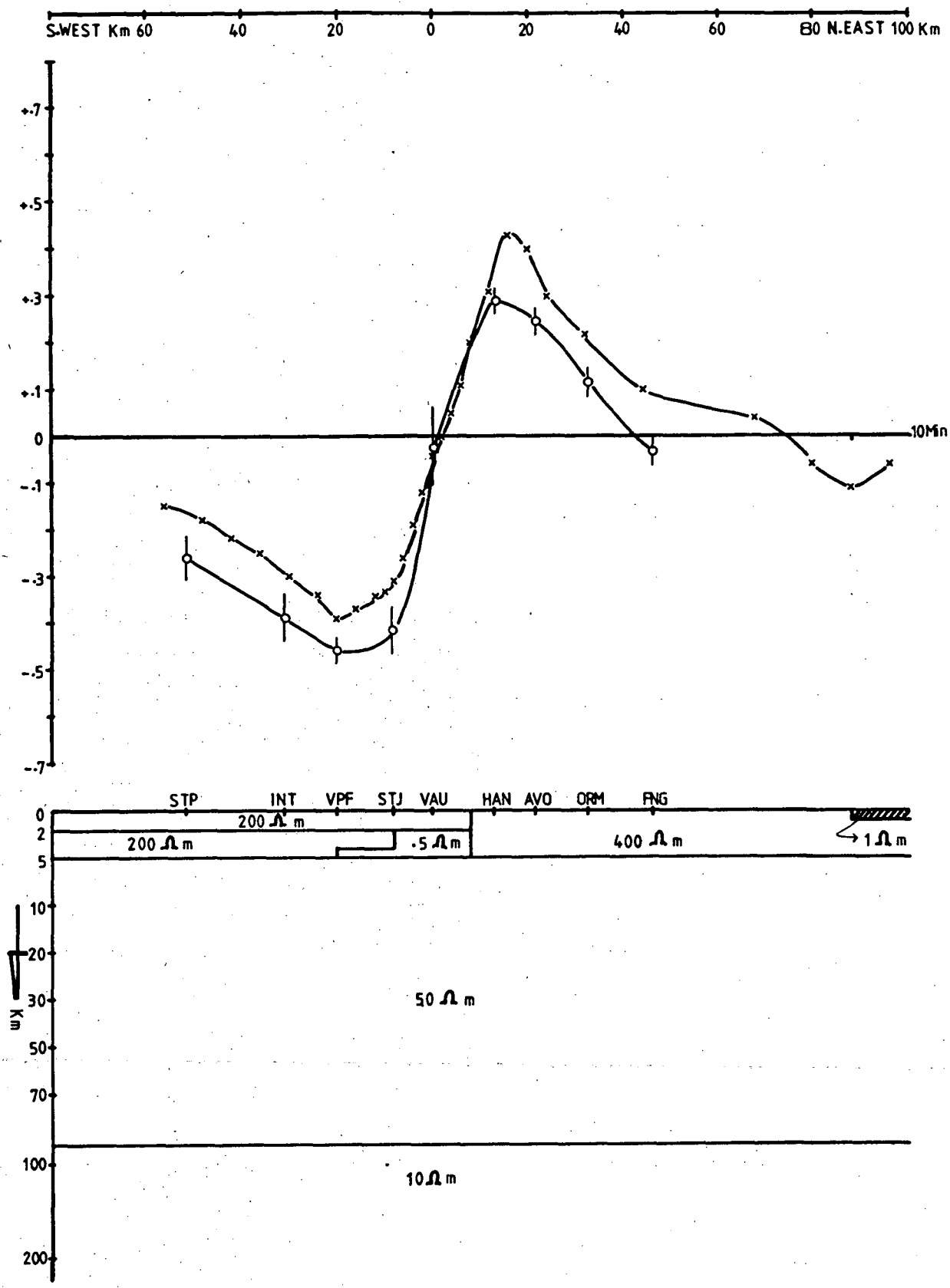

Fig. 5.18 Comparison of model (crosses) and observed (circles) in-phase results at period of 10 minutes and structural view of model 4 (type I).

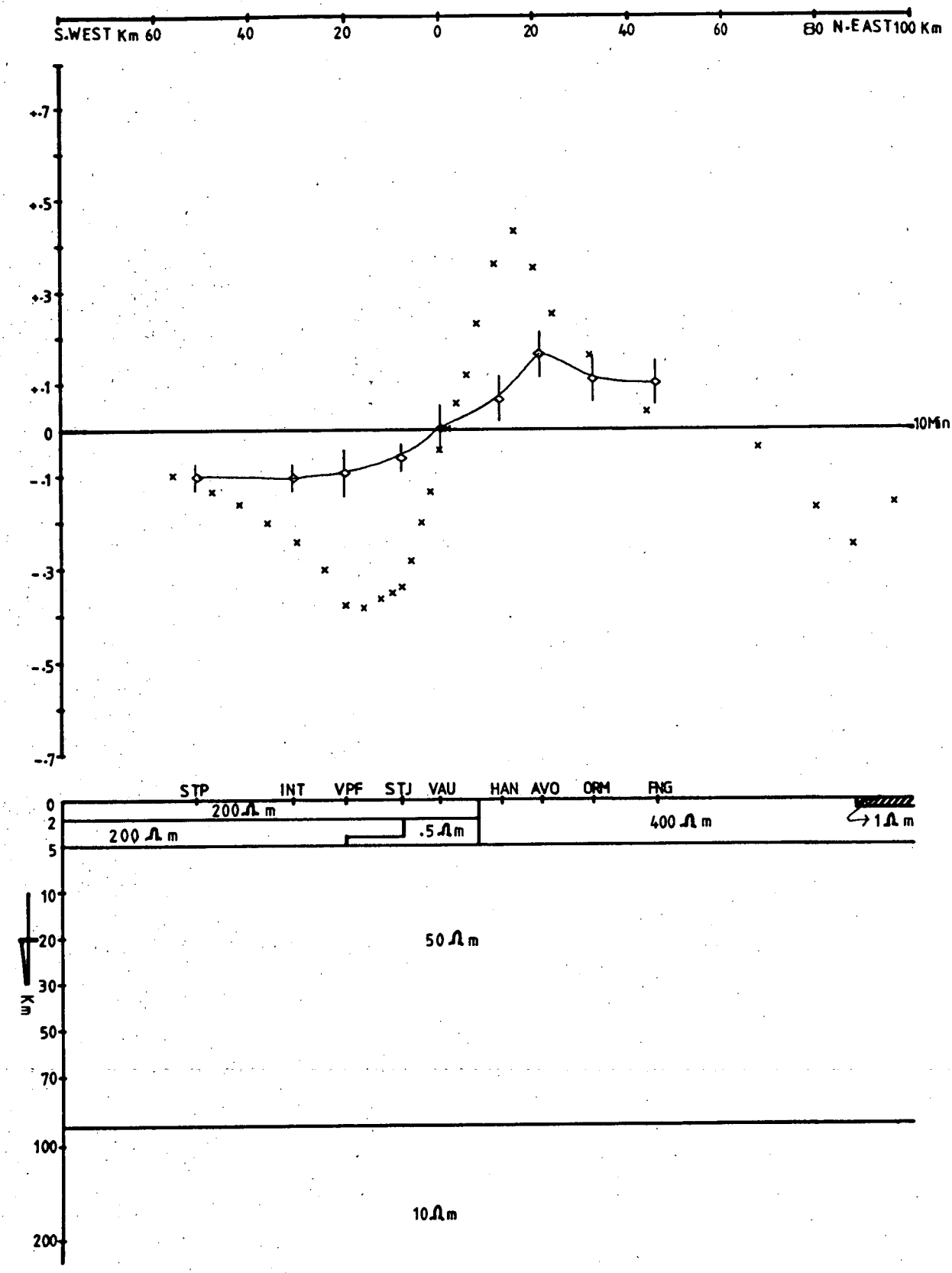

Fig. 5.19 Comparison of model (crosses) and observed (diamond symbols) quadrature results at period of 10 minute and structural view of model 4 (type I).

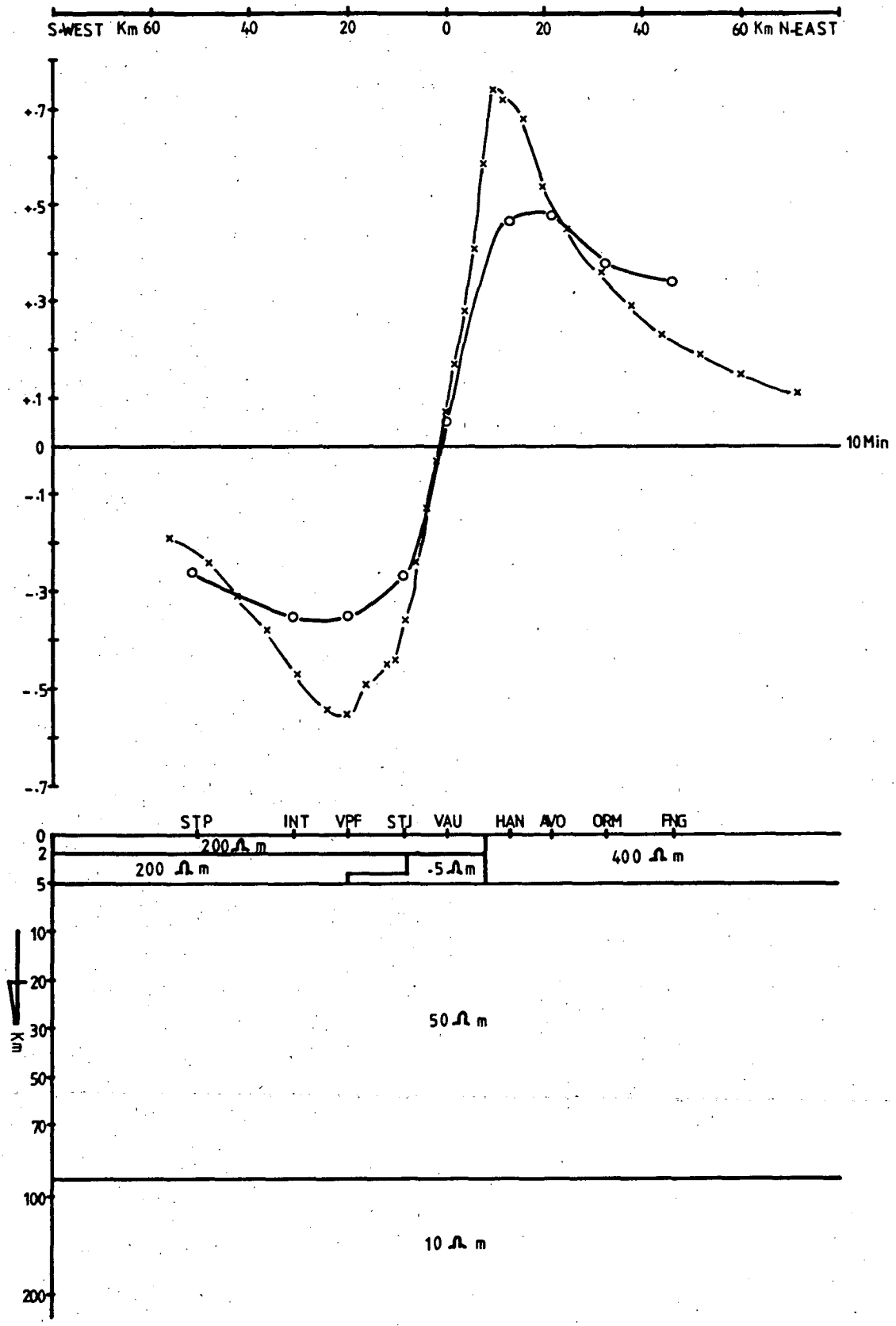

Fig. 5.20 Comparison of model (crosses) and difference (circles) in-phase results at period of 10 minutes and structural view of model 5 (type II).

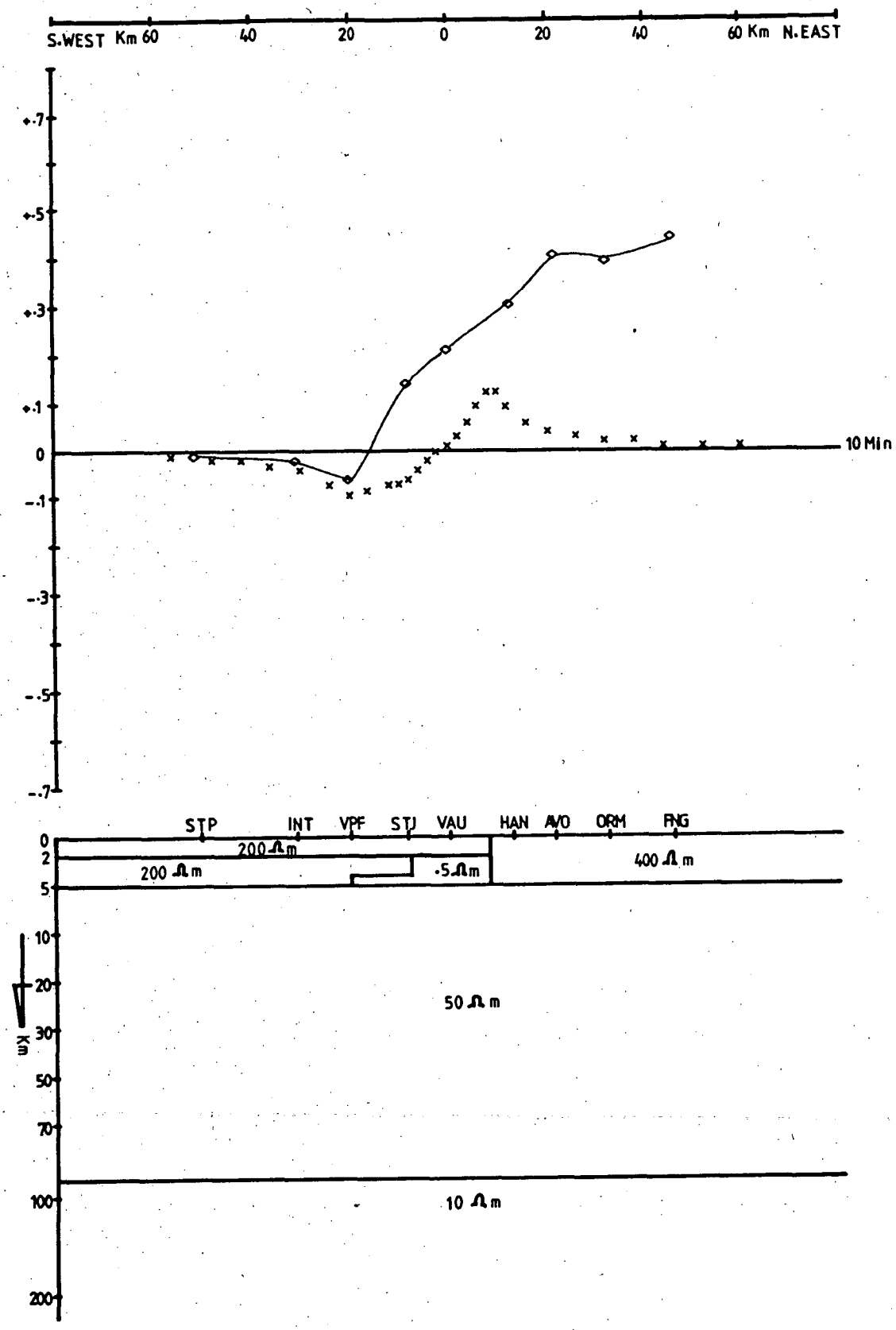

Fig. 5.21 Comparison of model (crosses) and difference (diamond symbols) quadrature results at period of 10 minutes and structural view of model 5 (type II).

similar to the previous models. A comparison of the results illustrated in the above-mentioned figures indicates that the in-phase components for the Type I model (see figure 5.18) fit quite well on both east and west sides. The quadrature components of model 4 (see figure 5.19), however, appear to increase again. The increase in the quadrature components is believed to be due to the effect of reducing the thickness of the conductive zone. On the other hand, the model for difference components (see figure 5.20) shows that the in-phase component is still too large. Reducing the thickness in this model (Type II) only reduces the in-phase component values slightly but for the quadrature component (see figure 5.21) reducing the thickness has a significant effect. The trend of the quadrature components has changed from reverse direction in model 2 (see figure 5.16), where the thickness of the conductive zone is 5 km, to the same direction as the difference results in model 4 (see figure 5.21) where the thickness of the conductive zone is 3 km. Reducing the thickness is therefore considered to be an improvement in the model. The best fit for the in-phase and quadrature components of the observed and model results can probably be obtained by adjusting the thickness of the conductive zone.

The best fitting models, i.e. models 6 and 7 for traverse 3, are shown in figures 5.22 and 5.23 and figures 5.24 and 5.25. The conductive zone has a thickness of 2 km. The model was calculated for periods of 4, 5, 10 and 20 minutes. Four minutes is the shortest period obtained from the observation while 5 minutes is the shortest period for which results of the analogue model are available.

The comparison for the observed in-phase components (see figure 5.22) shows a very good fit, especially on the east side, at all periods. Similar results are also obtained for the difference in-phase components (see figure 5.24) at periods of 10 and 20 minutes while at 5 minutes the in-phase model components to the east are slightly smaller than the difference results. The quadrature components of the Type I model (see figure 5.23) show relatively large discrepancies at periods of 4 and 10 minutes but agree reasonably well at 20 minutes. Meanwhile the quadrature results of the Type II model (see figure 5.25) for 5 minutes is oppositely directed but of very low amplitude. Note the big difference between this result and the result for the Type I quadrature model at 4 minutes (see figure 5.23). Since the difference between the two models is the presence

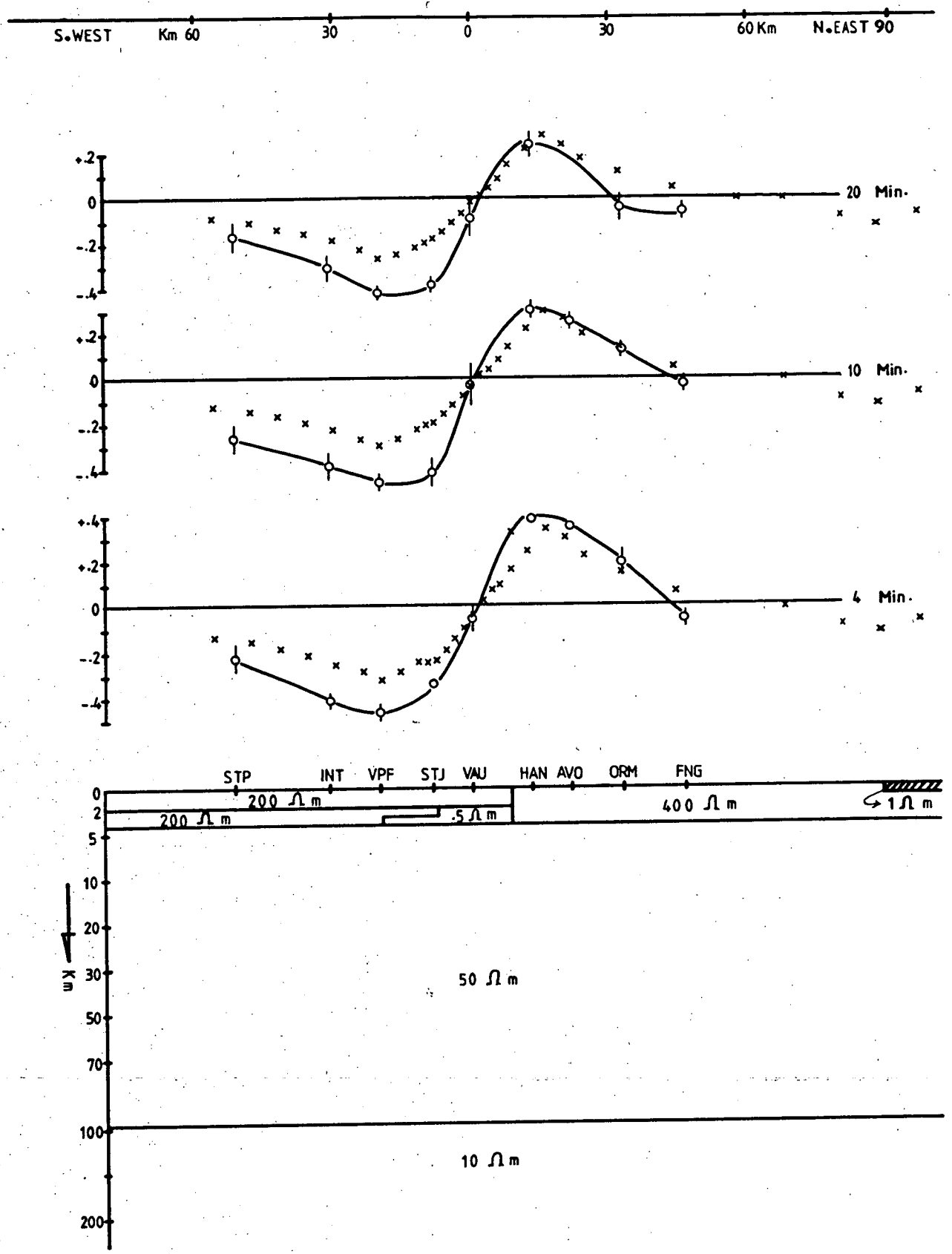

Fig. 5.22 Comparison of model (crosses) and observed (circles) in-phase results at periods of 4,10,and 20 minutes and structural view of model 6 (type I).

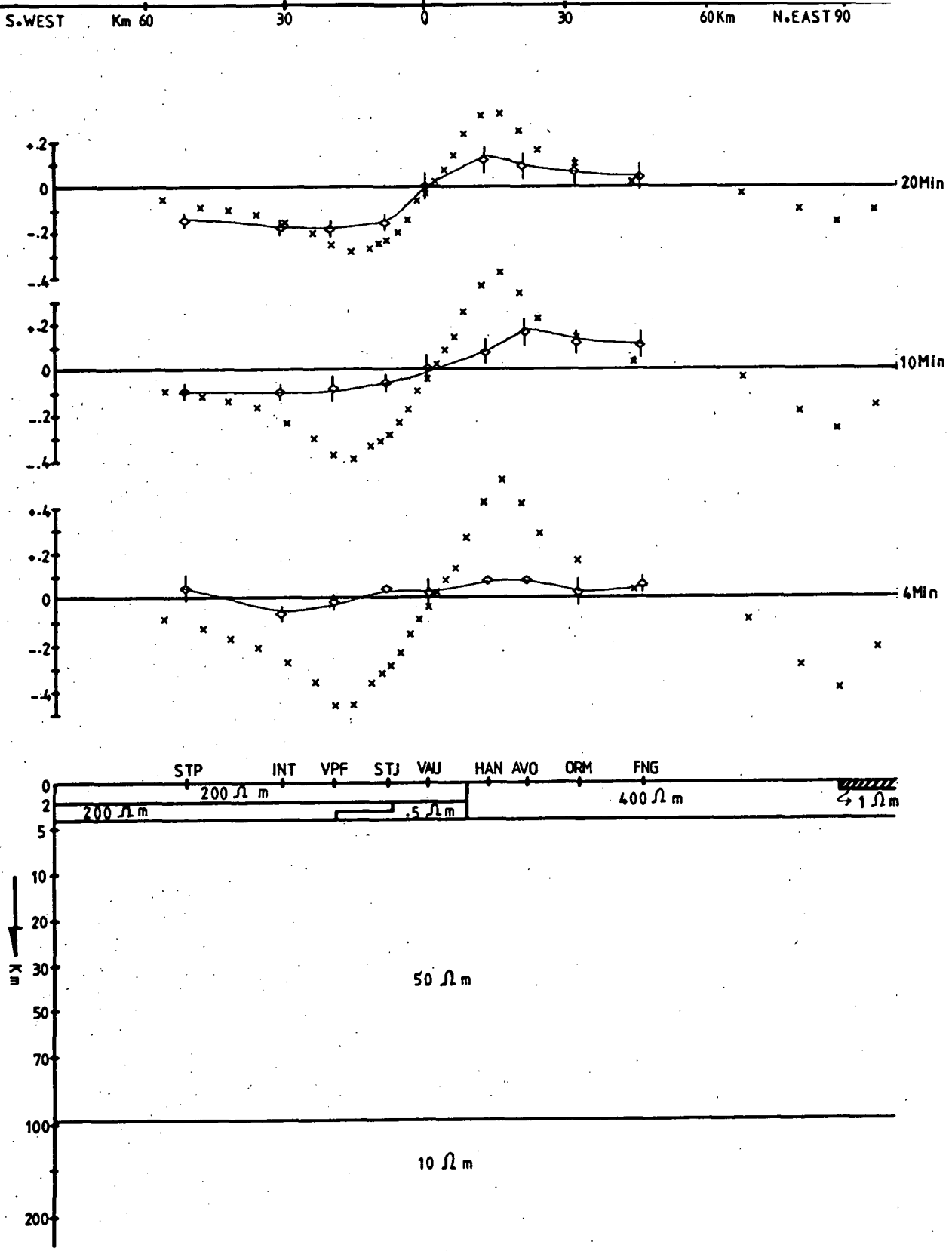

Fig. 5.23 Comparison of model (crosses) and observed (diamond symbols) quadrature results at periods of 4,10,and 20 minutes and structural view of model 6 (type I).

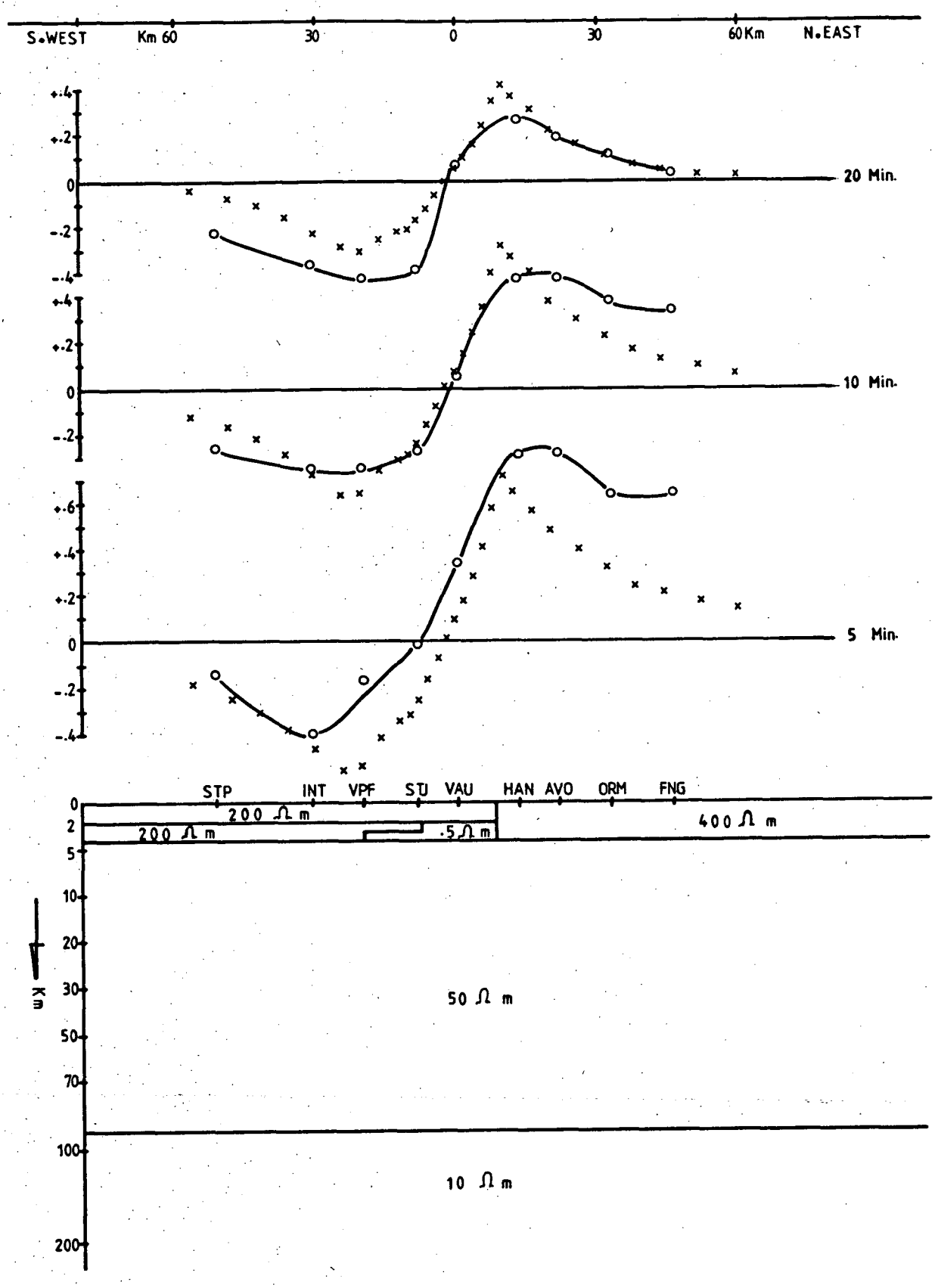

Fig. 5.24 Comparison of model (crosses) and difference (circles) in-phase results at periods of 5,10,and 20 minutes and structural view of model 7 (type II).

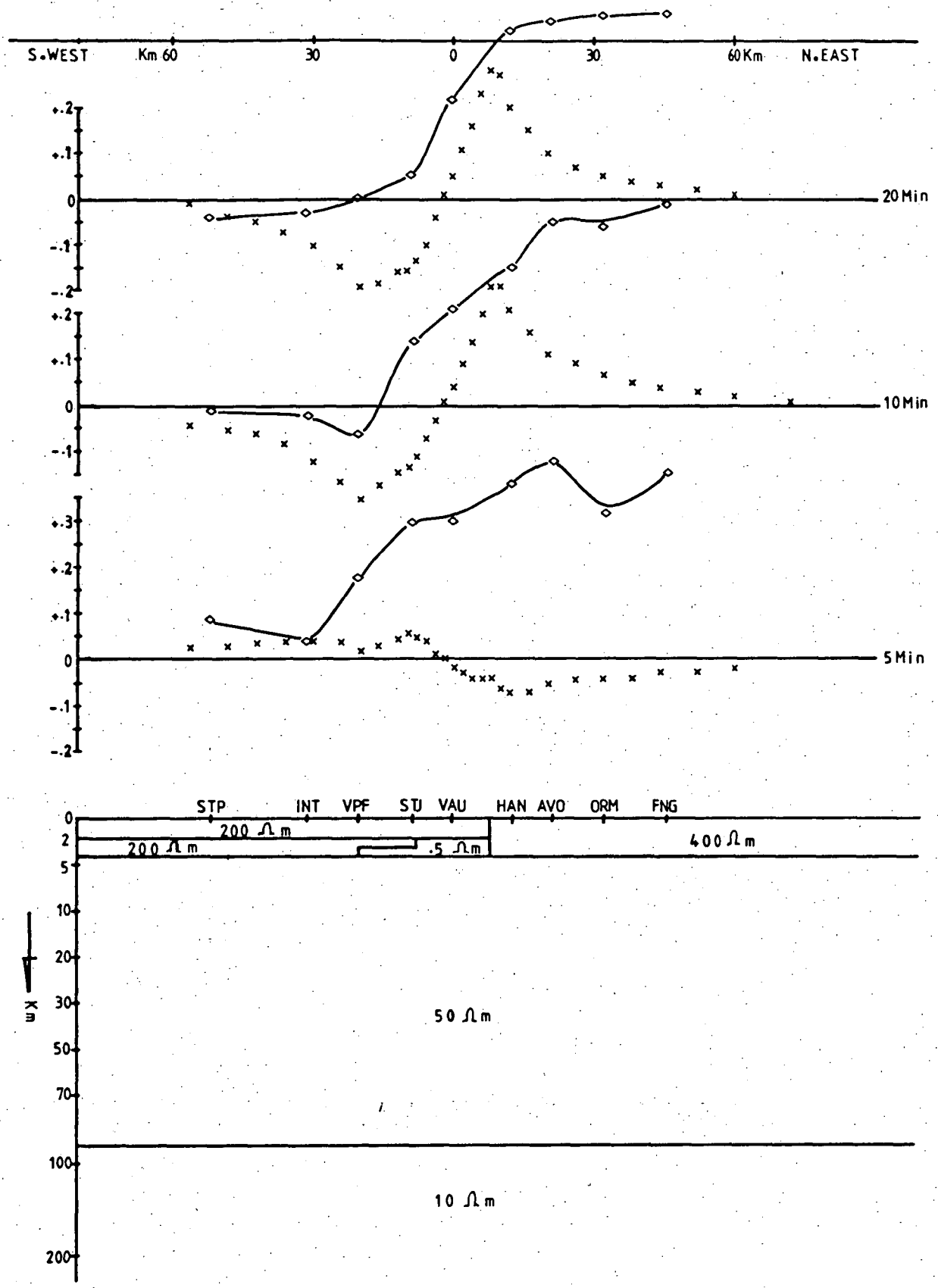

Fig. 5.25 Comparison of model (crosses) and difference (diamond symbols) quadrature results at periods of 5,10,and 20 minutes and structural view of model 7 (type II).

of the oceans (included in the Type I model), the large quadrature values for the Type I model are, therefore, due to the effect of oceans. The small and oppositely directed quadrature components for the Type II model at 5 minutes, on the other hand, seem likely to be due to the fact that for this model the quadrature component changes sign at a period near 5 minutes. The phenomenon of change of sign of the quadrature component with changing period can be seen very clearly in figure 4.11 at MTB. Note that the skin depth for the conductive zone at this period is 6.16 km. At periods of 10 and 20 minutes, however, this quadrature component reverts again to the same direction as the difference results when the skin depth is larger. The broad maximum shown by the quadrature difference component (see figure 5.25) suggests a thicker and more resistive block to the east, but this does not agree with the observed results shown in figure 5.23.

5.2.2 TRAVERSE 2

Traverse 2 (see figure 5.2) is located approximately 50 km north of traverse 3.

In general both of these models have a similar structure to the models for traverse 3. They also have a similar resistivity for the conductive zone, the surrounding regions and oceans. Similarly to traverse 3 the conductive zone is bounded by the much more resistive blocks to the east and west. The conductive zone which is located 2 km below the surface of the earth is believed to dip very gently to the west. It is also believed to occupy a much broader zone to the west than at traverse 3 as indicated by the much broader pattern of the in-phase components for the observed and difference results (see figures 5.3 to 5.6). In the first two models, i.e. models 8 and 9, for the observed and difference components (see figures 5.26, 5.27, 5.28 and 5.29) the conductive zone is 3 km thick. The width of the top and base of the conductive zone is approximately 26 and 68 km, respectively. The oceans which are included in the Type I models are located 132 km to the east and 275 km to the west of the centre of the anomaly, which is approximately at 0 position. In figures 5.26 and 5.27, however, the ocean to the west is not seen because it is located outside the limit of the diagram. Figure 5.26 shows model 8 and a comparison of the in-phase component for the observed and model results

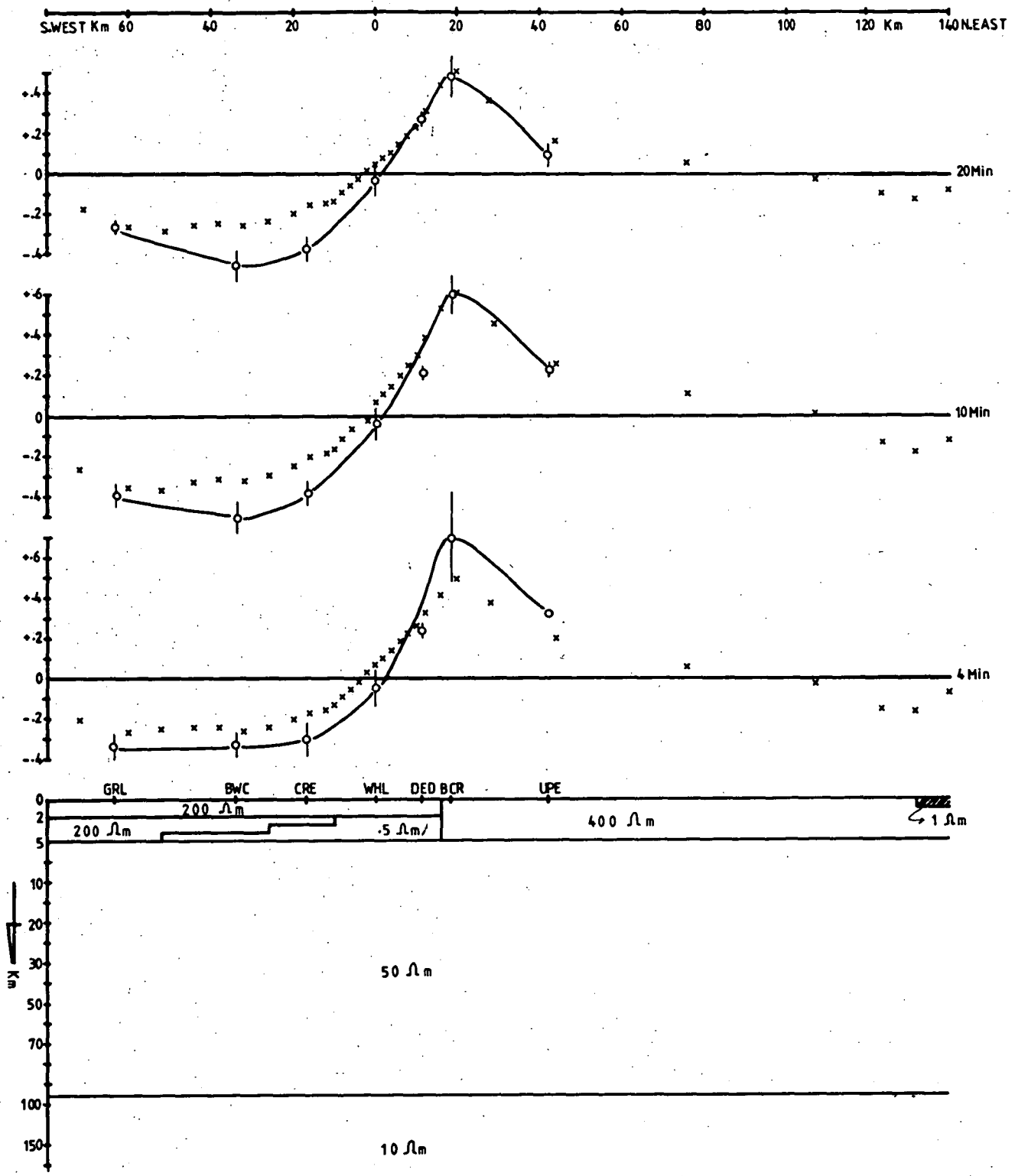

Fig. 5.26 Comparison of model (crosses) and observed (circles) in-phase results at periods of 4,10,and 20 minutes and structural view of model 8 (type I).

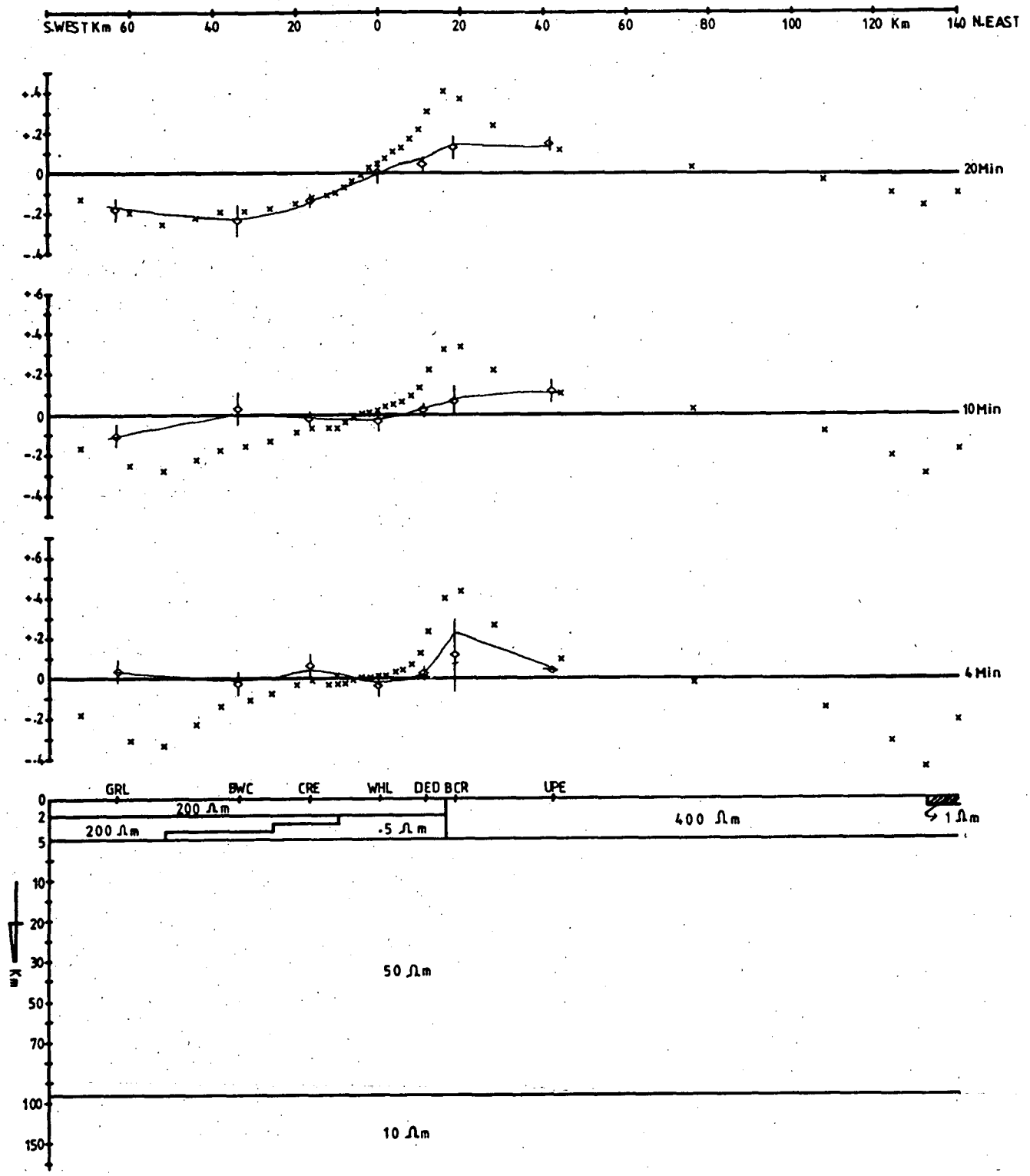

Fig. 5.27 Comparison of model (crosses) and observed (diamond symbols) quadrature results at periods of 4,10,and 20 minutes and structural view of model 8 (type I).

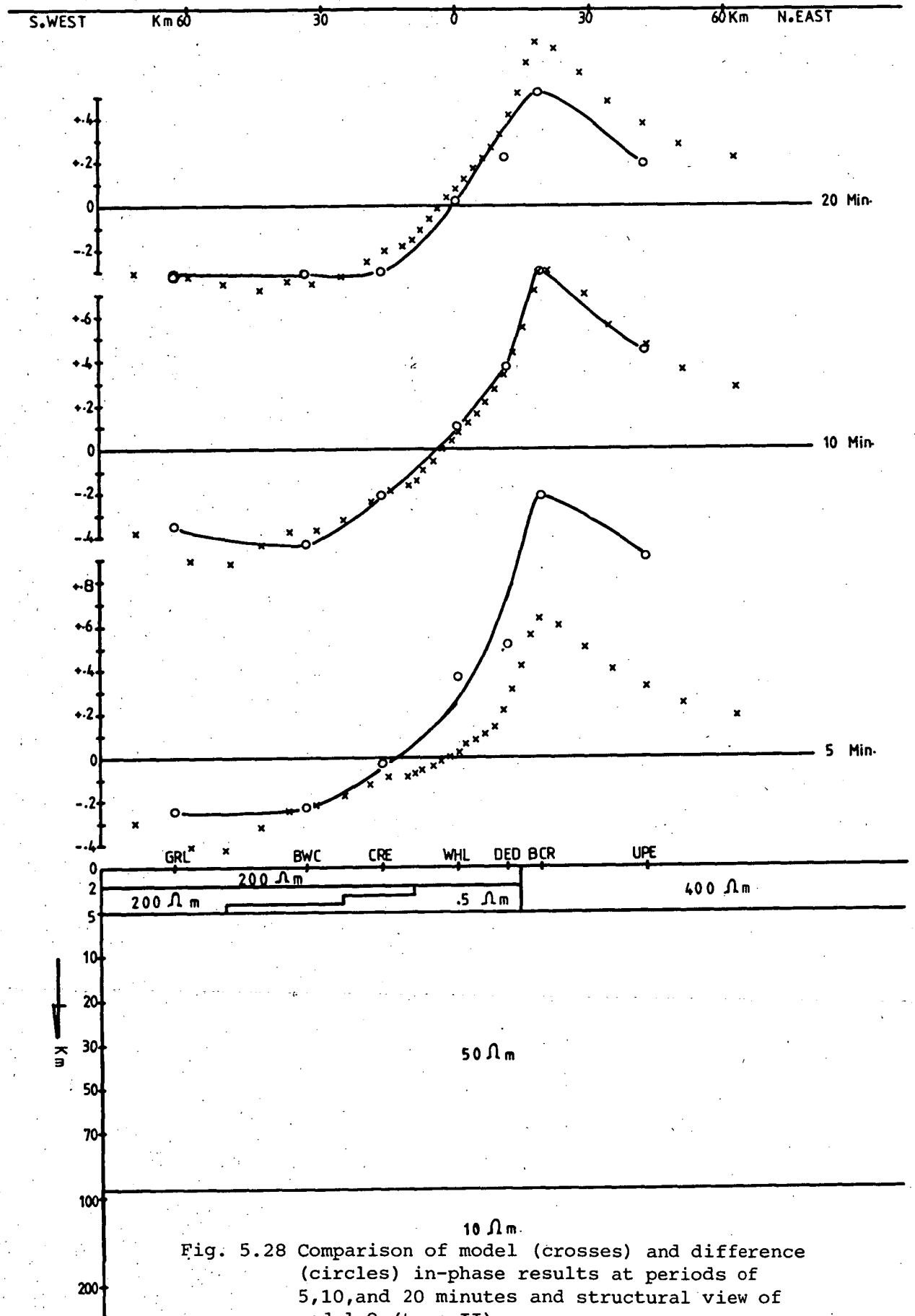

Fig. 5.28 Comparison of model (crosses) and difference (circles) in-phase results at periods of 5,10,and 20 minutes and structural view of model 9 (type II).

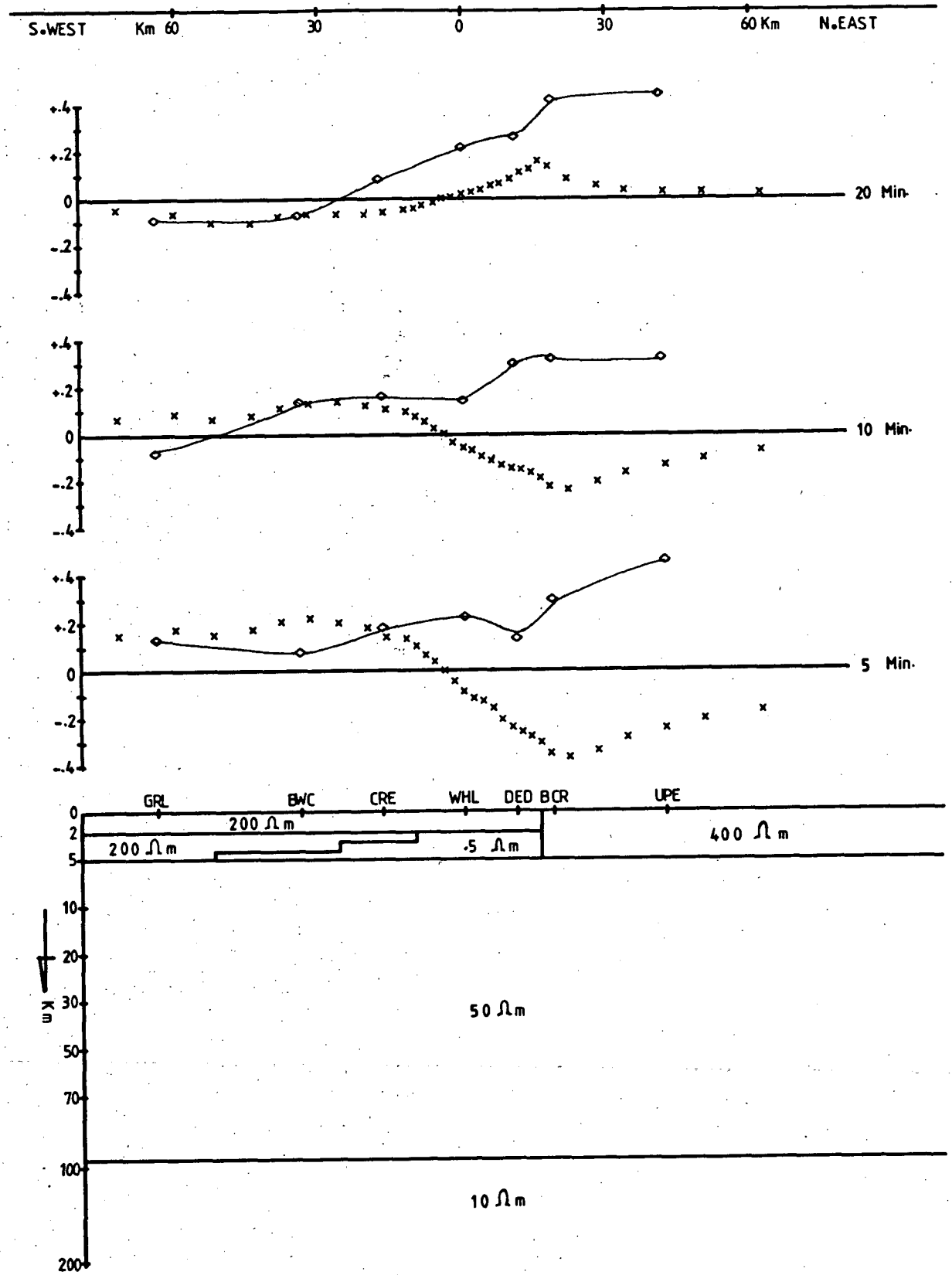

Fig. 5.29 Comparison of model (crosses) and difference (diamond symbols) quadrature results at periods of 5,10,and 20 minutes and structural view of model 9 (type II).

for periods of 4, 10 and 20 minutes, respectively. The model results at 10 and 20 minutes show a good fit to the observed results. A similar comparison is shown in figure 5.28 for the in-phase components of the difference results and the corresponding model (Type II) at the same periods. However, at a period of 4 minutes the Type I in-phase model results are slightly less than the observed ones. Note that the good fits obtained for the observed (Type I) and difference (Type II) models at 10 and 20 minutes, respectively, occur when the skin depth is large, thus implying that the effect of basement is more pronounced here. The skin depth at 5 minutes, on the other hand, is only a few kilometres thus indicating that the smaller in-phase results at 5 minutes, especially on the east side, of the Type II model (see figure 5.28), would be compatible with a less resistive block to the east.

A comparison of the quadrature of the observed and model results is shown in figure 5.27. At periods of 4 and 10 minutes the model responses are much bigger both on the east and west sides compared to the observed results. Note, however, that at 20 minutes the model results agree reasonably well. Again the results are good when the skin depth is large. Similarly, reasonable results are obtained for the Type II model (see figure 5.29) at a period of 20 minutes. But at periods of 10 and 5 minutes the results are very different. They reverse as the skin depth decreases thus implying that the effect of lateral conductivity inhomogeneities in the first few kilometres is more pronounced. The effect of thickness of the conductive zone can also cause the model quadrature results to reverse direction.

Figures 5.30, 5.31 and 5.32, 5.34 show models 10 and 11, which are alternative structures for Type I and Type II models of traverse 2, and a comparison between observed and model results for both in-phase and quadrature components. In these models the thickness of the conductive zone is reduced to 2 km. The resistivities of the conductive zone, surrounding regions and oceans are kept the same as in the previous models. The effect of reducing the thickness of the conductive zone is clearly seen both in the in-phase and quadrature components of the Type I model. At all periods the in-phase components of the model (Type I) are much smaller than observed results while the quadrature results, especially at 4 and 10 minutes, indicate only a slight increase compared to model 8 (see figure

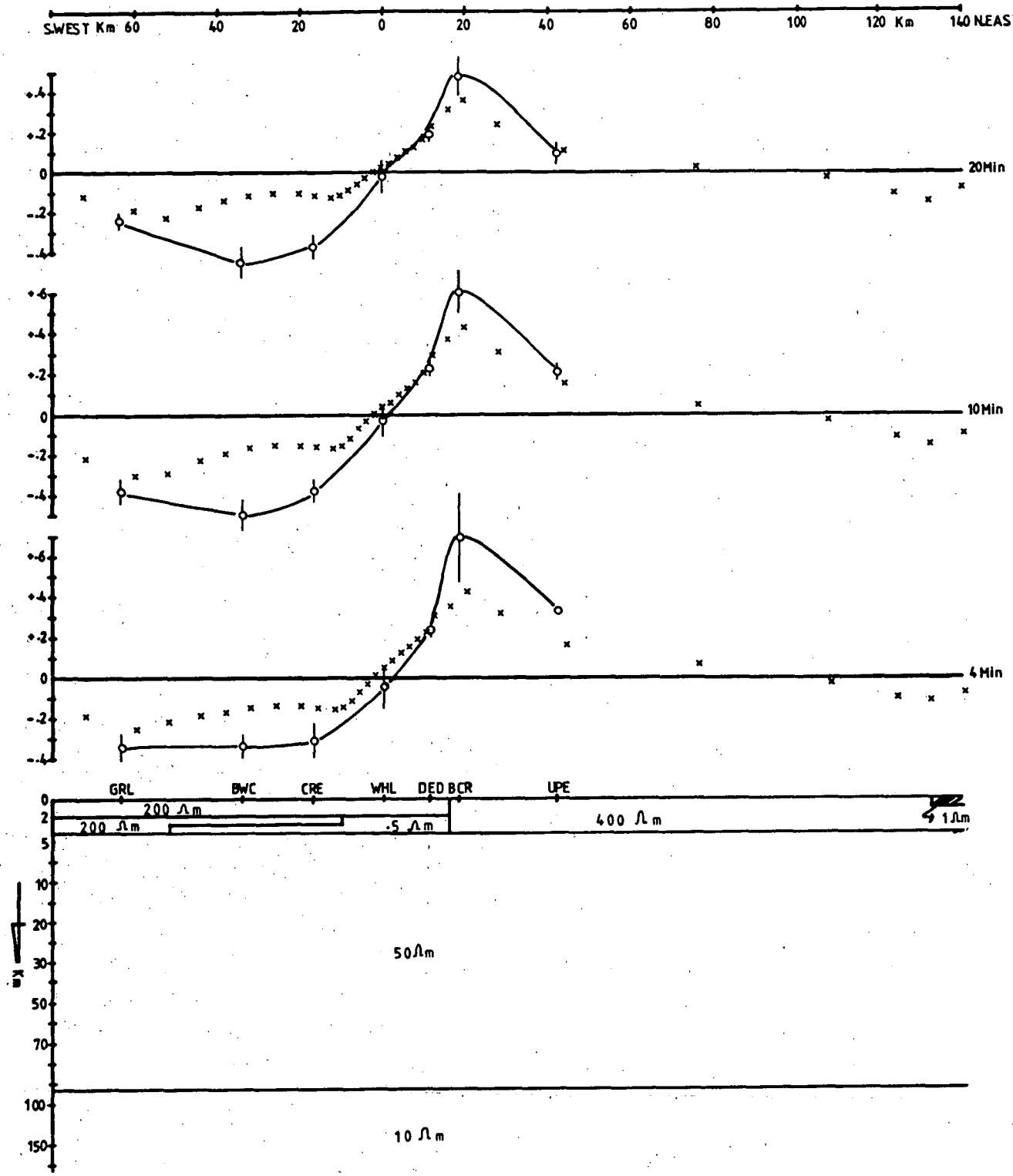

Fig. 5.30 Comparison of model (crosses) and observed (circles) in-phase results at periods of 4,10,and 20 minutes and structural view of model 10 (type I).

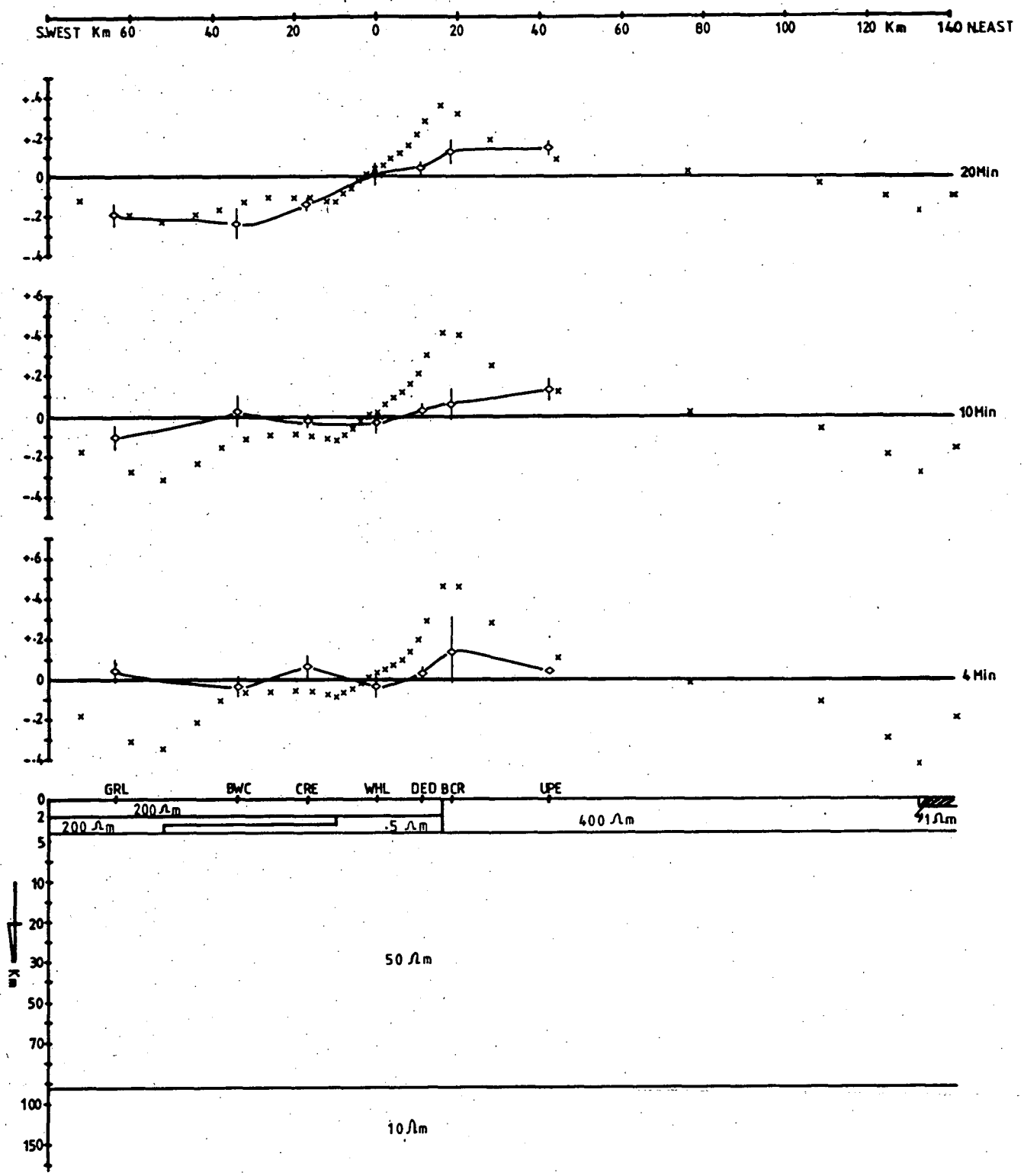

Fig. 5.31 Comparison of model (crosses) and observed (diamond symbols) quadrature results at periods of 4,10,and 20 minutes and structural view of model 10 (type I).

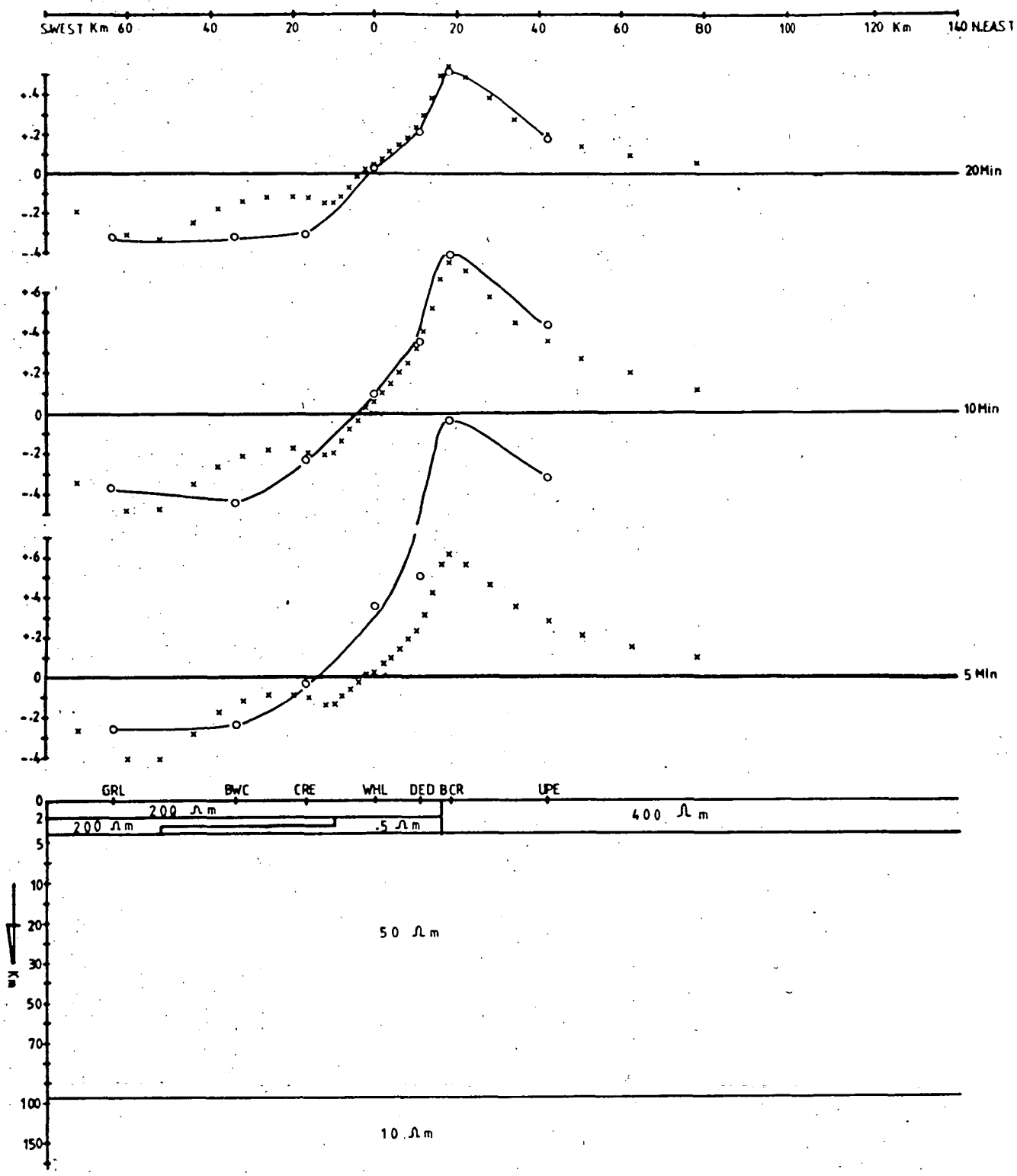

Fig. 5.32 Comparison of model (crosses) and difference (circles) in-phase results at periods of 5,10,and 20 minutes and structural view of model 11 (type II).

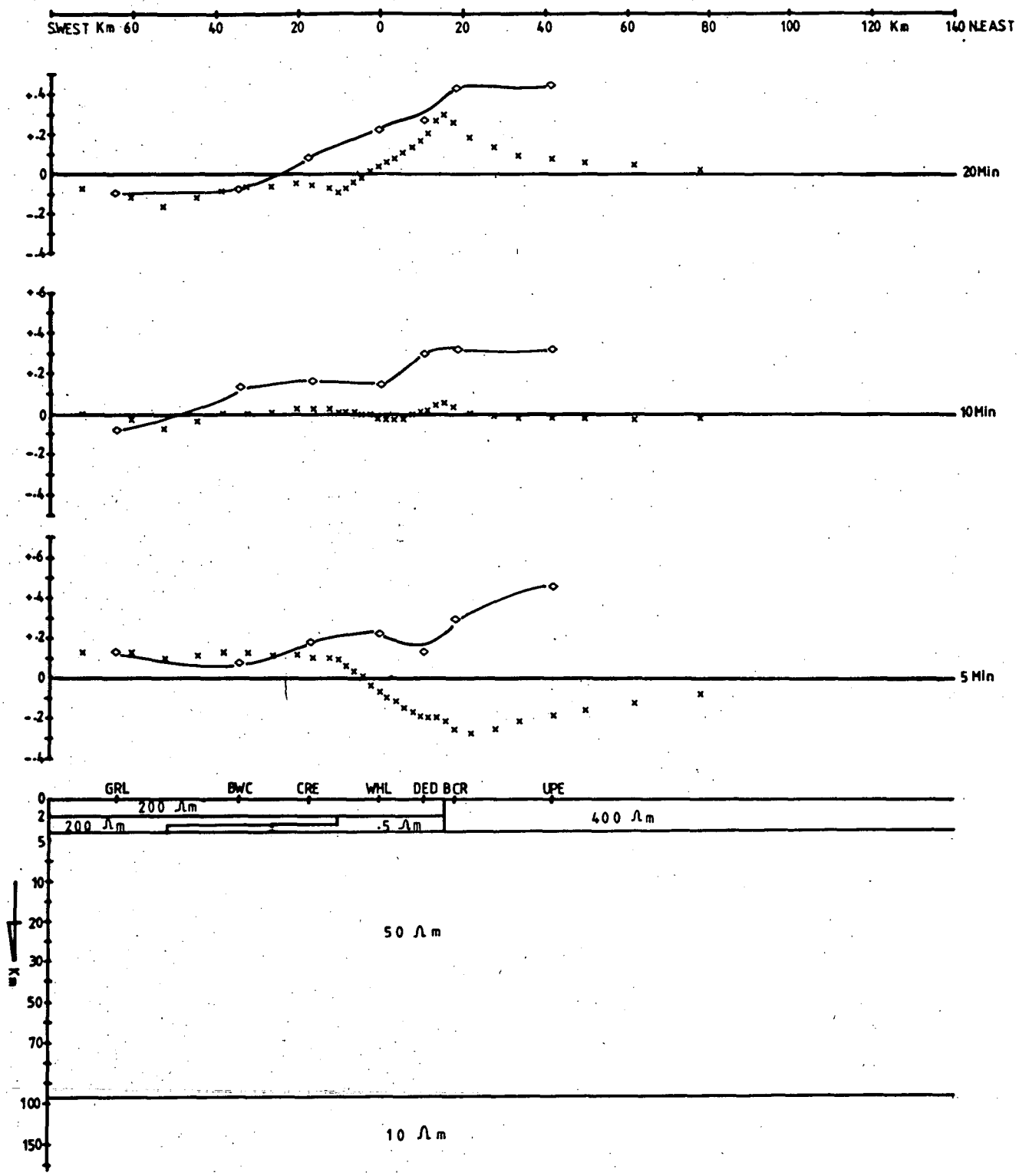

Fig. 5.33 Comparison of model (crosses) and difference (diamond symbols) quadrature results at periods of 5,10,and 20 minutes and structural view of model 11 (type II).

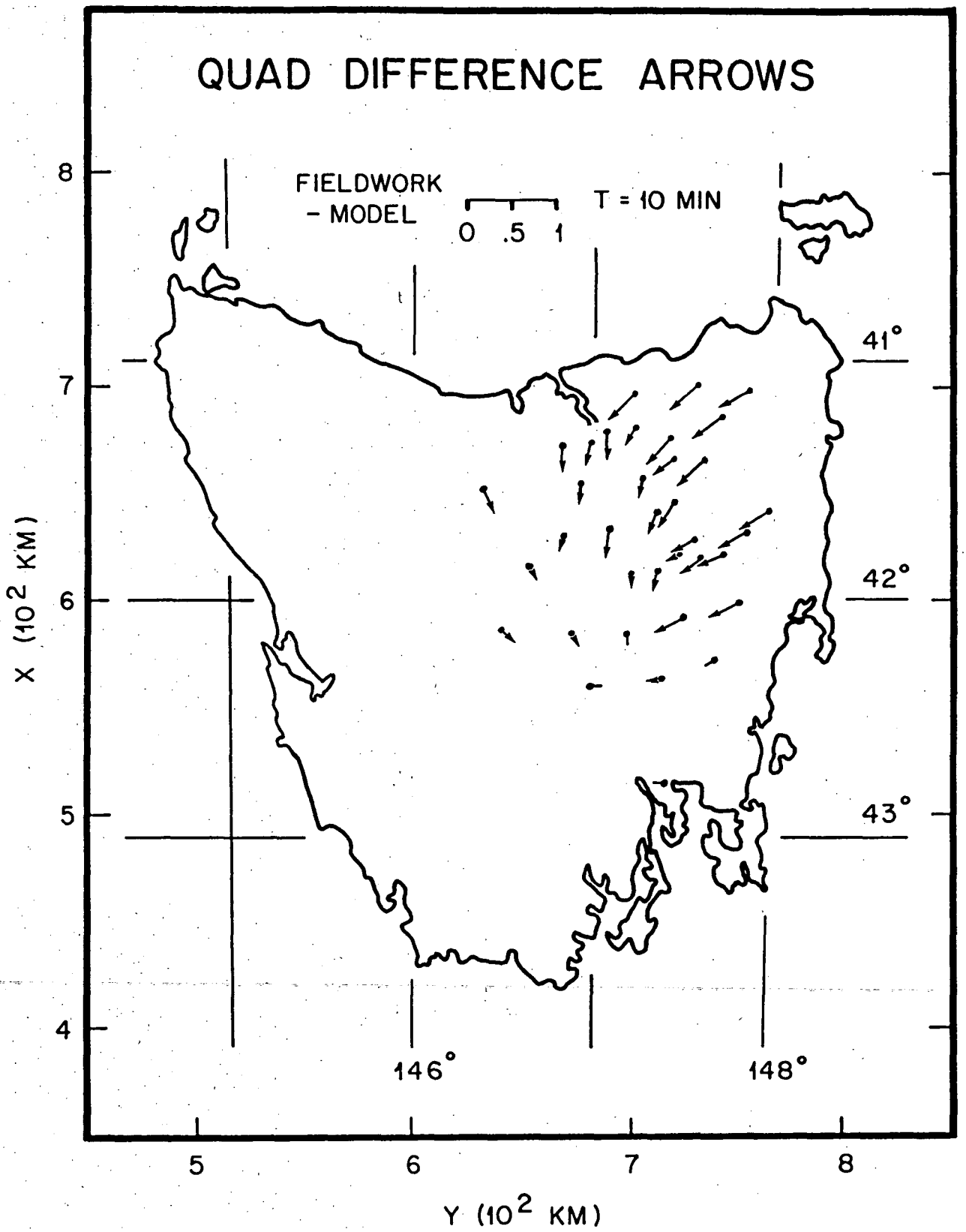

Fig. 5.34 Distribution of quadrature difference induction arrows at period of 10 minutes. (From Dosso, in press).

5.27) but at 20 minutes the result again are reasonable. The results for the in-phase component of the Type II model (see figure 5.32), however, give a better fit at periods of 10 and 20 minutes compared to model 9 (see figure 5.28) and indicate almost no change at a period of 5 minutes. As expected, by reducing the thickness of the conductive zone the quadrature components of the Type II model (see figure 5.33) show a large decrease in amplitude and a change in orientation especially at 10 minutes period. It also gives a better result at 20 minutes while at 5 minutes the result is still in the opposite direction. The quadrature difference induction vectors which are obtained from the Dosso's analogue model study are shown in figure 5.34 (H.W. Dosso, personal communication). The figure indicates that the arrows appear to have little to do with the conductivity anomaly. Dosso's values appear to exaggerate the coast effect because Tasmania has a higher conductivity than that used in the analogue model. The above model results (10 and 11) are, therefore, considered satisfactory but are inferior to those of models 8 and 9.

The error bars, which are plotted on all of the observed components results, were calculated by

$$\sigma_c = \sqrt{\sigma_{m(A)}^2 \cos^2 52^\circ + \sigma_{m(B)}^2 \sin^2 52^\circ} \qquad \ldots\ldots\ldots (5.2)$$

where σ_c is the standard deviation of the components, $\sigma_{m(A)}$ and $\sigma_{m(B)}$ are the standard deviation of the mean, similar to those determined in section 4.3.1, for A and B transfer function values, and 52° is the bearing of the traverse perpendicular to the strike of the anomaly measured from magnetic north.

5.3 GEOLOGIGAL SETTING

The differences in the geological environment to the east and west of the Tamar River have been discussed in detail by Williams (1979a).

To the east, the area is covered by thick folded Siluro-Devonian Mathinna beds which in some places are intruded by Devonian-Carboniferous granites. The sediments which consist of interbedded turbidite quartz-wacke and mudstones reflect a deep water depositional environment (Williams, 1979a). The thickness of these beds, interpreted from a gravity survey in the Scottsdale area, is about 4 km (Symonds, 1971, p. 32). This thickness is similar to the thickness of the resistive block to the east used during the modelling.

To the west and south-west, on the other hand, the area is generally dominated by Precambrian and Cambrian rocks. These rocks outcrop from Beaconsfield westward and include a dominantly quartzite-phyllite Precambrian sequence followed by a largely volcanic Cambrian sequence and a carbonate-dominated Ordovician section with some basal conglomerates and sandstones. The detailed distribution can be seen in Williams (1979b). The Precambrian rocks are also believed to act as the basement for the whole region. In the Midlands there is a basin-like structure mainly covered by Jurassic dolerite up to 330 m thick (Hinch, 1965, p. 22). The dolerite intrudes the sediments of Permian and Triassic age which probably overlie the older sedimentary sequences though little is known of the deeper structure. The Permian and Triassic sediments which crop out along the Great Western Tiers have a thickness of approximately 1300 m (Hinch, 1965, p. 21).

Figures 5.35 and 5.36, show the distribution of the Tertiary, Triassic and Permian rocks in Tasmania and distribution of the m-v stations across different geological environments. The Tamar Fracture Zone marks the junction between the two quite different types of geology (Williams, 1979a). The zone has been assumed by Williams (1979a) to continue to the south-east passing between Maria Island and Hobart. This agrees very well with the approximate strike of the anomaly determined from the short period induction arrows (see fig. 5.2).

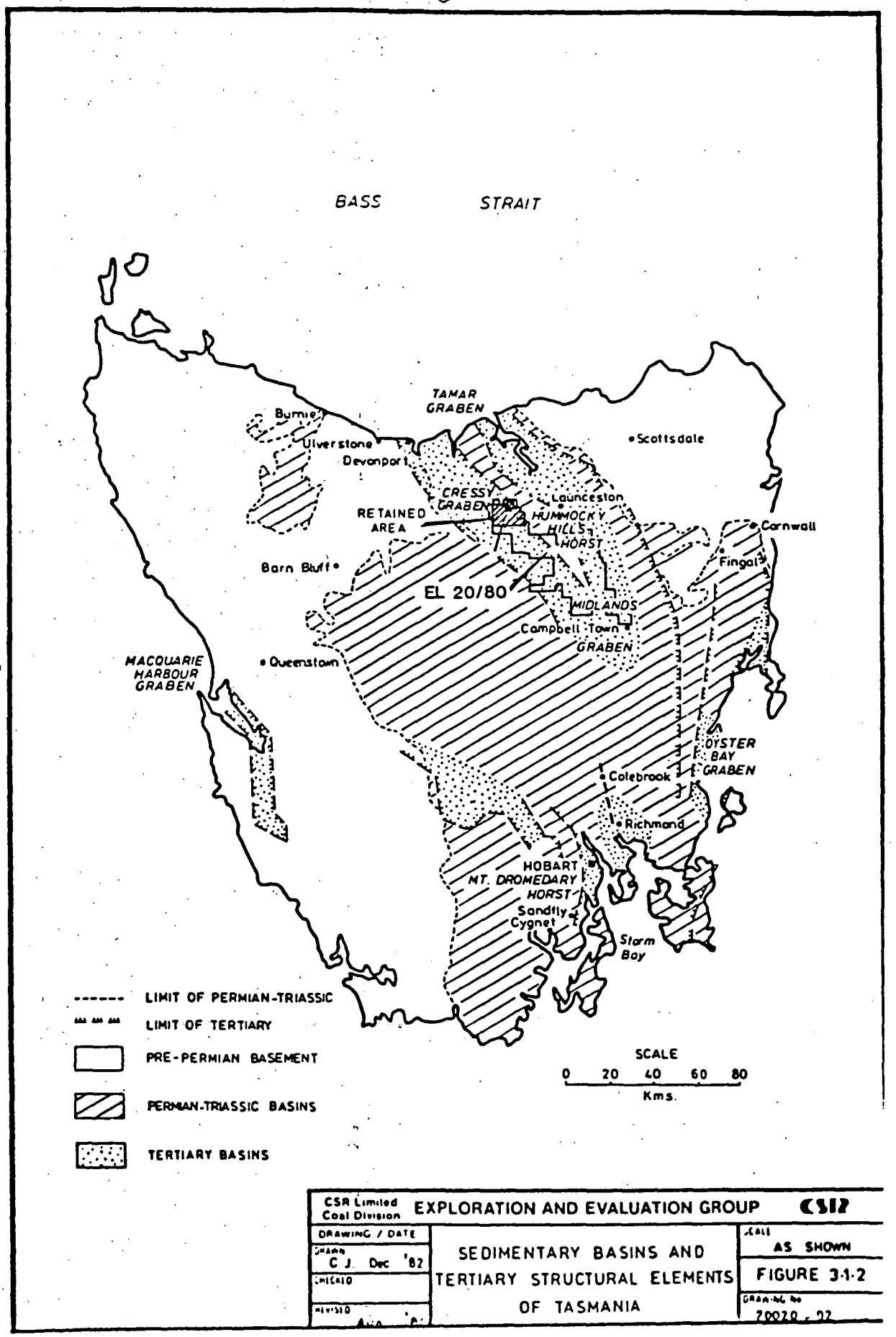

Fig. 5.35 Distribution of the Tertiary, Triassic, and Permian Rocks in Tasmania.

(From Carr, 1984).

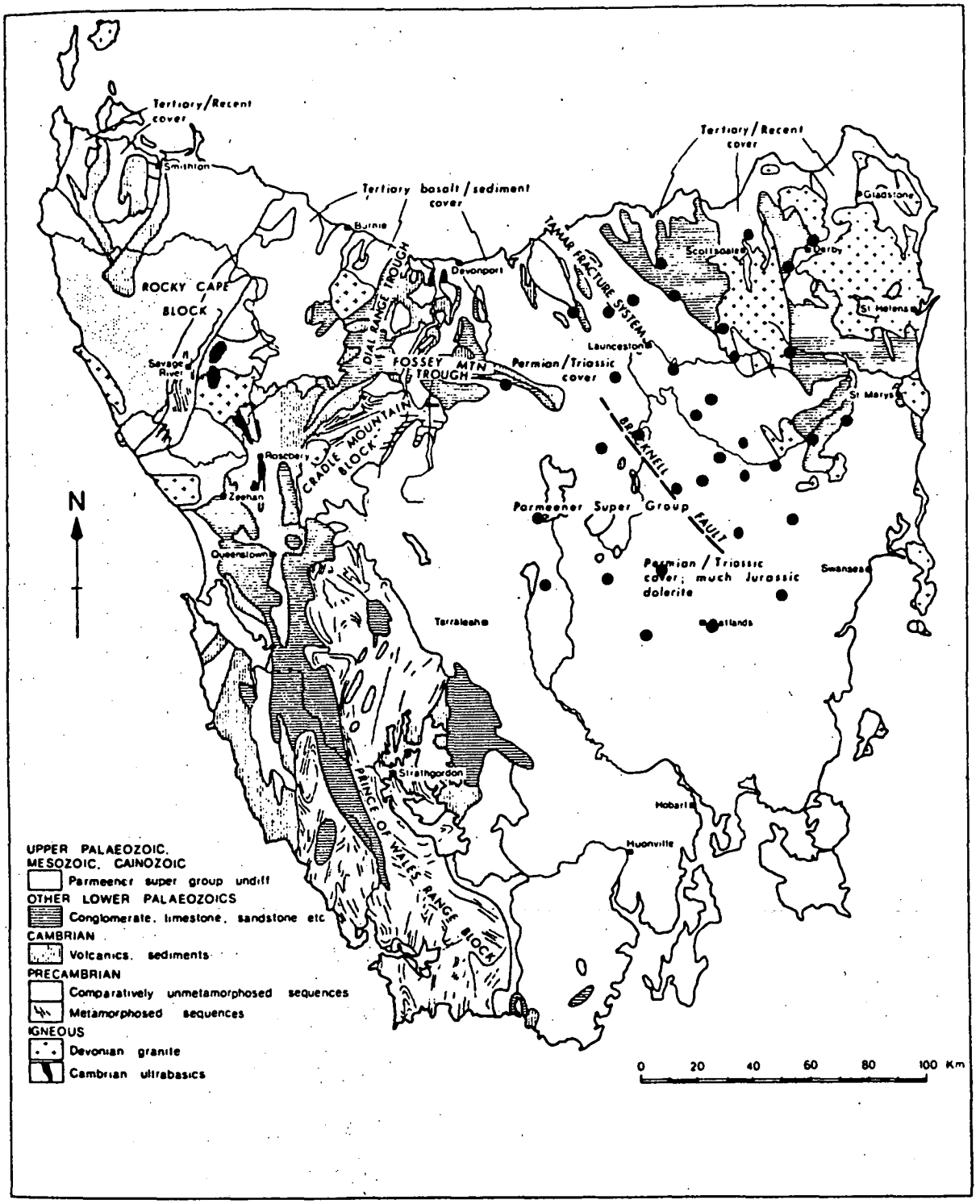

Fig. 5.36 Distribution of m-v stations across different geological environments.

(simplified geology from Leaman, 1973)

5.4 GEOPHYSICAL SIGNIFICANCE OF THE CONDUCTIVITY MODEL

Models 6, 7, 8, 9, 10 and 11, show progressively more probable underground conductivity structures in Tasmania. The conductive zone which has a resitivity of 0.5Ωm appears to have a thickness of about 2 to 3 km.

It is hard to explain the presence of the highly conductive zone that is associated with the occurrence of the Tamar Fracture Zone since it is located at very shallow depth, i.e. only 2 km from the surface. Rooney and Hutton (1977), for example, stated that solid conduction in dry rocks seems unlikely to explain such anomalies since the zone is very conductive. Similarly the idea that the anomaly could be associated with partial melting can be rejected since temperatures in excess of 700°C at only few kilometres depth are required to generate such a high conductivity and there is no evidence of thermal or volcanic activity in the area at present or since the middle Tertiary. The most likely cause of the highly conductive zone along the Tamar Fracture Zone is, therefore, a deep fault zone or extensive fracturing. The presence of this zone may facilitate the movement of electric current in electrolytic solutions. Hermance (1973) gave evidence from his laboratory experiments that water which saturates porous or cracked rocks has a very significant effect in lowering the resistivities of those rocks. A gravity survey in the Tamar graben area, conducted by Leaman et al. (1973), and Longman and Leaman (1971), revealed several major faults in that area. These faults formed after the displacement of the fracture zone and perhaps indicate that the older fracture zone continued to be a major structural control in subsequent geological time, and further, that not all the fracturing is associated with the initial large displacement.

It is possible that the response of the conductive zone may be enhanced if it forms part of a conducting loop in which current flows through the oceans around north-eastern Tasmania and then along the Tamar Fracture Zone. It is impossible to verify or disprove such a hypothesis with the presently available data. The pattern of the highly conductive anomaly, which runs approximately along the fracture zone, and the assumption by Williams (1979a) that the fracture zone continues to the south-east, may support this idea. A similar interpretation was made by

Porath and Dziewonski (1971) to explain the Eksdalemuir anomaly in Scotland. In this case, however, two-dimensional modelling of the Jones and Pascoe type would not be appropriate to analyse the structure of the conducting body.

CHAPTER 7

CONCLUSION

It is now confirmed that the highly conductive anomaly which was first discovered by earlier workers in the Tamar Graben area extends to the south-east coinciding with the Tamar Fracture Zone.

The anomaly is due to the concentration of current in the highly conductive structure along the fracture zone and this is clearly shown by the reversal of induction vectors at stations on the eastern and western sides of the fracture zone at periods less than 20 minutes. The effect of the oceans is clearly shown by the gradual change in the directions of the induction vectors with increasing periods. As period increases the induction vectors point toward the nearest coastline.

The most likely explanation of the highly conductive structure coinciding with the Tamar Fracture Zone is that it is due to large quantities of electrolyte solutions in porous or cracked rocks.

Two magneto-telluric surveys conducted by Bindoff (1983) and Sayers (1984) have contributed important data, especially in determining the depth to the surface of the conductor and its resistivity, these constraints giving more realistic results in the quantitative interpretation.

REFERENCES.

ASTEN, M.W., 1972. Magneto-telluric sounding in Tasmania. Honours thesis, Geology Department University of Tasmania, unpubl.

BINDOFF, N.L., 1983. A preliminary magneto-telluric survey of north-eastern Tasmania. Honours thesis, Geology Department University of Tasmania, unpubl.

BREWITT-TAYLOR, C.R., and WEAVER, J.T., 1976. On the finite difference solution of two-dimensional induction problems. Geophys. J.R. astr. Soc., 47, 375-396.

BUYUNG, N., 1980. A geomagnetic induction study in the north-east of Tasmania. M.Sc. thesis, Geology Department University of Tasmania, unpubl.

CAGNIARD, L., 1952. Basic theory of the magneto-telluric method of geophysical prospecting. Geophys., 18, 605.

CARR, J.M., 1984. Exploration Licence 20/80 Launceston. Final report on area relinquished 22 August 1984, C.S.R. No. 84/2206.

D'ERCEVILLE, I., and KUNETZ, G., 1962. The effect of a fault on the earth's natural electromagnetic field. Geophys., 27, no.5, 651-665.

DOSSO, H.W., NIENABER, W, and PARKINSON, W.D., in press. An analogue model study of electromagnetic induction in Tasmania region. Physics of the Earth and Planetary Interiors.

EVERETT, J.E., and HYNDMAN, R.D., 1967. Geomagnetic variations and electrical conductivity structure in south-western Australia. Physics of the Earth and Planetary Interiors, 1, 24-34.

GEYER, R.G., 1972. The effect of a dipping contact on the behaviour of electromagnetic field. Geophys., 37, no.2, 337-350.

GOUGH, D.I., and INGHAM, M.R., 1983. Interpretation methods for magnetometer arrays. Rev. of Geophys. and Space Phys., 21, no.4, 805-827.

HERMANCE, J.F., 1973. An electrical model for the Sub-Icelandic crust. Geophys., 38, no.1, 3-13.

HINCH, A.J., 1965. Cressy gravity survey. Honours thesis, Geology Department University of Tasmania, unpubl.

HONKURA, Y., 1978. Electrical conductivity anomalies in the Earth. Geophysical Survey, 3, 225-253.

JONES, F.W., 1970. Electromagnetic induction in a non-horizontally stratified two-layered conductor. Geophys. J.R. astr. Soc., 22, 17-28.

JONES, F.W., 1971. Electromagnetic induction in a two-dimensional model of an asymmetric two-layered conductor. Physics of the Earth and Planetary Interiors, 4, 417-424.

JONES, F.W., 1974. The effect of an island and bay structure on alternating geomagnetic fields at three-periods. Geophys. J.R. astr. Soc., 36, 627-639.

JONES, F.W., and AINSLIE, B.A., 1973. The perturbation of alternating geomagnetic fields by discontinuities with high conductivity contrast. Physics of the Earth and Planetary Interiors, 7, 97-110.

JONES, F.W., and LOKKEN, J.E., 1975. Irregular coastline and chanelling effect in three-dimensional geomagnetic perturbation models. Physics of the Earth and Planetary Interiors, 10, 140-150.

JONES, F.W., and PASCOE, L.J., 1971. A general computer program to determine the perturbation of alternating electric currents in a two-dimensional model of a region of uniform conductivity with embedded inhomogeneity. Geophys. J.R. astr. Soc., 24, 3-30.

JONES, F.W., and PASCOE, L.J., 1972. The perturbation of alternating geomagnetic fields by three-dimensional conductivity inhomogenities. Geophys. J.R. astr. Soc., 27, 479-485.

JONES, F.W., and PRICE, A.T., 1970. The perturbation of alternating geomagnetic fields by conductivity anomalies. Geophys. J.R. astr. Soc., 20, 317-334.

JONES, F.W., and PRICE, A.T., 1971a. Geomagnetic effect of sloping and shelving discontinuities of earth conductivity. Geophys., 36, no.1, 50-66.

JONES, F.W., and PRICE, A.T., 1971b. The geomagnetic effect of two-dimensional conductivity inhomogeneities at different depths. Geophys. J.R. astr. Soc., 22, 333-345.

JONES, F.W., and THOMPSON, D.J., 1974. A discussion of the finite difference method in computer modelling of electrical conductivity structures: A reply to the discussion by Williamson, Hewlett, and Tammemagi. Geophys. J.R. astr. Soc., 37, 537-544.

LEAMAN, D.E., 1973. Appied geophysics in Tasmania, Part 1 - Summary of surveys and rock properties. Austr. Soc. of Expl. Geophys. Bull., 4, 27-58.

LEAMAN, D.E., SYMONDS, P.A., and SHIRLEY, J.E., 1973. Gravity survey of the Tamar Region, Northern Tasmania. Geological Survey Paper, no.1, Tasmania Dept. of Mines.

LEWIS, R.J.G., 1965. Conductivity of the crust in Tasmania. Honours thesis, Geology Department University of Tasmania, unpubl.

LILLEY, F.E.M., 1976. A magnetometer array study across southern Victoria and the Bass Strait area, Australia. Geophys. J.R. astr. Soc., 46, 165-184.

LINES, L.R., and JONES, F.W., 1973. The perturbation of alternating geomagnetic fields by an island near a coastline. Can. J.Earth Sci., 10, 510-518.

LONGMAN, M.J., and LEAMAN, D.E., 1971. Gravity survey of the Tertiary basins in nothern Tasmania. Geological Survey Bulletin, no.51, Tasmania Dept. of Mines.

NIENABER, W., DOSSO, H.W., LAW, L.K., JONES, F.W., and RAMASWAMY, V., 1979. An analogue model study of electromagnetic induction in the Vancouver Island region. J. Geomag. Geoelectr., 31, 115-132.

PARKINSON, W.D., 1959. Direction of rapid geomagnetic fluctuations. Geophys. J.R. astr. Soc., 2, no.1, 1-28.

PARKINSON, W.D., 1962. The influence of continent and oceans on geomagnetic variations. Geophys. J.R. astr. Soc., 6, 441-449.

PARKINSON, W.D., 1964. Conductivity anomalies in Australia and the ocean effect. J. Geomag. Geoelectr., v.15, no.4, 222-226.

PARKINSON, W.D., 1983. Introduction to Geomagnetism. Scottish Academic Press.

PARKINSON, W.D., HERMANTO, R., SAYERS, J., BINDOFF, N.L., DOSSO, H.W., and NIENABER, W., in preparation. The Tamar conductivity anomaly.

PARKINSON, W.D., and JONES, F.W., 1979. The geomagnetic coast effect. Rev. of Geophys. and Space Phys., 17, no.8, 1999-2015.

PASCOE, L.J. and JONES, F.W., 1972. Boundary conditions and calculations of surface values for the general two-dimensional electromagnetic induction problem. Geophys. J.R. astr. Soc., 27, 179-193.

PATRA, H.P., and MALLICK, K., 1980. Geosounding Principles, 2 : Time-Varying Geoelectric Sounding. Elsevier.

PORATH, H., and DZIEWONSKI, A., 1971. Crustal resistivity anomalies from geomagnetic deep sounding studies. Rev. of Geophys. and Space Phys., 9, no.4, 891-915.

PRICE, A.T., 1950. Electromagnetic induction in a semi-infinite conductor with a plane boundary. Q. J. Mech. Appl. Math., 3, 385-410.

PRICE, A.T., 1973. The theory of geomagnetic induction., Physics of the Earth and Planetary Interiors, 7, 227-233.

RAMASWAMY, V., NIENABER, W., DOSSO, H.W., JONES, F.W., and LAW, L.K., 1975. Numerical and analogue model results for electromagnetic inductuion for island situated near a coastline. Physics of the Earth and Planetary Interiors, 11, 81-90.

RAMASWAMY, V., DOSSO, H.W., and WINTER, R., 1983. An electromagnetic scale model study of the Rhine Graben anomaly. J. Geomag. Geoelectr., 35, 17-27.

RANKIN, D., 1962. The magneto-telluric effect on a dike. Geophys., 27, no.5, 666-676.

RICHARDSON, R.G., 1980. Crustal seismology. Ph.D. thesis, Geology Department University of Tasmania, Unpubl.

ROKITYANSKY, I.I., 1975. The interpretation of anomalous fields by using their frequency characteristics. Physics of the Earth and Planetary Interiors, 10, 271-281.

ROKITYANSKY, I.I., 1982. Geoelectromagnetic Investigation of the Earth's Crust and Mantle. Springer-Verlag.

ROONEY, D., and HUTTON, V.R.S., 1977. A magneto-telluric and magneto-variational study of the Gregory Rift Valley, Kenya. Geophys. J. R. astr. Soc., 51, 91-119.

SAYERS, J., 1984. A magneto-telluric survey of the Midlands Area. Honours thesis, Geology Department University of Tasmania, unpubl.

SCHMUCKER, U., 1970. Anomalies of geomagnetic variations in the southwestern United States. Scripps. Inst. Oceanog. Bull., 13.

SWIFT, M.C., 1967. A magneto-telluric investigation of an electrical conductivity anomaly in the south-western United States. Ph.D. thesis, MIT.

SYMONDS, P.A., 1971. A regional gravity survey of the Scottsdale area., Honours thesis, Geology Department University of Tasmania, unpubl.

WAIT, J.R., 1954. On the relation between telluric currents and the earth's magnetic field. Geophysics, 19, 281-289.

WEAVER, J.T., 1970. The general theory of electromagnetic induction in a conducting half-space. Geophys. J.R. astr. Soc., 22, 83-100.

WEIDELT, P., 1971. The electromagnetic induction in two thin half-sheets. Z. Geophys., 37, 649-665.

WILLIAMS, E., 1979a. Tasman fold belt system in Tasmania. Explanatory notes for the 1:500.000 structural map of the pre-Carboniferous rocks of Tasmania: Tasmania Dept. of Mines.

WILLIAMS, E., 1979b. Structural map of the pre-Carboniferous rocks of Tasmania: Tasmania Dept. of Mines.

WILLIAMSON, K., HEWLETT, C, and TAMMEMAGI, H.Y., 1974. Computer modelling of electrical conductivity structures: letter to the editors. Geophys. J.R. astr. Soc., 37, 533-536.

Appendix 1.

Computer program for step 1 in the analysis (EMMTEE 1).

```
C                    "EMMTEE 1"
C A VERSION OF "DISPLAY MEMODYNE ",
C POLARISATION PLOTTING VERSION
C THIS PROGRAM READS BLOCKS (1440 READINGS) OF MEMODYNE TAPE AND
C DISPLAYS OR STORES ANY CHOSEN PART. PROGRAM IS CONTROLLED BY
C COMMAND NUMBERS; SINGLE DIGIT INTEGERS 1...9 TYPED BELOW THE
C C IN "COMMAND". TYPE THE INTEGERS II,JJJJ, UNDER "OM&"MAND", HAVING
C THE MEANINGS EXPLAINED IN COMMENTS BELOW. THE NUMBER OF
C DATA CHANNELS TO BE READ IS GIVEN BY "CHN"
C TO SUPRESS READ ERRORS    AS 400
C TO DISPLAY ON VIDEO       AS 442
C TO WRITE ON MAG TAPE      AS 185
C
C BEFORE STARTING CASSETTE SHOULD BE REWOUND BY ORDER "RW 9"
      INTEGER *2 INPUT(32)
      INTEGER*2 INGO(33)
      EQUIVALENCE(INPUT(1),INGO(1))
      INTEGER *2 MEM(7,1472)
      DIMENSION NTA(7),NTB(7), COF1(7),COF2(7),ZRO1(7),ZRO2(7)
      DIMENSION AMP(7), TEXT(7),LEVEL(7),KOLOR(7),F(16)
      DATA KOLOR/1,4,2,3,5,6,7/
      CALL PRIVLG
      CALL PLOTOM(1HT)
      CALL PLOT00(6)
      LIMIT=1440
      NBLOCK=0
      DO 220 I=1,7
      LEVEL(I)=0
  220 AMP(I)=20.
      WRITE(5,179)
  179 FORMAT('READING ERRORS ON L.U.4; OUTPUT ON L.U.1=ASSIGN')
      PAUSE
C INFORMATION FOR TASIGMA -- TYPE SITE NUMBER, TIME OF
C BEGINNING, DATA INTERVAL,  NUMBER OF CHANNELS
C DATA CAN BE CONDENSED BY AVERAGING MM (INTEGER) SUCCESSIVE VALUES
C MM SHOULD BE 2,4,8,16 OR 32. ZERO MM MEANS NO AVERAGING
  178 WRITE(5,79)
   79 FORMAT('CHN=CHANNELS; MM=AVERAGING WINDOW;
     * MISRD=TOLERANCE FOR BAD READING'//
     &'SITE DAY HOUR MIN DATA-INT CHN MM MISRD')
      READ(5,78)NSITE,JOUR,JORA,MIN,DI,KAN,MM,MISRD
      IF(DI.EQ.0.)GO TO 178
      IF(MM.NE.0)DI=DI*FLOAT(MM)
      IF(KAN.GT.7.OR.KAN.LT.1)GOTO 178
   78 FORMAT(I4,I4,I5,I4,F9.1,I4,I3,I6)
C COMMAND 4 -- READ ONE BLOCK FROM CASSETTE; IR=READING NUMBER
C IF II = ZERO READ NEXT BLOCK -- ELSE REWIND AND SKIP II BLOCKS
C PLUS JJJJ READINGS, THEN READ ONE BLOCK
      LA=0
      LB=0
      KK=0
      MISDFL=0
      GO TO 10
   24 NBLOCK=NBLOCK+1
      IF(LA.EQ.0.AND.LB.EQ.0) GO TO 70
C TO SKIP II BLOCKS AND JJJJ READINGS (TAKE ACCOUNT OF MM)
      REWIND 9
```

```
      PAUSE
      NBLOCK=1+LA
      MISDFL=LB
      LB=(FLOAT(LIMIT*KAN)/32.)*FLOAT(LA)+FLOAT(LB*KAN)/32.
      IF(MM.NE.Ø)LB=LB*MM
      DO 71 I= 1,LB
   71 READ(9)INPUT
   7Ø CONTINUE
CLEAR MEM
      DO 8 NC=1,KAN
      DO 8 I=1,LIMIT
    8 MEM(NC,I)=Ø
      IF(MM.GT.32)MM=32
      M=Ø
      IR=Ø
      KOUNT=Ø
      KL=Ø
      JR=Ø
C
C  MM=AVERAGING WINDOW;  KAN=NO OF CHANNELS
C
      IF(MISRD.EQ.Ø)MISRD=32ØØØ
      IF(MM.EQ.Ø)MM=1
      LOT=LIMIT*MM/32
      JJ=32/MM
      DO 2 L=1,LOT
      IRI=KOUNT/KAN+2
      IRJ=IRI+29
      DO 3 NMBR=1,KAN
      READ(9,ERR=49) INPUT
      DO 3 I=1,32
      CALL MEMOLY(INPUT,I,K,IDATA)
      K=K+1
      IF(M.EQ.Ø)KK=K
      KOUNT=KOUNT+1
      IR=(KOUNT-1)/KAN+1
      IF(K.EQ.KK)GO TO 191
      WRITE(4,19Ø)IR,K,KK
      M=Ø
      KC=KK
      GO TO 192
  191 CONTINUE
      KC=K
      M=1
  19Ø FORMAT(' READING',I5,I6,' INSTEAD OF',I2)
  192 CONTINUE
      IF(KC.GT.KAN)KC=KAN
      MEM(KC,IR)=IDATA-2Ø48
      KK=KK+1
      IF(KK.GT.KAN)KK=1
   43 CONTINUE
    3 CONTINUE
      IF(MM.EQ.1)GOTO    2
      DO 177 KC=1,KAN
      DO 177 IR=IRI,IRJ
      IF(IABS(MEM(KC,IR)-MEM(KC,IR-1)).GT.MISRD)
     *MEM(KC,IR)=(MEM(KC,IR-1)+MEM(KC,IR+1))/2
  177 CONTINUE
      DO 14Ø NC=1,KAN
      DO 14Ø J=1,JJ
```

```
      JRJ=JR+J
      IF(JRJ.GT.1472)GO TO 40
      T=0.
      DO 141 M=1,MM
      JRM=JR+(J-1)*MM+M
  141 T=T+FLOAT(MEM(NC,JRM))
  140 MEM(NC,JRJ)=T/FLOAT(MM)+0.5
      JR=JR+JJ
      KOUNT=KL+KAN*JJ
      KL=KOUNT
    2 CONTINUE
   40 WRITE(5,41)NBLOCK
      IF(MISRD.EQ.0)MISRD=32000
      DO 42 KC=1,KAN
      L=LIMIT-1
      DO 42 IR=2,L
      IF(IABS(MEM(KC,IR)-MEM(KC,IR-1)).GT.MISRD)
     *MEM(KC,IR)=(MEM(KC,IR-1)+MEM(KC,IR+1))/2
   42 CONTINUE
   41 FORMAT(7X,'BLOCK NO. ',I3)
C
COMMAND ALLOCATION
   10 WRITE(5,96)
   96 FORMAT('COMMAND')
      READ(5,95)KOM,LA,LB
      IF(KOM.NE.0)GOTO 44
      PAUSE
      GO TO 10
   44 CONTINUE
   95 FORMAT(I1,I2,I4)
      GO TO(21,22,23,24,25,26,27,28,29),KOM
C
COMMAND 1 -- IF II=0 254 READINGS STARTING WITH JJJ ARE DISPLAYED
C ELSE EVERY II-TH READING
   21 LF =LB
      IF(LF.EQ.0)LF=1
      LS=LA
      IF(LS.EQ.0)LS=1
      LL=LF+254*LS
      IF(LL.GT.LIMIT)LL=LIMIT
   31 CALL SCREEN(0)
  221 WRITE(5,48)
   48 FORMAT('CH?')
      READ(5,13.)NC
      IF(NC.EQ.0)GO TO 10
  122 Y=FLOAT(MEM(NC,LF)+LEVEL(NC))*AMP(NC)
      IF(ABS(Y).GT.32000.)Y=32000.
      JY=Y
      CALL PLOT(-2047,JY,1,7)
      DO 4 I=LF,LL,LS
      JX=-2047+(16*(I-LF))/LS
            Y=FLOAT(MEM(NC,I)+LEVEL(NC))*AMP(NC)
      IF(ABS(Y).GT.32000.)Y=32000.
      JY=Y
    4 CALL PLOT(JX,JY,0,KOLOR(NC))
      GOTO 221
C
COMMAND 2; RAISE COMPONENT II (NEGATIVE FOR LOWER) BY JJJJ T.V.SPACINGS
   22 CONTINUE
      IF(LA.EQ.0)GOTO 10
```

```
      NC=IABS(LA)
      LCH=ISIGN(LB,LA)
      LEVEL(NC)=LEVEL(NC)+LCH
      GOTO 31
C
COMMAND 3 -- CHANGE AMPLITUDE OF TRACE II   JJJJ =  % CHANGE
C   TO AMPLITUDE IN I3, E.G. 100 RESULTS IN  NO CHANGE, 50 HALVES AM
   23 CONTINUE
      IF(LA.EQ.0)GOTO 10
      IF(LB.EQ.0) LB=100
      EL=FLOAT(LB)
      I=LA/10
      J=LA-10*I
      IF(I.EQ.0.OR.I.GT.J)I=J
      DO 175 NC=I,J
  175 AMP(NC)=AMP(NC)*EL/100.
      GOTO 31
C
COMMAND 5 -- DISPLAY SCALE VALUE; FOR CHANNEL(II) JJJJ = SEPARATION
C   OF FIDUCIAL LINES IN GAMMAS. DEFAULT = 100
   25 CONTINUE
      IF(LB.EQ.0)LB=100
      IF(LA.EQ.0)LA=1
      EL=FLOAT(LB)
      DO 60 I=800,4000,200
      IX=I-2047
      CALL PLOT(IX,2047,1,0)
   60 CALL PLOT(IX,-2047,0,7)
      CALL PLOT(-2047,0,1,7)
      CALL PLOT(2047,0,0,7)
      I=0
    5 I=I+1
      IY=AMP(LA)*2.048*FLOAT(I)*EL
      IF(IY.GT.2048)GOTO 10
      CALL PLOT(-2047,IY,1,7)
      CALL PLOT(2047,IY,0,7)
      IY=-IY
      CALL PLOT(-2047,IY,1,7)
      CALL PLOT(2047,IY,0,7)
      GOTO 5
C
C
COMMAND 6 -- WRITE CHOSEN DATA IN NT ONTO L.U.1.
C   II=LENGTH OF OUTPUT RECORD; UNDER "BEGIN FINISH" TYPE FIRST AND
C   LAST READINGS OF EVENT WANTED ON L.U.1. OUTPUT FORMAT IS 16F7.1
   26 WRITE(5,92)NSITE,NBLOCK
   92 FORMAT('WRITE  SITE NO.',I4,' BLOCK NO.',I3/
     *'BEGIN FINISH EVENT')
      READ(5,91)KF,KL,NEVNT
   91 FORMAT(I5,I7,I6)
      NN=KL-KF+1
      WRITE(1,90)NSITE,DI,NEVNT,NN
   90 FORMAT(I4,F4.2,2I3)
  206 WRITE(5,48)
      READ(5,130)NC
      IF(NC.NE.0)GO TO 213
      PAUSE
      GO TO 10
  213 CONTINUE
C TELLURIC OUTPUT IN UNITS OF 55 MICROVOLTS
```

```
CORRECTION FOR TEMPERATURE - NT=TEMP CHANNEL,COEF IN
C  NTESLA/DECIKELVIN REDUCES VALUES TO ZERO TEMP.
      WRITE(5,172)
  172 FORMAT('TEMPERATURE'/'CH COEF  ZERO  CH COEF  ZERO')
      READ(5,174)NT1,COEF1,ZERO1,NT2,COEF2,ZERO2
  174 FORMAT(I1,2F6.1,I3,2F6.1)
      IF(NT1.EQ.9)GO TO 176
      COF1(NC)=COEF1
      COF2(NC)=COEF2
      NTA(NC)=NT1
      NTB(NC)=NT2
      ZRO1(NC)=ZERO1
      ZRO2(NC)=ZERO2
  176 CONTINUE
      WRITE(1,90)NC
      IF(LA.LT.1.OR.LA.GT.16)LA=16
      NL=NN/LA+1
      DO 6 I=1,NL
      JF=(I-1)*LA+KF
      IF(JF.GT.KL)GOTO 206
      JL=JF+LA-1
      IF(JL.GT.KL)JL=KL
      NT1=NTA(NC)
      NT2=NTB(NC)
      DO 171 J=1,LA
      JA=JF+J-1
      IF(JA.GT.KL)GOTO 6
      F(J)=FLOAT(MEM(NC,JA))/2.048
      IF(NT1.EQ.0)GO TO 171
      F(J)=F(J)-(FLOAT(MEM(NT1,JA))/2.048-ZRO1(NC))*COF1(NC)
      IF(NT2.NE.0)F(J)=F(J)-(FLOAT(MEM(NT2,JA))/2.048
     1   -ZRO2(NC))*COF2(NC)
  171 CONTINUE
    6 WRITE(1,89)(F(J),J=1,LA)
   89 FORMAT(16F7.1)
      GOTO 206
C
COMMAND 7 -- PRINT MEMORY NUMBER, LA=ELEMENT, LB=FIRST GUESS
   27 GO TO 230
   39 L=LB+9
      WRITE(5,87)(MEM(NC,K),K=LB,L)
   87 FORMAT(10I6)
      GOTO 10
C
COMMAND 8 -- PLOT EVENT; JJJJ IS NT SCALE (DEFAULT=20)
C IF II.LT.10 PLOT MAGNETOGRAM OTHERWISE PLOT POLARISATION WITH COMPO
C J AS ORDINATE AND K AS ABSCISSA, WHERE JK=II, E.G. II=12 PLOTS
C X AS ORDINATE AND Y AS ABSCISSA.
C IF II.GT.0 AND II.LT.10 MARK EVERY II HOURS ON ABSCISSA (DEFAULT=1)
   28 CALL PLOTOM(1HH)
      CALL PLOT00(6)
      IF(LB.EQ.0)LB=20
      WRITE(5,86)
   86 FORMAT('BEGIN FINISH EVENT')
      READ(5,91)KF,KL,NEVNT
      IF(KF.LT.1.OR.KL.LE.KF)GOTO 10
C SCRAWL SIZE OF NT SCALE, SITE & EVENT
  195 FORMAT('SITE NO.',I3,' EVENT NO.',I3,'&    ')
      WRITE(10,195)NSITE,NEVNT
      READ(10,196)TEXT
```

```
  196 FORMAT(7A4)
      CALL SCRAWL(0,2000,6,TEXT,7)
  104 FORMAT(I3,' NTS')
      WRITE(10,104)LB
      READ(10,103)TEXT
  103 FORMAT(2A4)
      CALL SCRAWL(-2047,2000,6,TEXT,7)
C PLOT NT SCALE
      ID=AMP(1)*FLOAT(LB)/0.4439
      IY=1940
      CALL PLOT(-2000,IY,1,7)
   13 CALL PLOT(-2047,IY,0,7)
      IY=IY-ID
      IF(IY.LT.-2047)GO TO 61
      CALL PLOT(-2047,IY,0,7)
      CALL PLOT(-2000,IY,0,7)
      GOTO 13
   61 CALL PLOT(-2047,-2000,1,7)
      IF(LA.LT.10)GO TO 150
      NCY=LA/10
      NCX=LA-10*NCY
      IF(NCY.GT.KAN.OR.NCY.EQ.0)GO TO 10
      IF(NCX.GT.KAN.OR.NCX.EQ.0)GO TO 10
      RXY=180./250.
      CALL PLOT(0,-1821,1,7)
      CALL PLOT(0,1934,0,7)
      CALL PLOT(1311,0,1,7)
      CALL PLOT(-1311,0,0,7)
C SCRAWL FIRST & LAST READINGS
      WRITE(10,151)KF,KL
  151 FORMAT(I4,' - ',I4,'S')
      READ(10,152)TEXT
  152 FORMAT(3A4)
      CALL SCRAWL(-2000,-2000,6,TEXT,7)
      DO 153 I=KF,KL
      KPEN=0
      IF(I.EQ.KF)KPEN=1
      JY=FLOAT(MEM(NCY,I)+LEVEL(NCY))*AMP(NC)
      JX=FLOAT(MEM(NCX,I)+LEVEL(NCX))*AMP(NC)*RXY
  153 CALL PLOT(JX,JY,KPEN,7)
      GO TO 38
  150 CONTINUE
      IF(LA.EQ.0)LA=1
      PPR=4096./FLOAT(KL-KF)
      JDAY=JOUR
      JHR=JORA+IA
      PPH=PPR*60.*FLOAT(LA)/DI
C IN CASE CASSETTE HAS BEEN REWOUND AND "MISDFL" FILES SKIPPED
      TSB=DI*FLOAT(KF+LIMIT*(NBLOCK-1)+MISDFL)
C TSB=TIME SINCE BEGINNING OF CASSETTE
      M=TSB+FLOAT(MIN)+0.4
   52 CONTINUE
      IF(M.LT.60*LA)GOTO 53
      M=M-60*LA
      JHR=JHR+LA
      IF(JHR.LT.24)GOTO 52
      JHR=JHR-24
      JDAY=JDAY+1
      GOTO 52
   53 WRITE(10,105)JDAY
```

```
  105 FORMAT('DAY',I3,'&')
      READ(10,103)TEXT
      CALL SCRAWL(-1980,-1800,6,TEXT,7)
      J=1
  211 IX=PPR*FLOAT(15*J*LA-M)/DI
      IF(IX.GT.0)GO TO 210
      J=J+1
      GO TO 211
C PLOT TIME MARKS
  210 CONTINUE
      IX=IX-2047
      CALL PLOT(-2047,-2000,1,0)
   54 CALL PLOT(IX,-2000,0,7)
      IF(LA.NE.1)GO TO 173
      IF(J.EQ.1.OR.J.EQ.3)CALL PLOT(IX,-2015,0,7)
      IF(J.EQ.2)CALL PLOT(IX,-2030,0,7)
  173 CONTINUE
      IF(J.NE.4)GO TO 212
      CALL PLOT(IX,-2047,0,7)
      WRITE(10,101)JHR
  101 FORMAT(I2,'&')
      READ(10,102)TEXT
  102 FORMAT(A3)
      CALL SCRAWL(IX-81,-1950,6,TEXT,7)
      CALL PLOT(IX,-2000,1,0)
  212 CALL PLOT(IX,-2000,0,7)
      IX=FLOAT(IX)+PPH/4.
      IF(IX.GE.2047)GO TO 63
      IF(J.EQ.4)JHR=JHR+LA
      IF(JHR.GE.24)JHR=JHR-24
      J=J+1
      IF(J.EQ.5)J=1
      GO TO 54
C
   63 WRITE(5,48)
      READ(5,130)NC
      IF(NC.EQ.0)GOTO 38
  130 FORMAT(I1)
      JY=FLOAT(MEM(NC,KF)+LEVEL(NC))*AMP(NC)
      CALL PLOT(-2047,JY,1,7)
      DO 12 I=KF,KL
      X=FLOAT(I-KF)*PPR
      JX=X-2046.999
      JY=FLOAT(MEM(NC,I)+LEVEL(NC))*AMP(NC)
      JY=JY+LEVEL(NC)
   12 CALL PLOT(JX,JY,0,7)
      GOTO 63
   38 CONTINUE
      CALL PLOTOM(1HT)
      GOTO 10
C
COMMAND 9 -- FIND & REMOVE SPURIOUS VALUES.  II =
C  NO OF COMPONENT ; JJJJ =  READING NUMBER AT WHICH TO START
C  SEARCHING FOR BAD VALUE .
C IF(II=NC+10) MEM IS REPLACED BY LINEAR INTERPOLATION BETWEEN
C "FROM" & "TO"
   29 CONTINUE
      IF(LA.LT.10)GOTO 230
      WRITE(5,231)
  231 FORMAT('FROM  TO')
```

```
      READ(5,232)KF,KL
      IF(KF*KL.EQ.0)GOTO10
  232 FORMAT(2I4)
      LA=LA-10
      IF(LA.GT.7.OR.LA.LT.1)GOTO 10
      K1=MEM(LA,KF)
      K2=MEM(LA,KL)
      KD=K2-K1
      LD=KL-KF
      DO 233 L=1,LD
      LK=KF+L
  233 MEM(LA,LK)=K1+(L*KD)/LD
      GO TO 31
  230 CONTINUE
      IF(LA.EQ.0.OR.LF.EQ.0)GOTO 10
      NC=LA
      L=LF
      JX=-2047+(16*(L-LF))/LS
      JY=FLOAT(MEM(NC,L)+LEVEL(NC))*AMP(NC)
      JY=JY+100
      CALL PLOT(JX,JY,1,0)
      IY=JY-200
      CALL PLOT(JX,IY,0,7)
      WRITE(5,85)LF
   85 FORMAT('MOVE - MARKER NOW AT',I4)
      READ(5,84)LD
      CALL PLOT(JX,JY,0,0)
   84 FORMAT(I4)
      IF(LD.EQ.0) GOTO 37
      LF=L+LD
      GOTO 230
   37 IF(KOM.EQ.7)GO TO 39
      MEM(NC,L)=(MEM(NC,L-1)+MEM(NC,L+1))/2
      GOTO 31
C
   49 WRITE(5,88)NBLOCK,IR,INGO(33)
   88 FORMAT(' STOPPED AT BLOCK NO.',I3,' READING',I5,I7,'
     : WORDS MISSING')
      GOTO 10
      END
```

Appendix 2.

Computer program for step 2 in the analysis (TASIGMA 1).

```
C          "TASIGMA 1"
C TO CALCULATE FOURIER COEFFS FROM GEOMAGNETIC DATA
C THIS VERSION FOR USE WITH MEMODYNE OUTPUT
      DIMENSION F(1025)
   50 READ(6,87,END=22)NS,DI,NE,NN
   87 FORMAT(I4,F4.2,2I3)
      WRITE(5,51)NS,NE,NN,DI
   51 FORMAT('SITE',I3,' EVENT',I3,I5,' DATA POINTS AT',F5.2,' MINS')
      PAUSE
      WRITE(5,70)
   70 FORMAT('OK?')
      READ(5,71)KEY
   71 FORMAT(I1)
      IF(KEY.EQ.0)GOTO 50
   10 READ(6,86)NC
   86 FORMAT(I1)
C FIND POWER OF 2
      J=2
    3 IF(J.GE.NN) GO TO 4
      J=J*2
      GO TO 3
    4 N=J
C  READ DATA TAPE
    1 READ(6,96)(F(K),K=1,NN)
   96 FORMAT(16F7.1)
C SUBTRACT LINEAR TREND FROM DATA
      M=NN/20
      B=0.
      DO 5 I=1,M
    5 B=B+F(I)
      FM=FLOAT(M)
      B=B/FM
      E=0.
      K=NN-M+1
      DO 6 I=K,NN
    6 E=E+F(I)
      E=E/FM
      FNN=FLOAT(NN-1)
      DO 7 I=1,NN
      AI=I-1
    7 F(I)=F(I)-(AI*(E-B))/FNN-E
C ADJUST TO POWER OF 2
      IF(N-NN.EQ.0)GO TO 34
      NP=NN+1
```

```
      DO 31 I=NP,N
   31 F(I)=0.
   34 FN=N
C
      CALL RFFT(N,F,-1.,0)
C REDUCE TO FOURIER COEFFICIENTS
      DO 8 I=4,N,2
    8 F(I)=-F(I)*2./FN
      DO 9 I=3,N,2
    9 F(I)=F(I)*2./FN
      F(2)=-F(2)/FN
      F(1) = F(1)/FN
C OUTPUT F.C. ON PAPER TAPE
   97 FORMAT(4I3,F7.2)
      WRITE(1,97)NS,NE,NC,N,DI
      DO 2 I=1,25
    2 WRITE(1,90) F(I)
   90 FORMAT(F5.2)
C PRINT OUTPUT
      WRITE(7,94)NS,NE,NC,N
   94 FORMAT(//'STATION',I3,'   EVENT',I3,'   COMPONENT',I2,
     1I6,' DATA PTS'
     1/'PERIOD(M) COSINE  SINE  AMPLITUDE PHASE(DEG) PHASE(MIN)'/)
      WRITE(7,81)F(1)
   81 FORMAT('      MEAN',F7.2)
      DL=FN*DI
      PI=3.1415925
      DO 11 J=1,12
      I=2*J+1
      FI=F(I)
      FJ=F(I+1)
      T=DL/FLOAT(J)
      A=SQRT(FI*FI+FJ*FJ)
      IF(ABS(FI).GT.0.00001) GO TO 20
      PH=PI/2.
      GO TO 21
   20 CONTINUE
      PH=ATAN(FJ/FI)
   21 CONTINUE
      IF(FI.LT.0.0) PH=PH+PI
      IF(PH.LT.0.0) PH=PH+PI+PI
      PH=PH*180./PI
      PM=PH*T/360.
   11 WRITE(7,93)T,FI,FJ,A,PH,PM
   93 FORMAT(F9.3,2F7.2,F10.4,2F11.4)
      IF(NC.NE.3)GO TO 10
      GO TO 50
   22 PAUSE
      GO TO 50
      END
```

Appendix 3.

Computer program for step 3 in the analysis (TASIGMA 2).

```
C          'TASIGMA 2"
C TO CALCULATE A S E TRANSFER FUNCTIONS BY EVERETT .E.E.P.I. 1
C NEV IS TOTAL NUMBER OF EVENTS FED IN
C ALL EVENTS USED IN ONE RUN MUST HAVE THE SAME DATA INTERVAL(DAT.
C OF READINGS (N).
C
C
COVARIANCE INCLUDED
C
      DIMENSION A(20,3),B(20,3),C(20),AI(20,36),BI(20,36)
     1  ,F(1025)
      COMPLEX XXX,PIP,QQQ,XXC,PPC,QQC,CCC,BNB,BWP,AA,EE,EEE
      COMPLEX ONE,EYE,HH(3),GAM(20),DEL(20)
      ONE=(1.,0.)
      EYE=(0.,1.)
      PI=3.1415926
      WRITE(5,98)
      READ(5,99,ERR=21)NS,NEV,DI,T1,T2,AMIN
   99 FORMAT(2I4,4F6.1)
   98 FORMAT('  NS NEV DAT.I MAX.P MIN.P MIN.A')
      NV=1
   10 READ(1,97,ERR=21)NSTA,NE,NC,N,DATIN
      IF(NV.EQ.1)NE1=NE
      IF(NV.EQ.NEV)NE2=NE
   97 FORMAT(4I3,F7.2)
      IF(NS.NE.NSTA) GO TO 1
      T=ABS(DI-DATIN)
      IF(T.GT.0.01) GO TO 1
      GO TO 2
    1 WRITE(5,96)
   96 FORMAT('DATA LENGTH OR STATION INCORRECT')
      PAUSE
      GO TO 10
    2 CONTINUE
      DO 3 I=1,26
    3 READ(1,95) F(I)
  999 FORMAT('REACHED',I4)
   95 FORMAT(F6.2)
      TF=FLOAT(N)*DI
      K1=TF/T1+0.1
      K2=TF/T2+0.1
      IF(K2-K1.GT.11)K2=K1+11
      DO 14 K=K1,K2
      KI=K-K1+1
      L=(NC-1)*12+KI
      AI(NV,L)=F(2*K+1)
      BI(NV,L)=F(2*K+2)
   14 CONTINUE
      IF(NC.LT.3) GO TO 10
      NV=NV+1
      IF(NV.LE.NEV)GO TO 10
```

```
   21 CONTINUE
      WRITE(7,92)NE1,NE2,AMIN
      AMIN=AMIN*AMIN
   92 FORMAT('EVENTS',I4,' TO', I4, '  MIN AMPLITUDE=',F4.1/)
      DO 13 K=K1,K2
      T=TF/FLOAT(K)
      KI=K-K1+1
      NVI=0
      DO 66 NE=1,NEV
C THIS LOOP TO DISCARD F.C. WITH LOW AMPLITUDE
      CS=0.
      DO 4 NC=1,3
      L=(NC-1)*12+KI
      ASQ=AI(NE,L)
      BSQ=BI(NE,L)
    4 CS=CS+ASQ*ASQ+BSQ*BSQ
      IF(CS.LT.AMIN)GO TO 66
      CS=SQRT(CS)
      NVI=NVI+1
      DO 6 NC=1,3
      L=(NC-1)*12+KI
      A(NVI,NC)=AI(NE,L)/CS
      B(NVI,NC)=BI(NE,L)/CS
    6 CONTINUE
   66 CONTINUE
      ENN=0.
      WWW=0.
      XXX=(0.,0.)
      PPP=(0.,0.)
      QQQ=(0.,0.)
      DO 7 NE=1,NVI
      AX=A(NE,1)
      BX=B(NE,1)
      AY=A(NE,2)
      BY=B(NE,2)
      AZ=A(NE,3)
      BZ=B(NE,3)
      ENN=ENN+AX*AX+BX*BX
      WWW=WWW+AY*AY+BY*BY
      DO 20 NC=1,3
   20 HH(NC)=A(NE,NC)*ONE+B(NE,NC)*EYE
      XXX=XXX+HH(1)*CONJG(HH(2))
      PPP=PPP+HH(1)*CONJG(HH(3))
      QQQ=QQQ+HH(2)*CONJG(HH(3))
    7 CONTINUE
      XXC=CONJG(XXX)
      PPC=CONJG(PPP)
      QQC=CONJG(QQQ)
C TO CALCULATE GAMMA & DELTA - PEPI 1 P 28
      CCC=XXX*XXC
      XX=REAL(CCC)
```

```
      DEN=ENN*WWW-XX
  998 FORMAT(4F12.5)
      DO 8 NE=1,NVI
      IF(ABS(DEN).GT.0.000001)GO TO 22
      WRITE(7,91)NS,T,NVI
   91 FORMAT('STATION',I3,' PERIOD',F7.2,I5,' EVENTS USED'/
     *'COEFFICIENTS UNOBTAINABLE'/)
      GO TO  13
   22 CONTINUE
      HNB=A(NE,1)*(1.,0.)-B(NE,1)*(0.,1.)
      HWB=A(NE,2)*(1.,0.)-B(NE,2)*(0.,1.)
      GAM(NE)=(WWW*HNB-XXC*HWB)/DEN
    8 DEL(NE)=(ENN*HWB-XXX*HNB)/DEN
      AA=(PPC*WWW-QQC*XXC)/DEN
      BB=(QQC*ENN-PPC*XXX)/DEN
      IF(NVI.LE.2)GO TO 11
C 10 CALCULATE E
      DA=0.
      DB=0.
      DO 9 NE=1,NVI
      EEE=A(NE,3)*(1.,0.)+B(NE,3)*(0.,1.)
     1-AA*(A(NE,1)*(1.,0.)-B(NE,1)*(0.,1.))
     2-BB*(A(NE,2)*(1.,0.)-B(NE,2)*(0.,1.))
      CCC=GAM(NE)*EEE
      D=CABS(CCC)
      DA=DA+D*D
      CCC=DEL(NE)*EEE
      D=CABS(CCC)
    9 DB=DB+D*D
      EN1=NVI-1
      EN2=NVI-2
      EN=EN1/EN2
      DA=SQRT(EN*DA)
      DB=SQRT(EN*DB)
      GO TO 12
   11 WRITE(7,94)
      DA=0.
      DB=0.
   94 FORMAT('INSUFFICIENT EVENTS FOR ERROR ESTIMATE')
   12 CONTINUE
      AR=REAL(AA)
      AY=-AIMAG(AA)
      BR=REAL(BB)
      BY=-AIMAG(BB)
C
C
C
      WRITE(7,93)NS,T,NVI,AR,AY,DA,BR,BY,DB
   93 FORMAT('STATION',I3,' PERIOD',F7.2,' NTRS',I5,' EVENTS USED'
     1'      A =',2F7.2,' +-',F5.2/
     2'      B =',2F7.2,' +-',F5.2)
   13 CONTINUE
      STOP
      END
```

Appendix 4.

Modified Jones and Pascoe computer program.

```
$ RESET LIST
$ SET LINEINFO
$ RESET FREE
C     STEP STRUCTURE PROGRAM FOR E-POLARIZATION MODIFIED FROM
C     PASCOE & JONES (1972).
C
C INPUT FORMAT:
C [1]  N,L IN (1X,2I2) N=NUMBER OF ZERO COND. LAYERS + 1
C                      L IS NON-ZERO IF COMPLETE E GRID WANTED IN OUTPUT
C
C [2]  H(40),K(40) IN (1X,20F3.0) GRID SPACING HORIZONTAL & VERTICAL
C
C [3]  T IN (F10.0) = PERIOD IN MINUTES
C
C [4]  STRUCTURE THUS:
C      N,(A,K) IN (1X,I2,8(A1,I2))  N=NUMBER OF LINES OF (A,K)
C      A IS A RESISTIVITY SYMBOL AND K IS THE NUMBER OF CONSECUTIVE
C      TIMES A OCCURS.  BRACKET CAN BE REPEATED UP TO 8 TIMES.
C      SUM OF K FOR EACH LINE MUST BE 40. LINES ARE REPEATRED
C      UNTIL SUM N = 40    E.G.
C           10A40
C           20B10C20B10
C           10D40
C
C [5]  A,RES(A)  IN (1X,A1,1X,F10.5)
C      WHERE A IS A RESISTIVITY SYMBOL AND RES(A) THE CORRESPONDING
C      RESISTIVITY IN OHM-M. INSULATORS ARE REPRESENTED BY RES=0.
C      EVERY RESISTIVITY SYMBOL USED IN [4] MUST BE EXPRESSED IN [5]
C
C
C
C EPOL/4 USES DOUBLE PRECISION IN BYCOND
C        PHASE OF Z REFERRED TO DPHAHY(40)
C        HZHY USES AMPY(J) WHICH IS DERIVED FROM DERIVZ
C        FIMAG (IMAGINARY PART OF TRANSFER FUNCTION) HAS SIGN CHANGED
C
      REAL K
      DIMENSION ALPHA(16), CONDUC(16), SKIDE(16)
      COMMON F(41,41),G(41,41),H(40),K(40),SCALE,FREQ,REGION(40,40)
      WRITE(6,230)
      MAXIT=900
      EPS=0.0002
      READ(1,302)N,LECTIC
  302 FORMAT(1X,2I2)
      READ (1,200) H
      READ (1,200) K
      READ(1,210)PERIOD
      FREQ=1./(PERIOD*60.)
      SCALE=100000.
      CALL LAZY
      DO 140 I=1,40
      WRITE(6,296)I,(REGION(I,J),J=1,40)
  140 CONTINUE
      WRITE(6,280) H
      WRITE(6,290) K
      WRITE(6,260)
      PI=3.141592654
      DO 50 I=1,16
      READ(1,220,END=115,ERR=115) ALPHA(I),CONDUC(I)

      NKOND=1
```

```
      IF(CONDUC(I) .EQ. 0.) GOTO 44
      RES=CONDUC(I)
      CONDUC(I)=1.0E-11/CONDUC(I)
      SKIDE(I)=1.0/(2.0*PI*SQRT(CONDUC(I)*FREQ)*SCALE)
      GOTO 45
   44 SKIDE(I)=999999999.
   45 WRITE(6,270) ALPHA(I),CONDUC(I),SKIDE(I),RES
   50 CONTINUE
  115 DO 110 L=1,40
      H(L)=H(L)*SCALE
  110 K(L)=K(L)*SCALE
      OMEGA=2.0*PI*FREQ
      DO 120 I=1,40
      DO 120 J=1,40
      RTEMP=REGION(I,J)
      DO 121 KINDX=1,NKOND
      IF(ALPHA(KINDX) .EQ. RTEMP) GOTO 120
  121 CONTINUE
      WRITE(6,297) RTEMP
      STOP
  120 REGION(I,J)=4.0*PI*CONDUC(KINDX)*OMEGA
      CALL BYCOND (N)
      CALL ITERE (EPS,MAXIT,N)
      CALL SURFVL (N)
      WRITE(6,300) SCALE,FREQ,PERIOD
      IF(LECTIC.NE.0)CALL EFIELD
      STOP
  200 FORMAT (1X,20F3.0)
  210 FORMAT (2F10.0)
  220 FORMAT (1X,A1,1X,F10.5)
  230 FORMAT (1H1,20H/* E-POLARIZATION *///)
  260 FORMAT (1H0,4X,5HSIGMA,5X,10HSKIN DEPTH,'  RESIST'/)
  270 FORMAT (1H ,2X,A1,E13.4,2F8.2)
  280 FORMAT (//1H0,8HH VALUES,3X,20F4.1/12X,20F4.1)
  290 FORMAT (1H0,8HK VALUES,3X,20F4.1/12X,20F4.1)
  295 FORMAT(40A1)
  296 FORMAT(1H ,I3,2H  ,40A1)
  297 FORMAT(' RESISTIVITY CODE ',A1,' IS UNDEFINED')
  298 FORMAT(I4,F10.0,I4)
  300 FORMAT (1H0,7HSCALE =,F10.0,7H FREQ =,F10.6,10H   PERIOD=,F6.2)
      END
C
      SUBROUTINE SURFVL (L)
      REAL K
      DIMENSION DELPH(41),AMPY(41)
      DIMENSION AME(41), AMHY(41), AMHZ(41), DPHASE(41), DPHAHY(41), DPH
     1AHZ(41), APPRES(41), HZHY(41)
      COMMON F(41,41),G(41,41),H(40),K(40),SCALE,FREQ,REGION(40,40)
      COMPLEX ROOTI,HO,HI
      DOUBLEPRECISION R2,EKI,REK,YEK,RRK,YRK,RNUM,YNUM
     &,RT,YT,RDZ,YDZ
      PI=3.141592654
      OMEGA=2.0*PI*FREQ
      WRITE(6,140)
      WRITE(6,150)
      I=L
      IP1=I+1
      IM1=I-1
      DO 110 J=2,40
      JP1=J+1
```

```
      JM1=J-1
      GIJ=G(I,J)
      FIJ=F(I,J)
      AETAL=SQRT(REGION(I,JM1))
      AETAR=SQRT(REGION(I,J))
      AETA=(AETAL+AETAR)/2.0
      ROOTI=CMPLX(1./SQRT(2.),1./SQRT(2.))
      HO=CMPLX(FIJ,GIJ)
      HI=CMPLX(F(IP1,J),G(IP1,J))
      R2=DBLE(1./SQRT(2.))
      EKI=DBLE(AETA*K(I))*R2
      CALL CXDP(EKI,REK,YEK)
      CALL DDIV(DBLE(1.),DBLE(0.),REK,YEK,RRK,YRK)
      CALL DMULT(DBLE(REAL(HO)),DBLE(AIMAG(HO)),REK+RRK,YEK
     &+YRK,RT,YT)
      RDZ=DBLE(2.*REAL(HI))-RT
      YDZ=DBLE(2.*AIMAG(HI))-YT
      CALL DMULT(RDZ,YDZ,DBLE(AETA)*R2,DBLE(AETA)*R2,RNUM,YNUM)
      CALL DDIV(RNUM,YNUM,REK-RRK,YEK-YRK,RDZ,YDZ)
      DPHASE(J)=ATAN2(GIJ,FIJ)
      DPHAHY(J)=ATAN2(SNGL(YDZ),SNGL(RDZ))
      TEMP=SNGL(RDZ*RDZ+YDZ*YDZ)
      AMPY(J)=SQRT(TEMP)/OMEGA
      DPHAHZ(J)=ATAN2(F(I,JM1)-F(I,JP1),G(I,JM1)-G(I,JP1))
      AME(J)=SQRT(FIJ*FIJ+GIJ*GIJ)
      AMHY(J)=(1./OMEGA)*(SQRT(((F(IM1,J)-F(IP1,J))/(K(I)+K(IM1)))**2+((
     1G(IM1,J)-G(IP1,J))/(K(I)+K(IM1)))**2))
      AMHZ(J)=(1./OMEGA)*(SQRT(((F(I,JP1)-F(I,JM1))/(H(J)+H(JM1)))**2+((
     1G(I,JP1)-G(I,JM1))/(H(J)+H(JM1)))**2))
  110 APPRES(J)=(2.0/FREQ)*((AME(J)/AMHY(J))**2)
      AMH=SQRT(AMHY(2)**2+AMHZ(2)**2)
      AMPY2=AMPY(2)
      DO 120 J=2,40
      AMHY(J)=AMHY(J)/AMH
      AMHZ(J)=AMHZ(J)/AMH
      AMPY(J)=AMPY(J)/AMPY2
      HZHY(J)=AMHZ(J)/AMPY(J)
      DPHASE(J)=DPHASE(J)-DPHASE(40)
      DPHAHY(J)=DPHAHY(J)-DPHAHY(40)
  120 DPHAHZ(J)=DPHAHZ(J)-DPHAHY(40)
      SUMH=0.
      DO 1 J=1,40
      H(J)=H(J)/SCALE
      K(J)=K(J)/SCALE
    1 CONTINUE
      DO 101 J=1,20
  101 SUMH=SUMH+H(J)
      HOR=H(1)-SUMH
C VALUES AT J ARE ON THE GRID LINE RIGHT OF SPACE J
      DO 130 J=2,40
      DIFPH=DPHAHZ(J)-DPHAHY(J)
      FREAL=HZHY(J)*COS(DIFPH)
      FIMAG=-HZHY(J)*SIN(DIFPH)
      WRITE(6,160) J,AME(J),AMHY(J),AMHZ(J),HZHY(J),DPHASE(J),
     1DPHAHY(J),DPHAHZ(J),APPRES(J),HOR,FREAL,FIMAG,DIFPH,AMPY(J)
  130 HOR=HOR+H(J)
      RETURN
  140 FORMAT (1H0,20H/* SURFACE VALUES *//)
  150 FORMAT (1H0,7X,'AME',3X,'AMHY',3X,'AMHZ',3X,'HZ/HY',1X,
     1'DPHASE',1X,'DPHAHY',1X,'DPHAHZ',1X,'APPRES',12X,
```

```
     2  'POSN F-REAL F-IMAG DELPH  AMPY'//)
  160 FORMAT (16,2F6.3,5F7.3,E10.3,10X,F5.0,2F7.2,2F6.3)
      END
C
      SUBROUTINE BYCOND (N)
      REAL K
      DOUBLEPRECISION RE(41,2),YE(41,2),RD1(40,2),YD1(40,2),
     &RD2(40,2),YD2(40,2),REP(41,2),YEP(41,2),DR,DY,DETA(40,2),
     &RENZ,YENZ,REMNZ,YEMNZ,RTEMP,YTEMP,RT2,YT2,RNORM,YNORM,R2
      COMMON F(41,41),G(41,41),H(40),K(40),SCALE,FREQ,REGION(40,40)
      DIMENSION DIST(41)
      DIST(1)=0.0
      DO 110 I=2,41
  110 DIST(I)=DIST(I-1)+K(I-1)
      R2=DBLE(1./SQRT(2.))
      DO 120 I=N,40
      DETA(1,1)=DBLE(SQRT(REGION(I,1)))
  120 DETA(I,2)=DBLE(SQRT(REGION(I,40)))
      DR=DBLE(-DIST(41))*DETA(40,1)*R2
      CALL CXDP(DR,RE(41,1),YE(41,1))
      DR=DBLE(-DIST(41))*DETA(40,2)*R2
      CALL CXDP(DR,RE(41,2),YE(41,2))
      CALL DMULT(-R2*DETA(40,1),-R2*DETA(40,1),RE(41,1)
     &,YE(41,1),REP(41,1),YEP(41,1))
      CALL DMULT(-R2*DETA(40,2),-R2*DETA(40,2),RE(41,2)
     &,YE(41,2),REP(41,2),YEP(41,2))
      DO 130 J=1,2
      DO 130 I=N,40
      IN=41-I+N
      I1=40-I+N
      DR=DBLE(DIST(IN))*DETA(I1,J)*R2
      CALL CXDP(DR,RENZ,YENZ)
      CALL DDIV(DBLE(1.),DBLE(0.),RENZ,YENZ,REMNZ,YEMNZ)
      CALL DMULT(RE(IN,J),YE(IN,J),DETA(I1,J)*R2,DETA(I1,J)*R2
     &,RTEMP,YTEMP)
      CALL DMULT(RENZ,YENZ,RTEMP,YTEMP,RT2,YT2)
      CALL DMULT(REP(IN,J),YEP(IN,J),RENZ,YENZ,RTEMP,YTEMP)
      RTEMP=RT2-RTEMP
      YTEMP=YT2-YTEMP
      CALL DDIV(RTEMP,YTEMP,DETA(I1,J)/R2,DETA(I1,J)/R2,
     &RD1(I1,J),YD1(I1,J))
      CALL DMULT(REP(IN,J),YEP(IN,J),REMNZ,YEMNZ,RTEMP,YTEMP)
      CALL DMULT(RE(IN,J),YE(IN,J),R2,R2,RT2,YT2)
      CALL DMULT(RT2,YT2,REMNZ*DETA(I1,J),YEMNZ*DETA(I1,J)
     &,DR,DY)
      RTEMP=RTEMP+DR
      YTEMP=YTEMP+DY
      CALL DDIV(RTEMP,YTEMP,DETA(I1,J)/R2,DETA(I1,J)/R2
     &,RD2(I1,J),YD2(I1,J))
      CALL CXDP(DBLE(DIST(I1))*DETA(I1,J)*R2,RENZ,YENZ)
      CALL DDIV(DBLE(1.),DBLE(0.),RENZ,YENZ,REMNZ,YEMNZ)
      CALL DMULT(RD1(I1,J),YD1(I1,J),REMNZ,YEMNZ,RTEMP,YTEMP)
      CALL DMULT(RD2(I1,J),YD2(I1,J),RENZ,YENZ,RT2,YT2)
      RE(I1,J)=RTEMP+RT2
      YE(I1,J)=YTEMP+YT2
      CALL DMULT(DETA(I1,J)*R2,DETA(I1,J)*R2,RD1(I1,J)
     &,YD1(I1,J),RTEMP,YTEMP)
      CALL DMULT(RTEMP,YTEMP,REMNZ,YEMNZ,RT2,YT2)
      CALL DMULT(DETA(I1,J)*R2,DETA(I1,J)*R2,RD2(I1,J)
     &,YD2(I1,J),RTEMP,YTEMP)
```

```
      CALL DMULT(RTEMP,YTEMP,RENZ,YENZ,DR,DY)
      REP(I1,J)=DR-RT2
      YEP(I1,J)=DY-YT2
  130 CONTINUE
      L=N-1
      DO 140 J=1,2
      DO 140 I=1,L
      NMI=N-I
      N1=N-I+1
      RD1(NMI,J)=RE(N1,J)-REP(N1,J)*DBLE(DIST(N1))
      YD1(NMI,J)=YE(N1,J)-YEP(N1,J)*DBLE(DIST(N1))
      RD2(NMI,J)=REP(N1,J)
      YD2(NMI,J)=YEP(N1,J)
      RE(NMI,J)=RD1(NMI,J)+RD2(NMI,J)*DBLE(DIST(NMI))
      YE(NMI,J)=YD1(NMI,J)+YD2(NMI,J)*DBLE(DIST(NMI))
      REP(NMI,J)=RD2(NMI,J)
      YEP(NMI,J)=YD2(NMI,J)
  140 CONTINUE
      RNORM=RE(N,1)
      YNORM=YE(N,1)
   99 FORMAT(2E10.2)
      DO 150 I=1,41
      CALL DDIV(RE(I,1),YE(I,1),RNORM,YNORM,RTEMP,YTEMP)
      RE(I,1)=RTEMP
      YE(I,1)=YTEMP
      CALL DDIV(REP(I,1),YEP(I,1),RNORM,YNORM,RTEMP,YTEMP)
      REP(I,1)=RTEMP
      YEP(I,1)=YTEMP
  150 CONTINUE
      CALL DDIV(REP(N,2),YEP(N,2),REP(N,1),YEP(N,1)
     &,RNORM,YNORM)
      DO 160 I=1,41
      CALL DDIV(RE(I,2),YE(I,2),RNORM,YNORM,RTEMP,YTEMP)
      RE(I,2)=RTEMP
      YE(I,2)=YTEMP
      CALL DDIV(REP(I,2),YEP(I,2),RNORM,YNORM,RTEMP,YTEMP)
      REP(I,2)=RTEMP
      YEP(I,2)=YTEMP
  160 CONTINUE
      DO 170 I=1,41
      F(I,1)=SNGL(RE(I,1))
      F(I,41)=SNGL(RE(I,2))
      G(I,1)=SNGL(YE(I,1))
  170 G(I,41)=SNGL(YE(I,2))
      DIST(1)=0.0
      DO 180 I=2,41
  180 DIST(I)=DIST(I-1)+H(I-1)
      DO 190 I=1,41
      DFDY=(F(I,41)-F(I,1))/DIST(41)
      DGDY=(G(I,41)-G(I,1))/DIST(41)
      DO 190 J=2,40
      F(I,J)=F(I,1)+(DFDY*DIST(J))
  190 G(I,J)=G(I,1)+(DGDY*DIST(J))
      RETURN
      END
C
      SUBROUTINE EFIELD
      REAL K
      COMMON F(41,41),G(41,41),H(40),K(40),SCALE,FREQ,REGION(40,40)
      DO 140 L=32,64,32
```

```
      THETA=(FLOAT(L))*0.0490873
      DO 110 I=1,41
      DO 110 J=1,41
  110 F(I,J)=F(I,J)*COS(THETA)-G(I,J)*SIN(THETA)
      WRITE(6,150) L
      DO 120 I=1,41
  120 WRITE(6,160) (F(I,J),J=1,21)
      DO 130 I=1,41
  130 WRITE(6,160) (F(I,J),J=21,41)
  140 CONTINUE
      RETURN
  150 FORMAT (1H1/////,21H/* PRINT OF EFIELD AT,I3,17H/64 PI RADIANS */)
  160 FORMAT (1H0,11F6.3/11F6.3)
      END
C
      SUBROUTINE  ITERE (EPS,MAXIT,N)
      REAL K
      COMMON F(41,41),G(41,41),H(40),K(40),SCALE,FREQ,REGION(40,40)
      ITER=0
      WRITE(6,150) EPS,MAXIT,N
      DO 130 L=1,MAXIT
      ITER=ITER+1
      BIGF=0.0
      BIGG=0.0
      DO 120 I=2,40
      IM1=I-1
      IP1=I+1
      AKI=K(I)
      AKIM=K(IM1)
      AKI2=AKI*AKI
      AKIM2=AKIM*AKIM
      DO 120 J=2,40
      JP1=J+1
      JM1=J-1
      HJ=H(J)
      HJM=H(JM1)
      HJ2=HJ*HJ
      HJM2=HJM*HJM
      IF (HJ2.EQ.0..OR.HJM2.EQ.0..OR.AKI2.EQ.0..OR.AKIM2.EQ.0.)
     * WRITE(6,700) I,J,HJ2,HJM2,AKI2,AKIM2
  700 FORMAT(' ZERO:',2I6,8E15.6)
      A=4.0*(2.0/(HJM*HJ)+2.0/(AKIM*AKI))
      B=-(REGION(I,J)+REGION(IM1,JM1)+REGION(IM1,J)+REGION(I,JM1))
      C1=8.0/(HJ*(HJM+HJ))
      C2=8.0/(AKIM*(AKIM+AKI))
      C3=8.0/(HJM*(HJM+HJ))
      C4=8.0/(AKI*(AKIM+AKI))
      C=F(I,JP1)*C1+F(I,JM1)*C3+F(IP1,J)*C4+F(IM1,J)*C2
      P=G(I,JP1)*C1+G(I,JM1)*C3+G(IP1,J)*C4+G(IM1,J)*C2
      DENOM=A*A+B*B
      TEMPF=(C*A-B*P)/DENOM
      TEMPG=(A*P+C*B)/DENOM
      RESIDF=ABS(TEMPF-F(I,J))
      RESIDG=ABS(TEMPG-G(I,J))
      IF (RESIDF.GT.BIGF) BIGF=RESIDF
      IF (RESIDG.GT.BIGG) BIGG=RESIDG
      F(I,J)=TEMPF
  120 G(I,J)=TEMPG
      IF ((BIGF.LT.EPS).AND.(BIGG.LT.EPS)) GO TO 140
C     WRITE(6,180) L,BIGF,BIGG
```

```
C 180 FORMAT(' ITERATION',I6,2E15.6)
      LL=(L/10)*10
      IF(LL.EQ.L)WRITE(6,90)L,BIGF,BIGG
   90 FORMAT(I4,2E10.2)
  130 CONTINUE
C     WRITE(6,160) BIGF,BIGG
      RETURN
  140 WRITE(6,170) ITER
      RETURN
  150 FORMAT(9H0/* EPS =,F9.6,28H MAXIMUM NO. OF ITERATIONS =,I6,20H NO.
     # OF AIR LAYERS =,I4,2H*/)
  160 FORMAT (1H0,45H/* STOPPED ON MAX. NO. OF ITERATIONS, FDIFF =,F10.6
     1,11H AND GDIFF=,F10.6,3H */)
  170 FORMAT (1H0,23H/* STOPPED ON ITERATION,I6,3H */)
      END
C
      SUBROUTINE LAZY
      REAL K
      DIMENSION KK(8),A(8)
      COMMON F(41,41),G(41,41),H(40),K(40),SCALE,FREQ,REGION(40,40)
      KN=0
    5 READ(1,9)N,(A(J),KK(J),J=1,8)
      N1=KN+1
      N2=N1+N-1
      DO 3 II=N1,N2
      L=0
      DO 2 J=1,8
      M=KK(J)+L
      L=L+1
      DO 1 I=L,M
      REGION(II,I)=A(J)
      IF(I.EQ.40)GO TO 3
    1 CONTINUE
    2 L=M
    3 CONTINUE
      KN=KN+N
      IF(KN.LT.40)GO TO 5
    9 FORMAT(1X,I2,8(A1,I2))
      RETURN
      END
C
C
      SUBROUTINE CXDP(X,DREX,DYEX)
      DOUBLEPRECISION X,DREX,DYEX
      DREX=DEXP(X)*DCOS(X)
      DYEX=DEXP(X)*DSIN(X)
      RETURN
      END
C
      SUBROUTINE DMULT(XR,XY,YR,YY,PR,PY)
      DOUBLEPRECISION XR,XY,YR,YY,PR,PY
      PR=XR*YR-XY*YY
      PY=XR*YY+YR*XY
      RETURN
      END
C
      SUBROUTINE DDIV(XR,XY,YR,YY,QR,QY)
      DOUBLEPRECISION XR,XY,YR,YY,QR,QY,DD
      DD=YR*YR+YY*YY
      QR=(XR*YR+XY*YY)/DD
```

```
      QY=(XY*YR-XR*YY)/DD
      RETURN
      END
```

Appendix 5.

Example of substorm type variations.

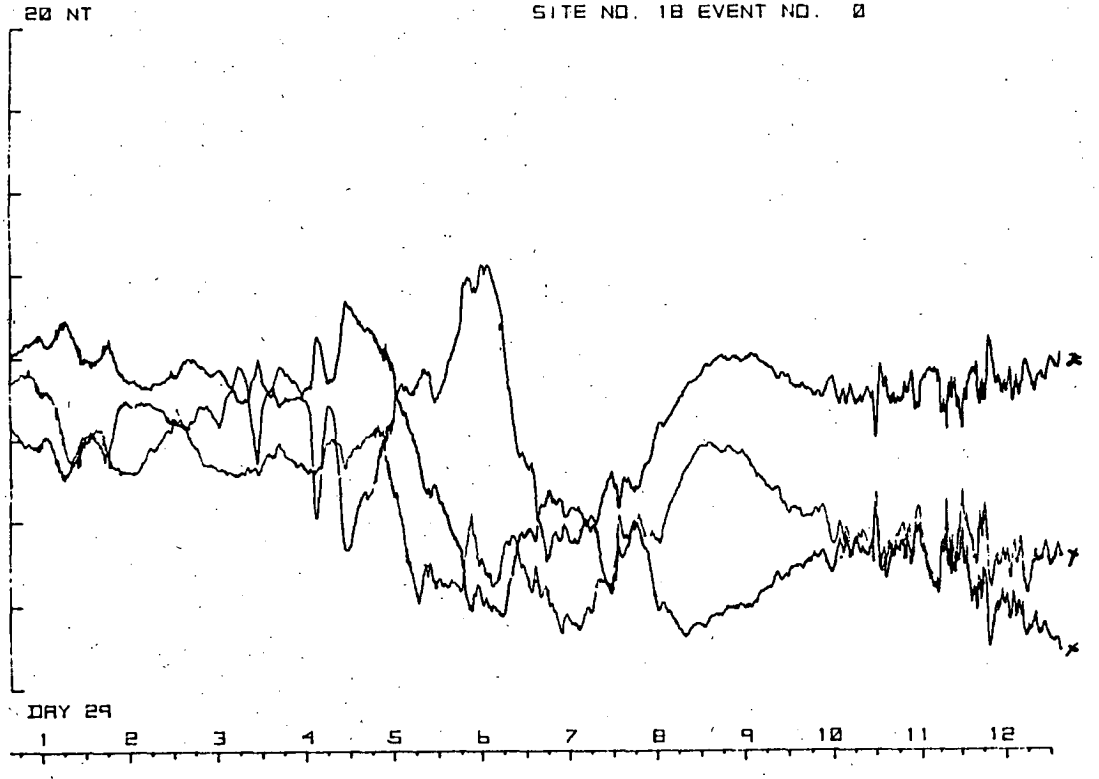

Appendix 5.1 Substorm type variations from Burns Creek (BCR).

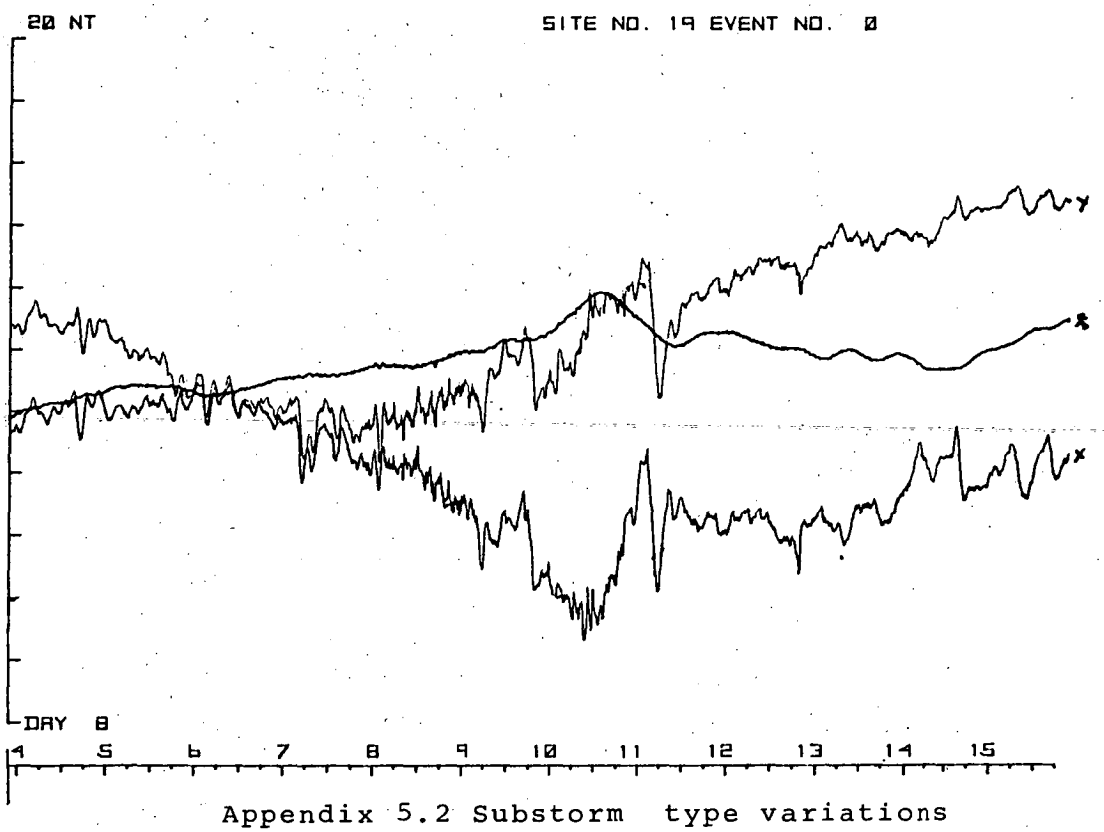

Appendix 5.2 Substorm type variations from White Hills (WHL).

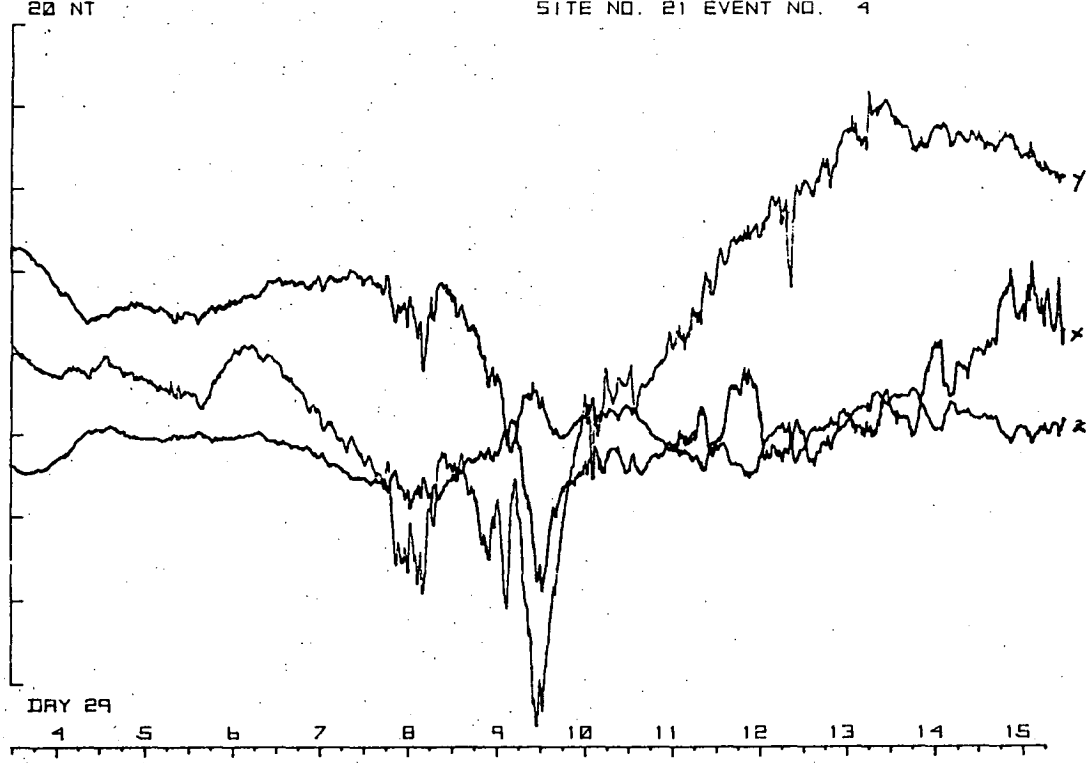

Appendix 5.3 Substorm type variations from Hanleth (HAN).

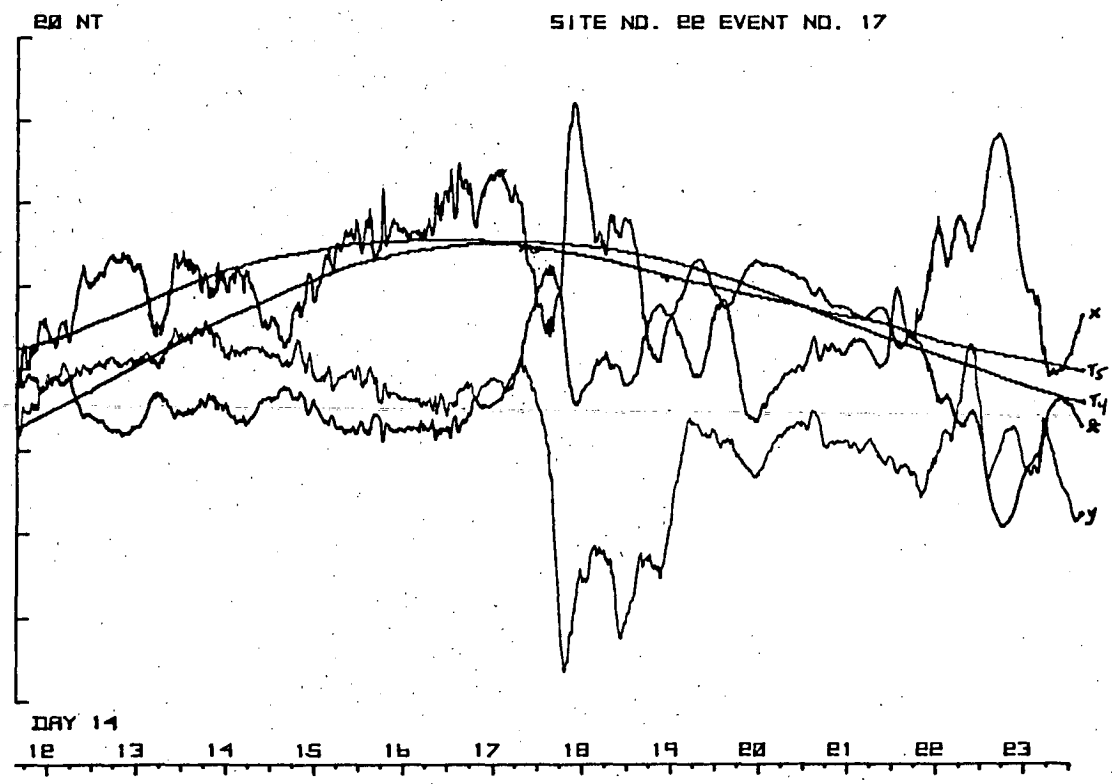

Appendix 5.4 Substorm type variations from Avoca (AVO).

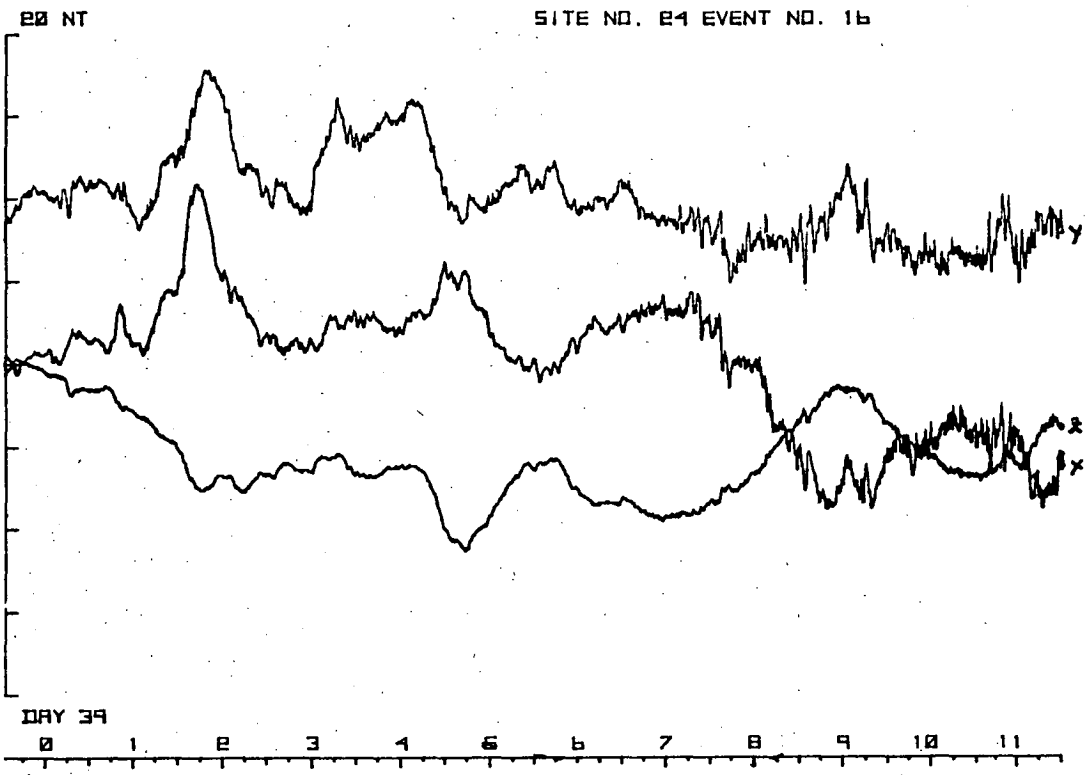

Appendix 5.5 Substorm type variations from Fingal (FNG).

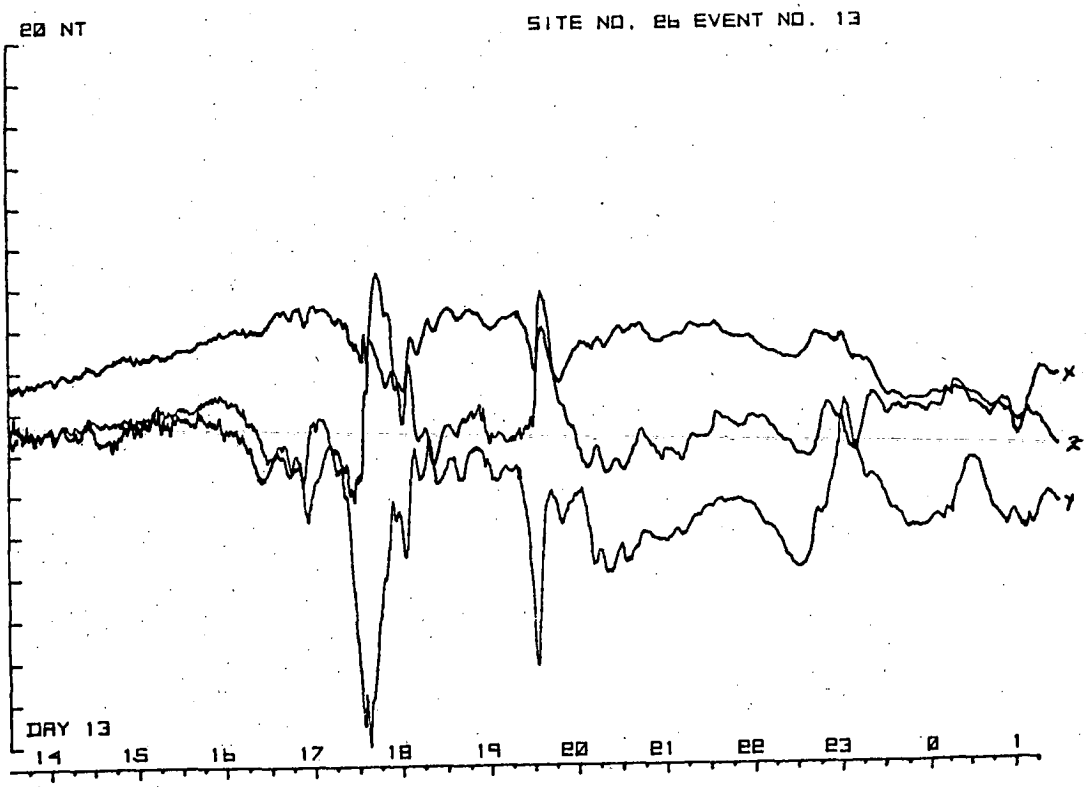

Appendix 5.6 Substorm type variations from View Point Farm (VPF).

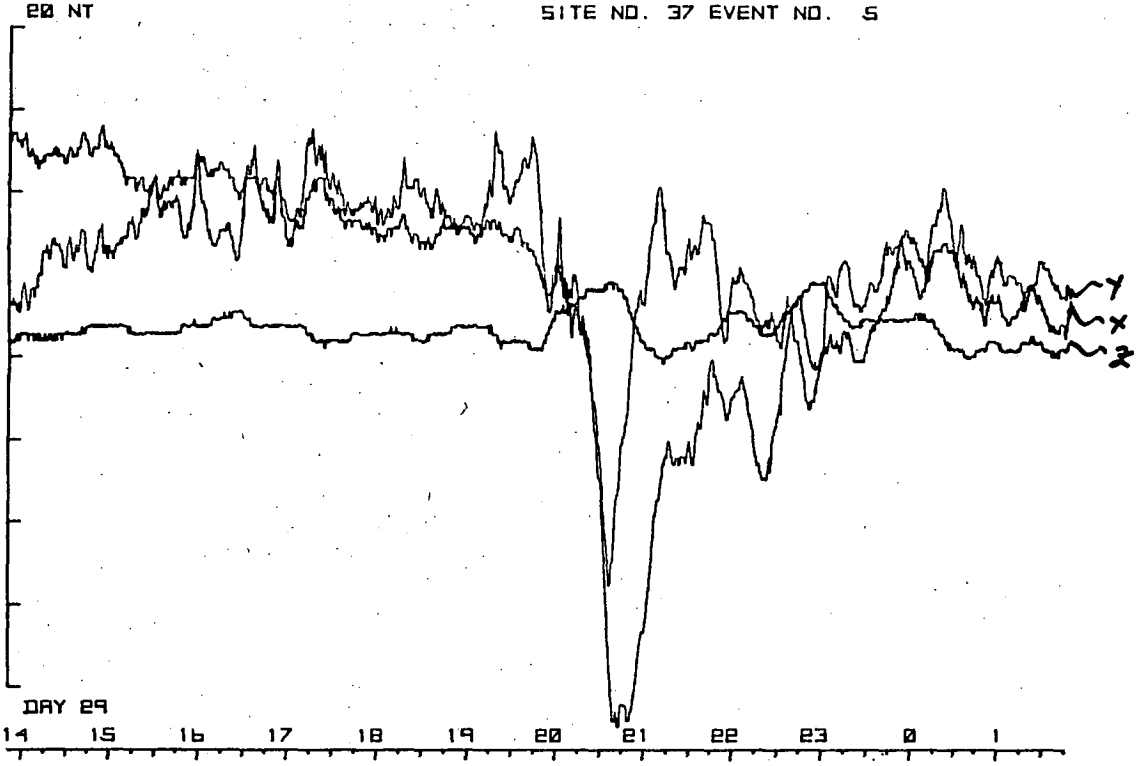

Appendix 5.7 Substorm type variations from Nile (NIL).

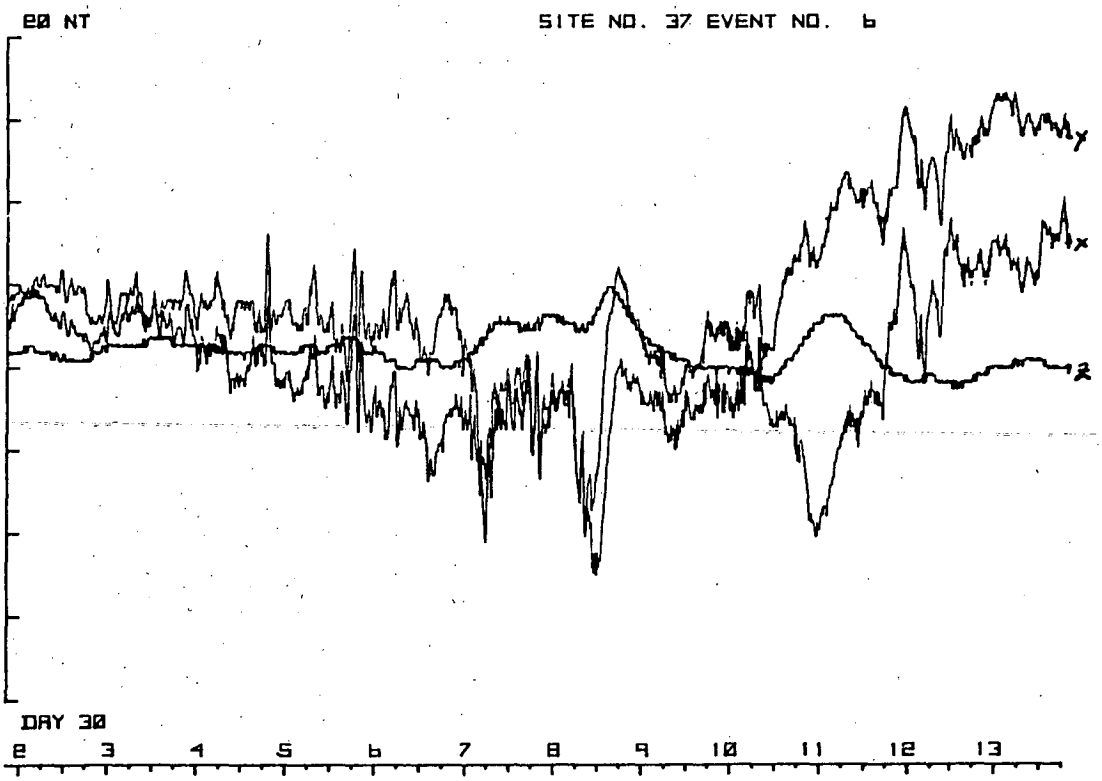

Appendix 5.8 Substorm type variations from Nile (NIL).

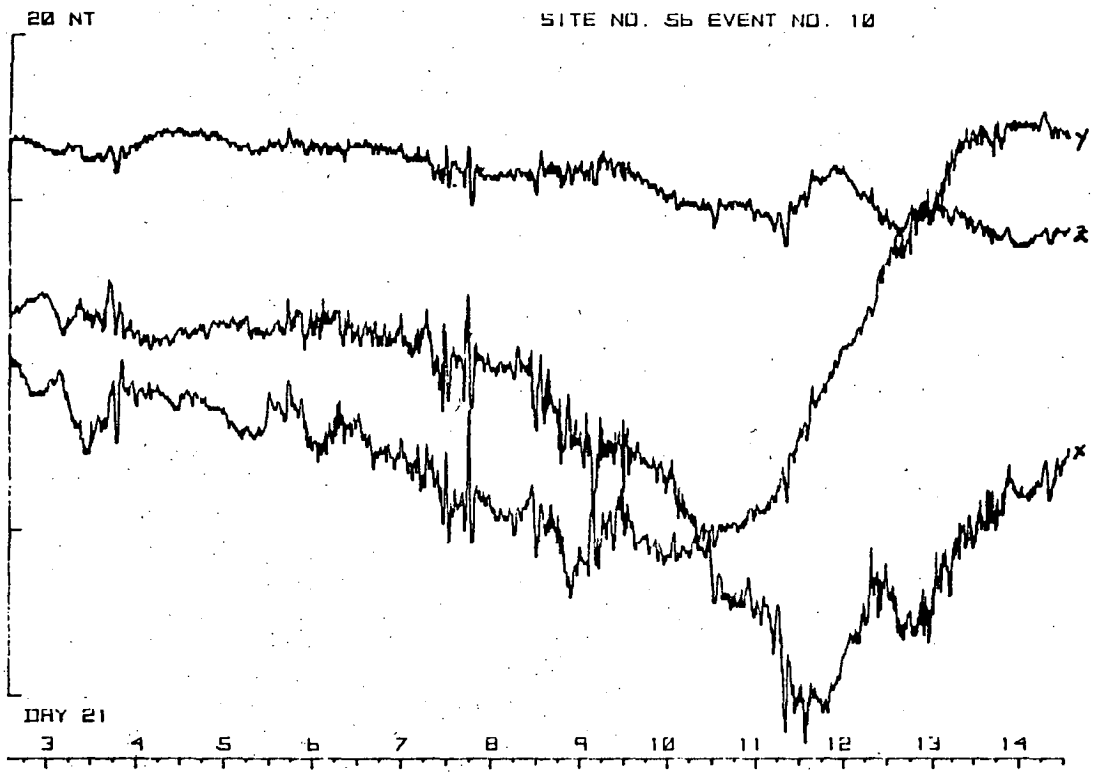

Appendix 5.9 Substorm type variations from Great Lake (GRL).

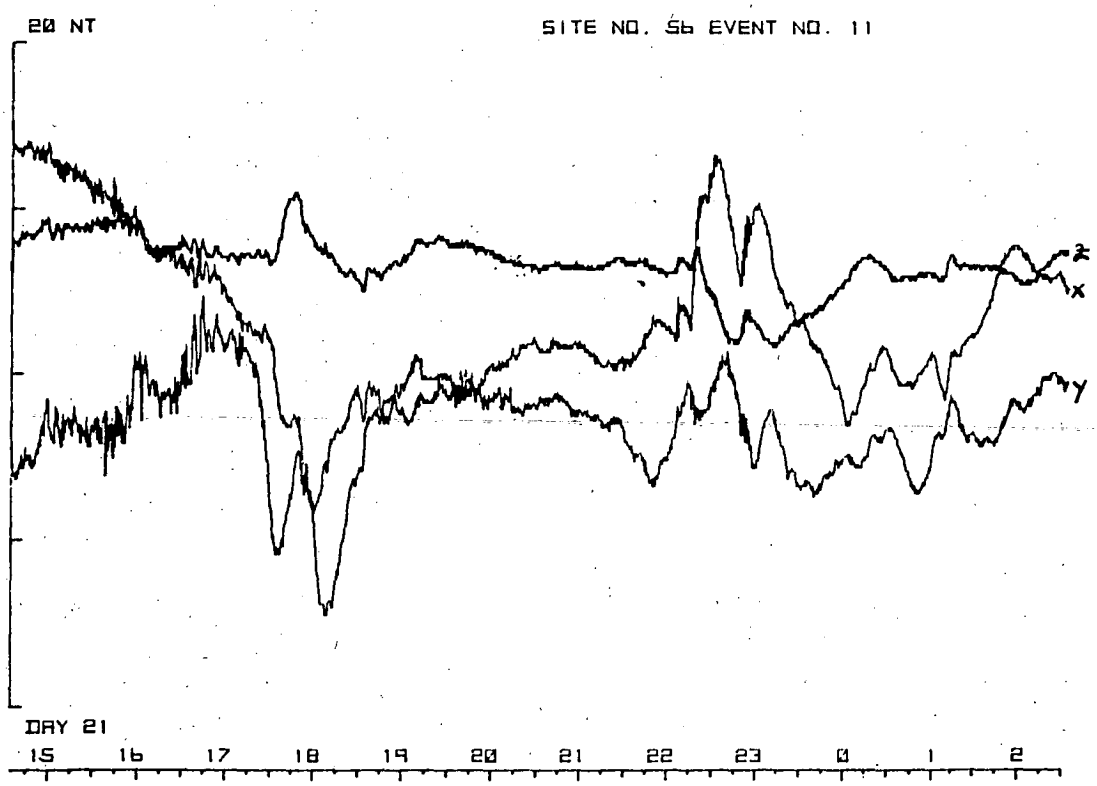

Appendix 5.10 Substorm type variations from Great Lake (GRL).

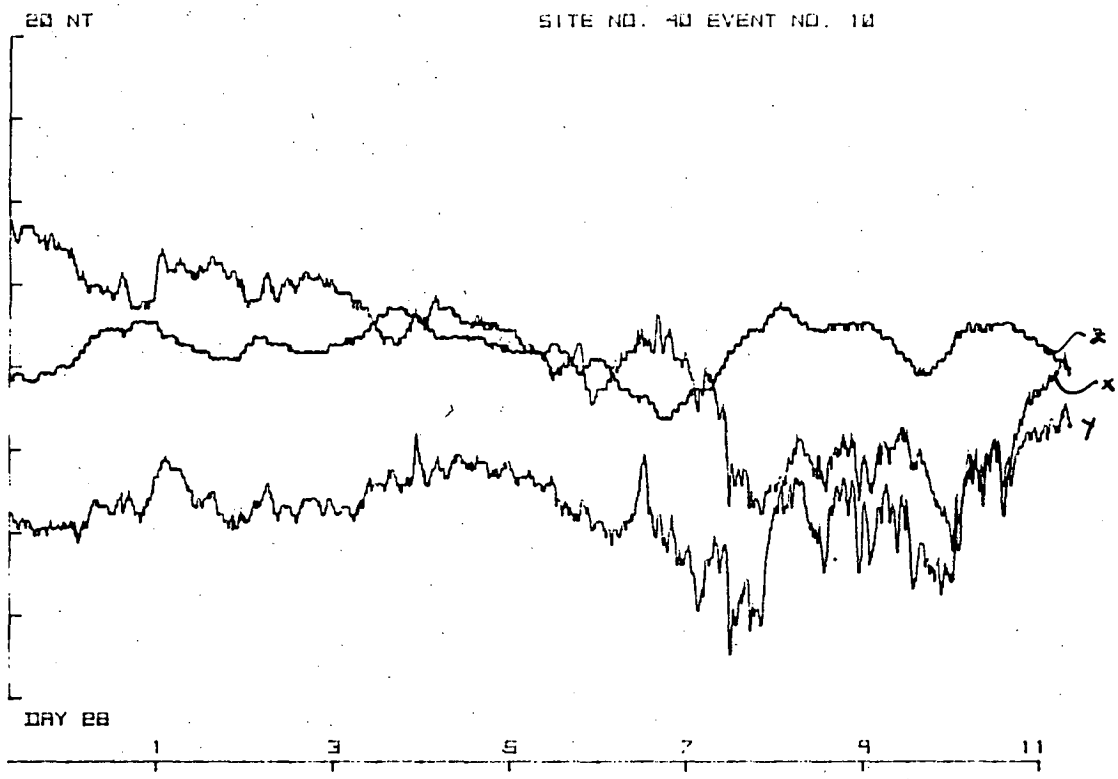

Appendix 5.11 Substorm type variations from Lemont (LEM).

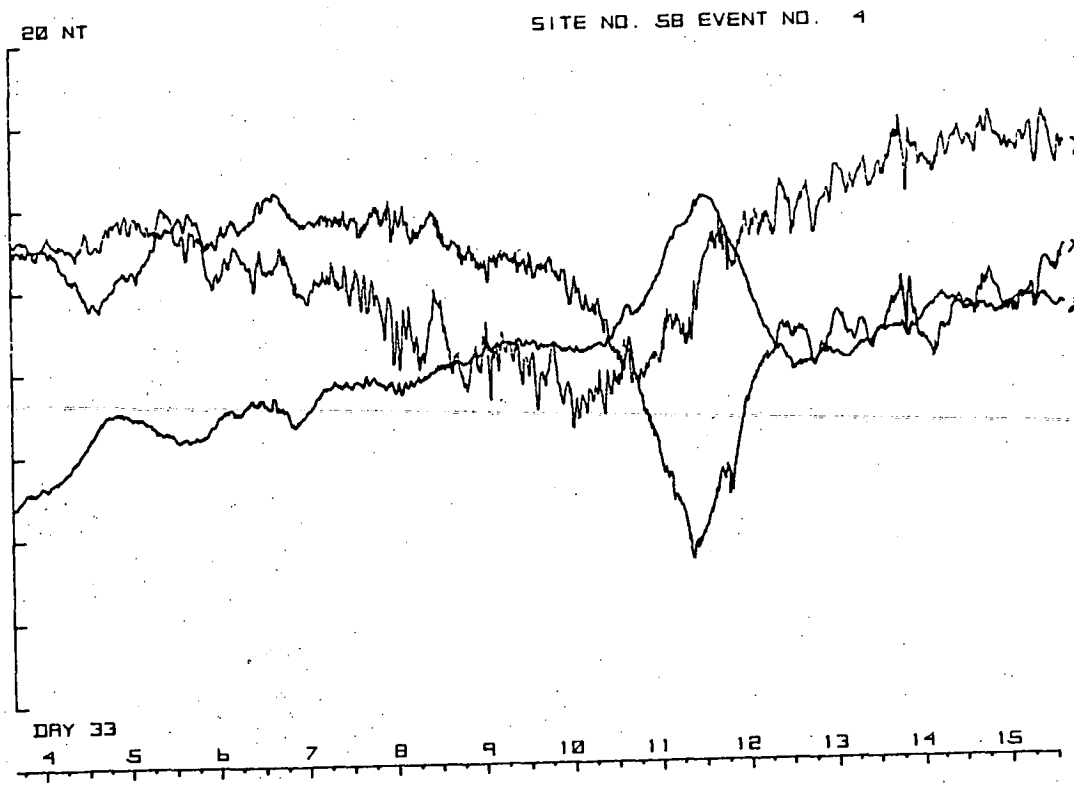

Appendix 5.12 Substorm type variations from Oatlands (OAT).